AD-648 078

MODELING TECHNIQUES FOR
SONIC FATIGUE PREDICTION

P. WANG
NORTH AMERICAN AVIATION, INC./LOS ANGELES DIVISION

TECHNICAL REPORT AFFDL-TR-65-171
JUNE, 1966

Distribution of this
document is unlimited.

2007091909S

AIR FORCE FLIGHT DYNAMICS LABORATORY
RESEARCH AND TECHNOLOGY DIVISION
AIR FORCE SYSTEMS COMMAND
WRIGHT-PATTERSON AIR FORCE BASE, OHIO

MODELING TECHNIQUES FOR SONIC FATIGUE PREDICTION

P. WANG
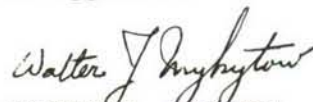
FOREWORD

The research work reported herein was conducted by North American Aviation, Inc., Los Angeles, California. The work was administered by the Aero-Acoustics Branch, Vehicle Dynamics Division, AF Flight Dynamics Laboratory, Wright-Patterson Air Force Base, Ohio, under Contract Nr. AF33(615)-1743. This research is part of a continuing effort to obtain tolerance levels and design criteria for flight vehicles and is part of the Research and Technology Division, Air Force Systems Command's exploratory development program. The work was conducted under Project 1471 "Aero-Acoustic Problems," Task 147101 "Sonic Fatigue". Mr. M. J. Cote of the Aero-Acoustics Branch was the Project Engineer.

This report covers the period from May 1964 through October 1965. The manuscript for this report was released by the author for publication as an AFFDL Technical Report in November 1965. Contractor's report number is NAA TFD 64-490-13.

This report has been reviewed and is approved.

WALTER J. MYKYTOW
Asst. for Research & Technology
Vehicle Dynamics Division

ABSTRACT

The principles of static and dynamic similitude were applied to typical complex structural components for the purpose of examining the application of modeling techniques to sonic fatigue predictions. Modeled specimens of curved panels, honeycomb sandwich flat panels, and honeycomb sandwich cantilever beams have been tested. The tests were conducted on full scale, 5/8, and 3/8 size models. The tests and analyses demonstrated that scale reductions of linear panel dimensions, and other size factors necessary in the fabrication of models, may be separately considered in maintaining the established similitude relationships. Both random spectra and discrete frequency acoustic excitation are considered.

Correlation of available data from other sources has established a frequency parameter defining the effects of radius of curvature along one side of a curved panel. This frequency parameter converts to a stress reduction factor that has been verified experimentally in many modes. Although the section modulus for honeycomb sandwich panels need not be controlled by the scaling factors, the generation of response modes is significantly related to the aspect ratios of surface dimensions. This panel aspect ratio effect can yield a dominant excitation of higher complexity modes at low stresses and impose difficulties in fatigue duration tests. Experimental data are used to identify these complexities and differences between modes without introducing consideration of coupling effects.

Stress correlation is the critical parameter in modeling for acoustic fatigue. True models with exact geometric scaling in all elements are not necessary. Adequate modeling is obtained by maintaining the same aspect ratio and modes for the specimen and model. The frequency and stress then vary at predetermined magnitudes with a functional relationship to damping, amplitude, and cross-section (thickness) geometric parameters. Non-linear effects are dependent on excitation levels. In general, a prerequisite to sonic fatigue tests is a knowledge of the non-linearity induced by damping and amplitude for each specimen. The experimental data confirms the application of basic procedures formulated by Miles, Palmgren, and Miner which minimize the requirement for random excitation in the use of modeling techniques for sonic fatigue predictions.

TABLE OF CONTENTS

LIST OF ILLUSTRATIONS

LIST OF SYMBOLS

A	effective area, in^2
A.R.	amplification ratio
C	a dimensional frequency constant
D	total system damping work per cycle, in-lb per cycle
E	modulus of elasticity, lb per sq. in.
I	moment of inertia, in^4
K_t	a stress concentration factor
M	bending moment, in-lb.
N	number of life-cycles at fatigue failure
N'	a scale factor = scale reduction
P	total force, lbs.
R	algebraic ratio of fatigue stresses, $= S_{min}/S_{max}$
R	radius of curvature, in.
S	bending stress, lbs per sq. in. (psi)
T	a time duration at specified unit
V	shear force, lb.
W	total weight, lb.
a	a length factor or the short side of a rectangular plate element, in.
b	long side of a rectangular plate element, in.
c	the depth of a honeycomb core (between face sheets), in.
c	coefficient of damping force, lb/in. per sec.
c_c	coefficient of force at critical damping velocity, lb./in. per sec.
c_i	a nonlinear coefficient of damping force, lb./in. per sec.

d	distance of an extreme fiber in bending to neutral axis, in.
f	frequency, cps
f_r	linear resonance frequency, cps
g	acceleration due to gravity, ft per sec^2
h	thickness of a rectangular plate, in.
i	the number of complete waves in the circumference of a ring
k	radius of gyration, in.
k	a spring constant, lb. per in.
ℓ	a length factor, in.
m, n	the number of half-waves in dimensions b and a
n	an exponential constant, dimensionless
p	pressure intensity, lb. for a particle
	lb./in. for a beam
	lb./in^2 for a plate
r	subscript for a linear resonance mode
t	thickness of face sheets in a honeycomb sandwich section, in.
t	time, sec.
u	a function of nonlinearity in bending response, dimensionless
w	unit weight of a vibrating beam, lb per in.
	plate, lb per sq in.
y	amplitude, in.
α	S-N curve parameter = $\log N_2/N_1 \Big/ \log S_1/S_2$
β	coefficient of bending stress
λ	a dimensional constant, $in.^{-1}$
ρ	density of material
σ	dynamic stress, psi

ϕ	a nonlinear deflection coefficient
ψ	a nonlinear bending stress coefficient
ω_r	linear resonance frequency, rad./sec.
ω, Ω	frequencies in nonlinear resonance conditions, rad./sec.

1.   INTRODUCTION

On the question of fatigue failures in structural components of aerospace vehicles, there is little doubt that a major contribution comes from acoustically induced vibrations. In recent years, considerable research work has been oriented towards a better definition of the acoustical loading that these components should be designed to sustain, and towards a more critical analysis of the vibratory responses induced by the acoustical loading. Progress and advancement to meet newer challenges in the technology of acoustically induced fatigue of structure is dependent upon an optimum achievement in both these undertakings. Like all engineering accomplishments of the past, however, analytical results must be subjected to proof tests before acceptance. As vehicles become more and more complex and loading requirements are more and more severe; the performance of these tests would incur a great deal of engineering effort and expense. This situation has drawn attention to the potential use of models, as specifically in the current program, for studying a technique by which acoustically induced fatigue strength can be predicted.

In a technological sense, models have been used and are used in almost any engineering task. In the determination of physical properties of newer or more exotic materials, sample specimens of any shape or form are fabricated and tested. These are essentially models; for example, in the case of the tensile strength of a round bolt or a rectangular pin, one would simply refer to the unit strength of a modeled specimen in the same loading environment and determine the desired strength from the cross-sectional area of the bolt or pin. The area is, therefore, the essential modeling parameter. Because a tensile specimen is usually round, it can be considered as a true model of the bolt and a distorted model of the rectangular pin. If an additional consideration is required in this case to determine fatigue strength, the question of loading conditions will naturally arise. Similitudes are extended to the case of fatigue only if the stress reversals or variations are compatible in magnitudes. For the bolt and pin, possible differences in the most likely stress concentrations of model (test specimen) and the bolt or pin must be considered and evaluated. For the purpose of this program satisfactory fatigue properties commonly expressed in the form of S-N curves for the specimen material are assumed available for loading conditions representative of those imposed; the intrinsic variation in an S-N curve is not an investigation objective.

Specifically, therefore, a premise is established that under identical environments, the behavior of a specimen and its models are alike. Indeed, the designation of a "specimen" or a "model" is merely symbolic. The knowledge that is being sought in modeling studies for sonic fatigue is no more exclusive than in other cases. The response of a given elastic assemblage must be ascertained under given conditions that are common to both specimens and models, which incidentally need not be restricted to true models only. The program is one of defining the parameters relevant to both response and loading.

1

The purpose of this study is to demonstrate through analysis and experimentation that some basic relationships remain applicable in modeling complex structures for acoustic fatigue analyses. For providing information on the more pertinent simulation requirements of desirable structural components, two structural assemblages in the form of honeycomb sandwiched panels and curved plates were chosen for study. Neither of these structural unit types have been completely delineated in its physical properties - only those considered of major importance were defined in the study. The objective is to extend the parameters as defined in this study towards a prediction of the fatigue strength of each unit in an acoustical environment.

2. DYNAMIC MODELING REQUIREMENT AND PARAMETERS

2.1 Background

Dynamic similitude through the use of models as a method of solving many engineering problems has long been recognized. In fatigue investigations of structural components exposed to random excitations, acoustically or otherwise induced, the application as reported in Reference 1 will of course be anticipated. The advocated reduction of a prototype specimen in all its linear dimensions by the same scale factor i.e., into "true" models, however, poses severe limitations that must be overcome. The theoretical background on the use of "adequate" models, not exactly scaled, is provided in Reference 2.

Generally speaking, the use of models is predicated upon the premise that in dynamic stress similitude, a structure is correctly modeled if its stress under a given dynamic load can be predicted from the measured stress in the model. Thus in true models, the same stress is merely duplicated. Insofar as fatigue strength is concerned, the equivalent knowledge (S-N curves) applies. For the same life-cycle duration, the product of frequency and time is a constant. Since the frequency is inversely proportional to the true model geometric scale, the duration on a time basis becomes directly related to scale factors. However, quite frequently geometric variations and changes in response modes require that differences in resultant stresses must be taken into account in fatigue considerations. Available data from Reference 1 and other sources have been, therefore, re-examined in this direction whereby some of the reported discrepancies may be resolved.

2.2 Fatigue Data Correlation

2.2.1 Stress Variations between Modeled Specimens

Some typical examples of stress variations are found in the data of Reference 1 and reproduced here in Figures 1a and 1b. Spectrum analyses of strain gage signals from similar locations are indicated as S_1, S_2, and S_3 of Figure 1 for 1/3 and 1/6 scaled models of a ribbed square plate excited by random noise of appropriately scaled acoustic powers. To reproduce the same stress in both cases, all corresponding spectra should follow the same shape after a downward shift in frequencies at a scaled ratio of 2 for the smaller model (frequency scaling for the 1/2 :1 geometric scaling). The power spectrum difference should then be +3dB (=10 log 2) for the larger model. In the data shown, this difference is +6dB for the maximum stress indicated.

2.2.2 Mode Frequency Variations between Modeled Specimens and Fatigue Correlation

By comparing the shapes shown in Figures 1a and 1b, it is also observed from the spectrum differences at location S_1 that the square element within the ribs responded differently between models. This may serve to explain the increased stress in the 1/3-model plate. The relationship between excitation powers was separately determined to have been

3
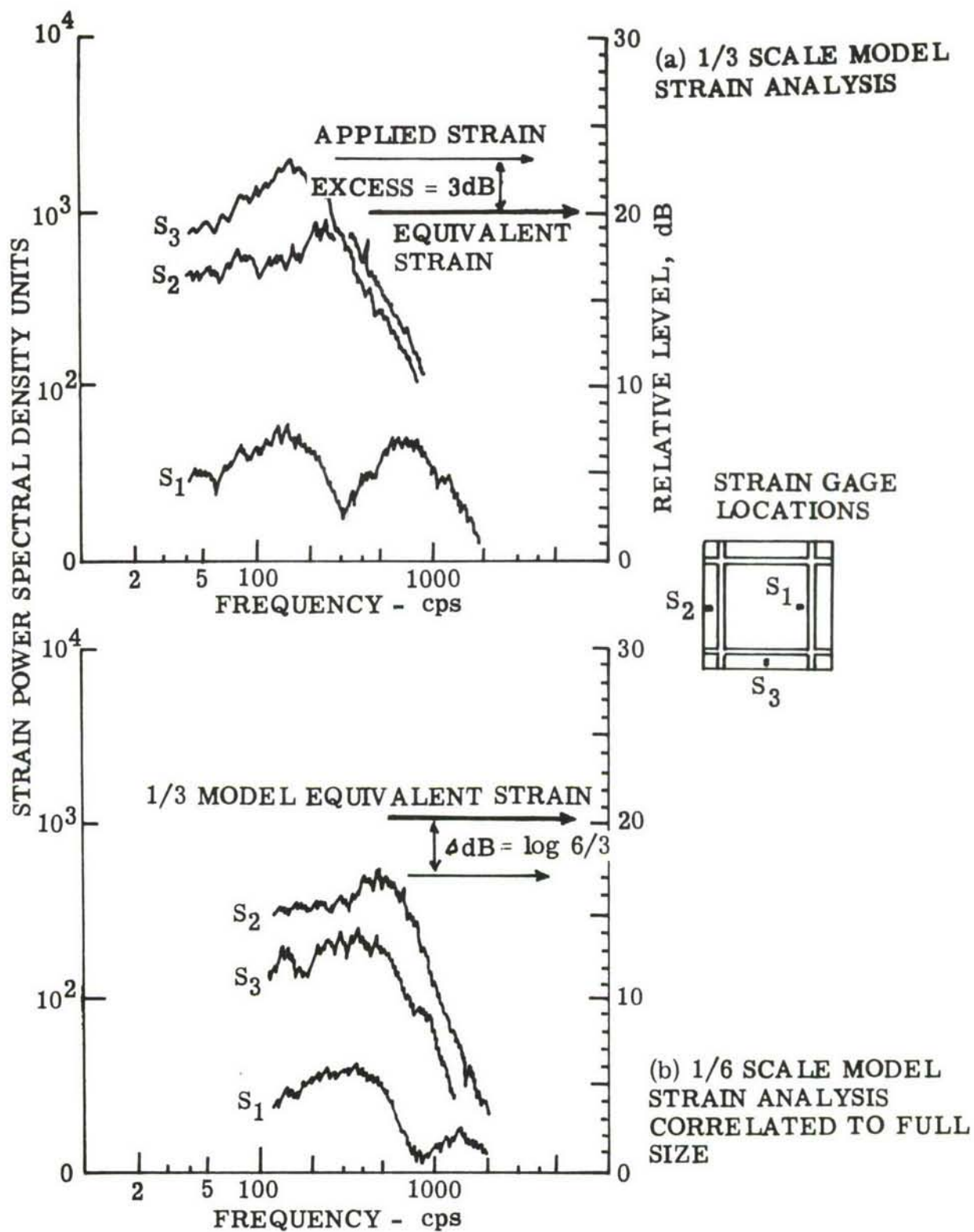
Figure 1. Strain Power Spectral Analyses
(Design I Plate Data From Ref 1)

properly applied between all specimens (See Ref. 1). If the increase in maximum stress is taken into account, it is very likely that the reduced fatigue time of the 1/3-model plate would fit an acceptable S-N curve or could be corrected to show a constant "N" for the same "S" as in the other specimens. In this respect, it must be mentioned that locations S_2 and S_3 are essentially the same insofar as plate vibrations are concerned. Failures induced by transverse bending could occur along either side. For this reason the spectra at S_2 and S_3 are compared as respective maxima. The mode frequencies observed at 165 and 500 cps, not being precisely an inverse ratio of geometric scale factors provide a necessary correction factor in converting fatigue cycles to the indicated duration time. Because the stress is the criterion in fatigue, such a correction is always necessary when a time duration is used.

2.2.3 Fatigue Time Corrected

The average S-N curves for aluminum, when plotted on log-log scales, exhibit a nearly uniform slope beyond 10^4 cycles without significant variations between material classifications or stress concentration factor changes. On this basis, for a stress difference corresponding to +3dB (= 20 log stress ratio) or 1.4 times higher stress, the number of cycles affected is approximately 10 times. Thus the observed durations of the higher stress at 165 cps should be multiplied by 10 if the frequency had been correct at the modeled stress for the 1/3-model. Based on 65 cps for the full size panel mode of Reference 1, the 1/3-model frequency should be 195 cps. To correct for the frequency differences, the actual time observed at 165 cps is to be shortened by a ratio of 165/195 making a total correction of 8.5 times.

Examination of the details of the 1/6-scaled specimens (Design I of Reference 1) reveals that a reduced corner radius at the advocated scaling law would very likely incur an increased stress concentration factor. Based on the given full scale reference, the observed fatigue duration of the 1/6-scale specimens should be adjusted by a ratio of 1.5 for stress concentration differences. Concurrently the time correlation required is based on the observed response at 500 cps (Fig. 1b) divided by the scaled frequency of 6 x 65. The total correction factor is $1.92 \left(= \frac{500}{6 \times 65} \times 1.5 \right)$ which is applicable in an interpretation of fatigue

time T between true models at scale factors N'. The corrected failure time result for the Reference 1 specimens is shown in Fig. 2. A linear relationship is clearly indicated which verifies the theoretical result that duration time is directly proportional to geometric scale factors. The range in data scatter which is represented by either the vertical or horizontal spread between the two lines, is attributed partly to damping coefficient variations, currently undetermined in extent, and partly to normal scatter in fatigue data.
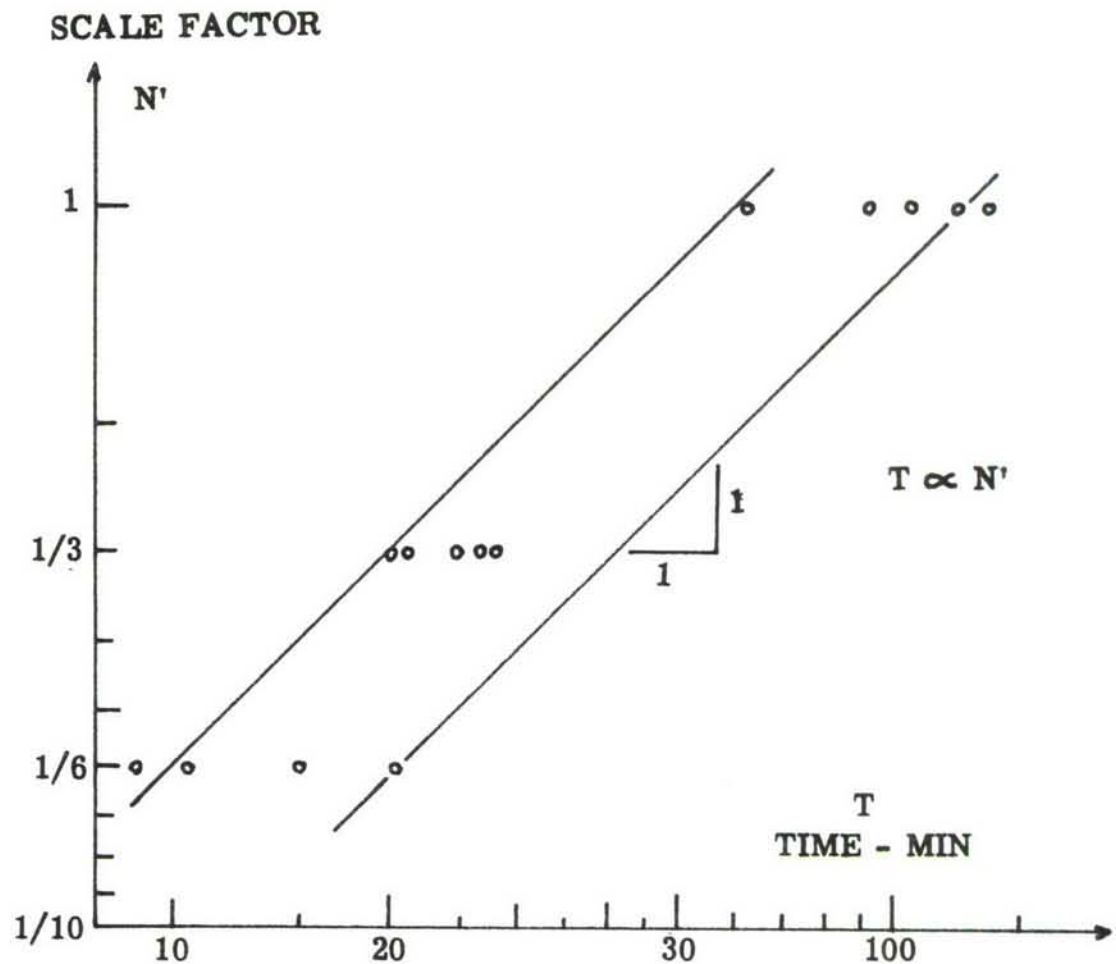
SCALE FACTOR

Figure 2.   Failure Time and Scale Factor of Test Specimens
(Design I Plates From Ref 1)

2.3   Similarity of Restricted Temperature Effect and Some
Nonlinear Characteristics of a Soft Spring Variety

In Figure 46 of Reference 3 an extensive change was reported in the
resonance frequency accompanying a temperature change of only a few
degrees Fahrenheit in a clamped beam specimen. This temperature change was
limited, however, to the beam itself through localized heating in such a

manner that the main clamping fixture remained essentially free of a thermal strain. This must be considered as a unique case in variance with steady state operational environments where both the clamping and the clamped generally assumed same temperatures. Only a slight drift in frequency was usually observed unless the difference in thermal expansions was extremely great. A large change in resonance frequency of the order reported must be attributed to the induced compressive stress. As the temperature of the beam was increased, the natural extension in its physical length caused it to exert an axial force on the clamping fixture. This action is the same as a compressive force applied axially on the beam. Before the Euler's load is reached, at which point the beam buckles as a column, the effect of such an induced compressive force is to reduce the tensile stress of bending in response to an applied transverse load. It is, therefore, feasible and relatively straightforward to calculate the ratio of the change in tensile stresses due to temperature changes as if a static compressive load was applied. A dynamic similarity of this restricted temperature effect is also found in a cylinder under torsional vibrations. For any particular mode, an elementary block or column may be considered as an elastic unit between nodal axes, subjected to axial compression and lateral bending at the same time. This was discussed in Reference 4 based on data extracted from Reference 5. The two cases are plotted in Figure 3 to compare the temperature effect and torsional vibration characteristics. The advantage in using logarithmic scales is evidenced in the fact that differences in readings are reflected merely in scales and that a geometric similarity is revealed in the curves. Thus, the general result is defined in the sloping lines which are parallel with a common slope of 12 dB per octave. As the compressive load is increased, the maximum vibratory stress increases for decreasing frequencies characteristic of nonlinear soft springs. It appears, therefore, unwarranted to emphasize merely the effect of restricted temperature changes on a vibrating unit without a complete investigation. It is interesting, however, to observe that if a temperature differential exists between the clamping fixture and the vibrating unit, a frequency shift is inevitable. Consequently in normal test set-ups, clamped boundaries must be released between tests to relieve residual axial forces and to minimize the expected frequency drift.

2.4   Sinusoidal versus Random Excitation in Response & Fatigue Tests

A useful correlation of the fatigue damage sustainable by an elastic unit responding in a single mode under random loading has been mathematically determined by Miles (Reference 6). Miles' theory was based in terms of the same damage that would be cumulated if a given random stress expressed by its rms spectrum or power spectral density, had been replaced by an equivalent sinusoidal power spectrum whose level is raised α/e (e = 2.72) times, or $10 \log \alpha/e$ decibels. Supporting data may be found in Reference 7 from which Figure 4 is reproduced, α (=7 for aluminum) being the indicated slope of a log S-log N curve. It is readily observable that both the random and constant amplitude fatigue curves exhibited the same general slope and were spaced apart to a degree in accordance with Miles' deductions. Accordingly for the equal damage condition   represented by any ordinate
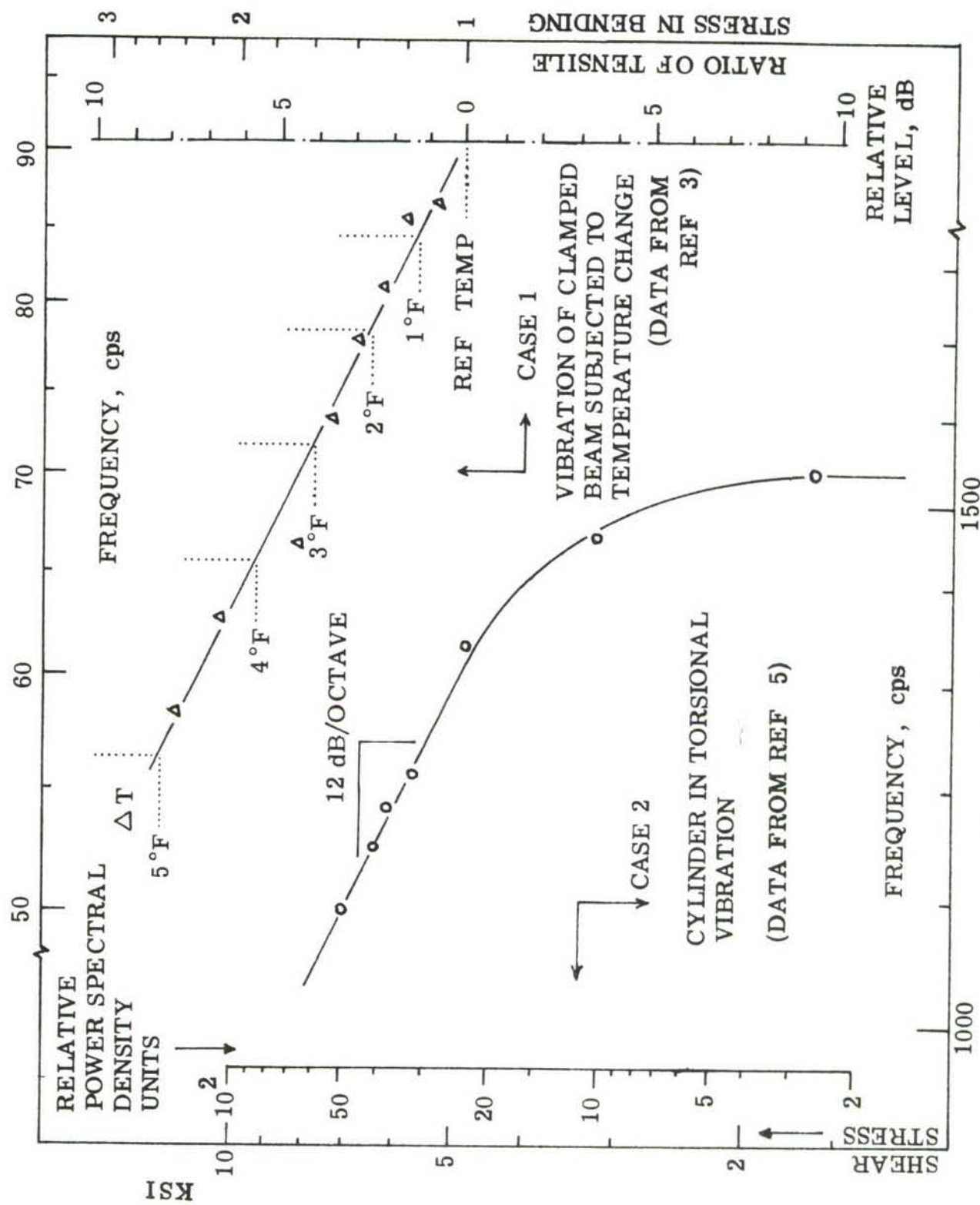
Figure 3. Soft Spring Characteristics

8
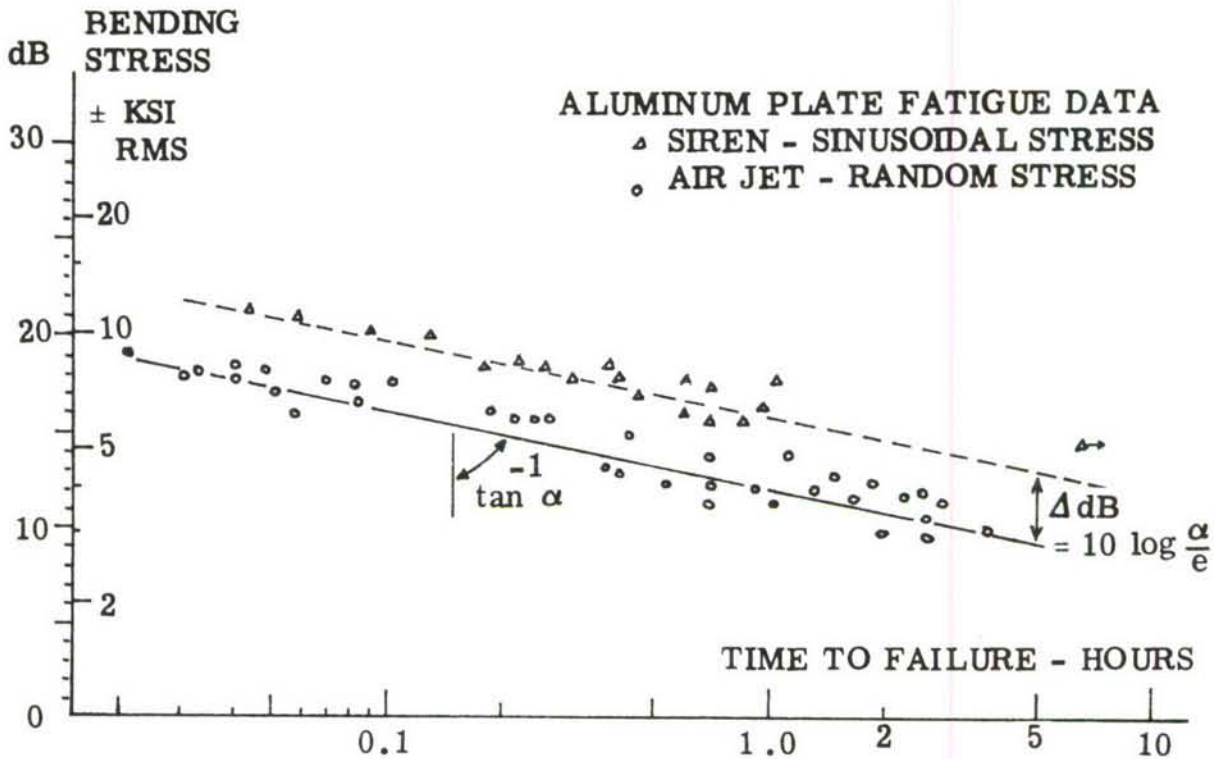
Figure 4. Typical Fatigue Data (From Ref 7)

in Figure 4, the observed sinusoidal stress level exceeds the random stress by 3 to 4 dB versus the calculated difference of 10 log α/e which is 4 dB. The use of Miner's cumulative damage index, Reference 8, in this analysis by Miles can be considered as quantitatively substantiated.

In achieving a satisfactory correlation of damages between a random and a sinusoidal stress, it becomes quite evident that under laboratory conditions either method may be used in obtaining relevant fatigue data. However, it must be emphasized that the solution by Miles is predicated upon an idealized solution of a single mode in linear response. The use of random forces in general implies large forcing amplitudes and almost necessarily induces nonlinear response in the resultant stress unless the specified spectrum is very moderate in level. Frequently, many mode components contribute to the same damage. Due to the difference in modes, the maximum stress may not be the damage stress pertaining to a particular mode. For example, a clamped beam would have its maximum bending and damage stress at the clamped ends in the first mode. The maximum stress in a 3rd mode would probably be located elsewhere while the contribution of the third mode to the ultimate damage at the ends was a much lesser stress. To assure the maximum stress in the modes of importance (generally the low order modes), the separation of modes is necessary. For this purpose, the use of sinusoidal forces, either acoustically or mechanically applied, becomes most suitable.

9

2.5   Modeling Parameters Extended to Complex Configurations

The evaluation of previous results introduced in the foregoing discussion demonstrates that for fatigue considerations, particularly between scaled models, it is important to secure a basic knowledge of the stresses induced in each specimen. For simple structures in rectangular sections, the geometric similarity achieved in true models results in equal static stress being generated in all cases under equal forcing powers or loading pressures. The expression of fatigue (S-N solutions) at any one stress level transformed into a relationship between model scale factors N' and a time duration T (See Fig. 2) is a particular solution and should not be extended to complex structures without necessary qualifications. For this program, a honeycomb sandwich structure and a curved panel will be used to illustrate the qualification procedures.

2.5.1   Modeling Parameters in Honeycomb Sandwich Panels

The geometrical representation of a honeycomb sandwich section is given in Figure 54c, Appendix A.

2.5.1.1   Stress Parameters

The bases for stress correlation are represented by equation A2 and A3 given in Appendix A, yielding the following relationship for the same stress conditions being modeled,

$$\left[\frac{M_o d}{2(c/c_c) I_{1-1}} \right]_{Full\ Scale} = \left[\frac{M_o d}{2(c/c_c) I_{1-1}} \right]_{Model} \tag{1}$$

where I_{1-1}/d is the section modulus, M_o is the maximum static bending moment, and c/c_c is the damping coefficient ratio. A more useful form of this same equation is given in Appendix A as Eq. A3a which expresses M_o in terms of the maximum forcing pressure intensity p and the ratio $1/2\ c/c_c$ as an amplification factor (A.R.). Thus, the equation of the modeled stress σ is

$$\sigma = \frac{\beta p a^2 d\ (A.R.)}{6\ A\ k^2} \tag{1a}$$

with $\beta p a^2/6 = M_o$ where $(\beta/6)$ is the moment coefficient and a is the relevant length factor; and $Ak^2 = I_{1-1}$ where A is the sectional area of the plate and k is its radius of gyration.

Note that for uniformly distributed loading intensity on rectangular plates, for which all linear dimensions are identically scaled, the above relationship is automatically maintained. This was designated in Reference 1 as a scaling law, where the damping coefficients were considered as being the same. For honeycomb sandwich sections, numerical values of I_{1-1} and d are subjected to other practical considerations such as the thickness t of the face sheets and the depth c of the core used. The result is that as the static bending moment M_o is exactly proportional to the square of the size factor, the ratio of I_{1-1}/d is not. It is, therefore, necessary to consider each parameter separately, including the damping coefficient ratio as an additional variable. For fatigue considerations, it is convenient (but not necessary) to keep the lumped ratios in the above relationship at

10

some given level. This can be accomplished by adjusting the loading conditions after c/c_c, I_{1-1} and d are determined for the full scale unit and its modeled specimen. The necessity of scaling every linear dimension is hereby removed.

2.5.1.2 Frequency Parameters

The required parameters in a frequency correlation between modeled specimens are given in the following equation which is a modified version of Equation A6 introduced in Appendix A.

$$f_r = C \frac{\sqrt{12}k}{a^2} \left[\frac{\text{weight of face sheets}}{\text{total section weight}} \right]^{1/2} \qquad (2)$$

where f_r is the resonance frequency in cps, C is a constant dependent on panel shape (b x a) or aspect ratio (b/a) and constraint conditions, k is the radius of gyration due to the face sheets, and the bracketed weight correction is due to the core weight adding inertial forces during vibration (the bending stiffness being provided by only the face sheets). The values of the constant C are given in References 9, 10, 11, 12 and shown in Fig. 5. It is evident that only identical modes may be considered if the above equation is applied to modeled specimens. For the modeled plates of Reference 1, the frequency is inversely proportional to the scale factor. For honeycomb sandwich sections, the weight correction cannot be held constant in view of the requirements set forth upon the values of I_{1-1} and d for stress parameters discussed in the preceding section. It is, therefore, necessary to consider the frequency of the mode to be investigated in each case and avoid a general correlation of fatigue time to scale ratios.

2.6 Selection of Honeycomb Sandwich Panels and Model Dimensions

2.6.1 Scale Ratios and Number of Specimens

While the selection of scale ratios is entirely arbitrary, practical considerations as to the minimum size that can be conveniently handled in experimental investigations usually impose an upper limit in scale reductions. In order to fulfill the programmed requirement of using two model sizes, these were established at 5/8 and 3/8, full size being 1. Three specimens were provided in each size. As indicated in Section 2.5, parametric requirements in comparative stress and frequency changes between models dictate specific ratios indicated in Sections 2.5.1.1 and 2.5.1.2. The given scale ratios are, therefore, nominal sizes only and not to be used in calculations.

2.6.2 Panel Sizes and Aspect Ratio

The largest size was based upon the size of the fixtures available which established the full scale panel dimension at 41 x 28 inches with an aspect ratio of 1.46. At an overall section height of one inch, preliminary design calculations indicate that a reasonable fatigue strength could be expected if the face sheets were 0.012 inch in thickness. The section modulus I_{1-1}/d is a routine calculation.

As indicated in Section 2.5.1.1, it is not necessary to change the section modulus in precise proportion to the square of the scale ratios. The choice of modeled specimen dimensions is in fact quite large. How-
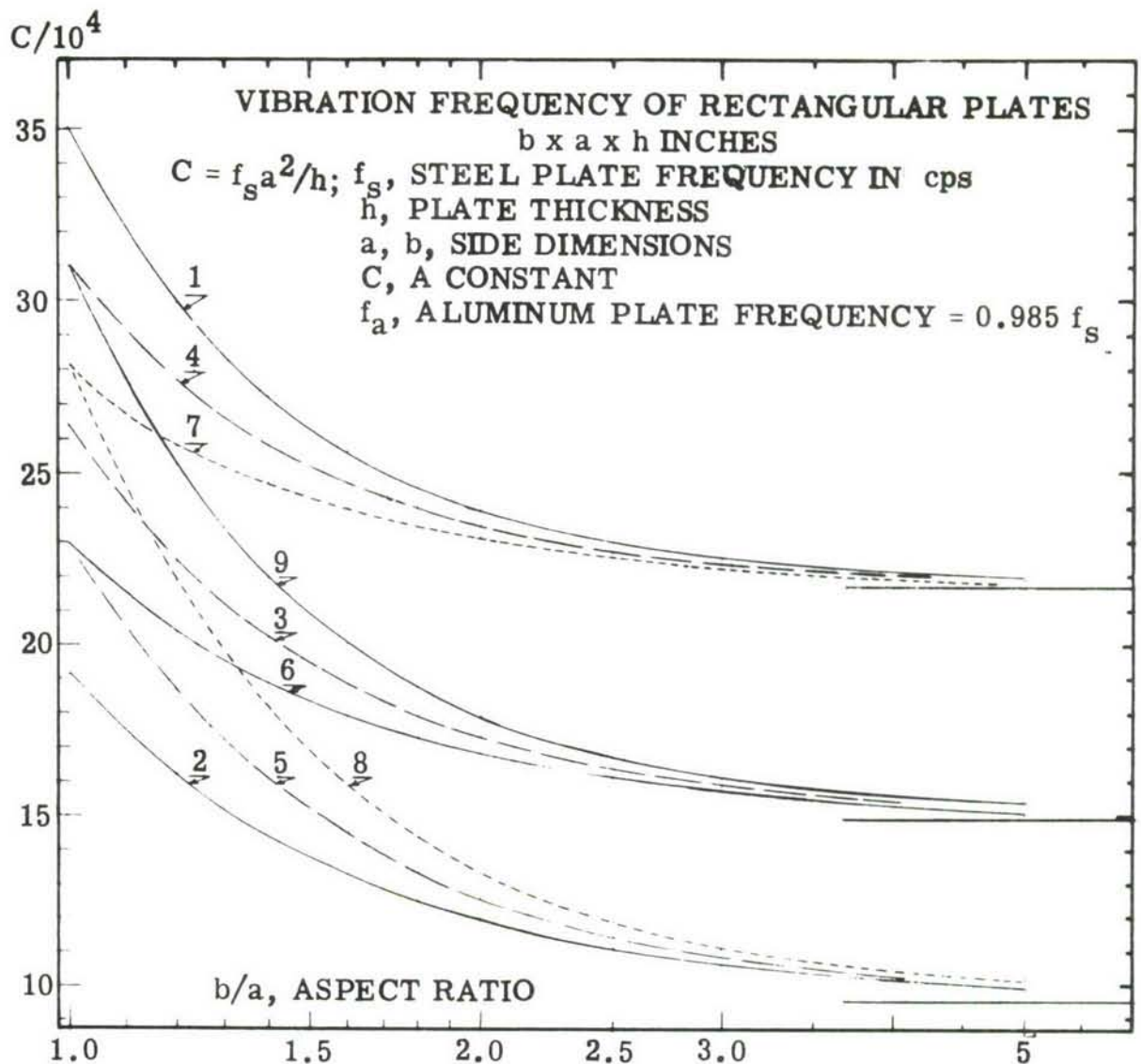
Boundary Conditions
1. All Sides Clamped
2. All Sides Simply Supported
3. Two Adjacent Sides Clamped
   Other Sides Supported
4. Three Sides Clamped, Short
   Side Supported
5. Three Sides Supported,
   Short Side Clamped

6. Three Sides Supported,
   Long Side Clamped
7. Two Long Sides Clamped,
   Opp. Short Sides Support
8. Two Short Sides Clamped,
   Opp. Long Sides Support
9. Three Sides Clamped,
   Long Side Supported

Figure 5. Frequency Constants for Rectangular Plates

12

ever, some convenient starting point can be realized by making the respective core depth at 5/8" and 3/8" for the present models. The same convenience cannot be extended in scaling face sheet thickness without incurring excessive fabrication costs.   Accordingly for the 5/8-size specimen, 0.012" face sheets were used again and 0.010" for the 3/8-size models. The overall panel dimensions were respectively 23-3/8 x 16-1/4 and 14-1/4 x 9-3/4 (unchanged after an original full size panel of 38 x 26 was modified to 41 x 28). A summary of these dimensions is shown in Table 1.

2.6.3   Bending Rigidity and Core Selections

As indicated in Appendix A, optimum achievement of complete bending rigidity in the face sheets is dependent on the provision of adequate core strength in resistance to the shear force V which is approximately a linear function of specimen size. An analysis on the strength of hexagonal honeycombs and core selections is given in Appendix B. The requirement can be simply stated that the density of core required is directly proportional to scale sizes. The lightest honeycomb density was, therefore, determined by the 3/8-size panel dimensions for which the shear stress safety dictated a density requirement of 6 lbs/ft^3. For full size and 5/8-size specimens, the cores used (as supplied) are the nearest proportionate in densities required. Other geometric characteristics are given in Table 1.

TABLE I   SUMMARY OF SPECIMEN DIMENSIONS

Nominal Size	Plate Dimensions		Face Sheet Thickness t, in.	Honeycomb Sandwich				Core Selection Al.5052-H39			
	b x a in.	Aspect Ratio		Core Depth c, in.	I_{1-1} in in.^{4} x 10^4	Rad. of Gyration k, in.	Ratio	Cell Size inch	Foil Size inch	Density lb/ft^3	Ratio
Full Scale	41 x 28	1.46	0.012 2024-T3 Clad	0.980	59.1	0.496	Ref.	1/8	.005	17.1	Ref.
5/8 Scale	23-3/4 x 16-1/4	1.46	0.012 2024-T3 Clad	0.625	24.4	0.319	0.642	1/8	.003	14.3	.84
3/8 Scale	14-1/4 x 9-3/4	1.46	0.010 2024-T3 Bare	0.375	7.41	0.193	0.390	1/4	.003	6.0	.35

14

2.7   Selection of Models for Curved Plates

The stiffening effect in curved plates is a highly complex phenomenon. A definition of this stiffening effect was one of the test objectives to be obtained before a proper fatigue correlation could be attempted through model tests. The selection of specimen sizes was, therefore, based on true models where all linear dimensions were scaled arbitrarily at these ratios: 1, 5/8 and 3/8. The net dimensions of each size are shown in Table II. The plates were rolled to the correct radii before mounting and clamped on all sides. It is assumed that such a specimen panel simulates very closely a curved plate element within a structural component unit confined in undistorted boundaries. Three specimens were fabricated in each case.

TABLE II   CURVED PANEL SPECIMEN DIMENSIONS, 2024 ALUMINUM

Nominal Specimen Size	Thickness of Plate inch	Plate Size, inch Net, between clamps			R, Radius of Curvature on side a, inch
		b	x	a	
Full	0.064	33	x	24	36
5/8	0.040	21	x	15	22-1/2
3/8	0.024	13	x	9	13-1/2

3.   EXPERIMENTAL OBSERVATIONS IN HONEYCOMB SANDWICH MODELING

3.1   Weight Analysis of Specimen Samples

In order to determine the weight correction required in the frequency equation, Eq. 2 (Section 2.5.1.2), an accurate weight analysis is needed in each case. For this purpose a beam section was carefully weighed after curing and compared to the total weight of separate elements and adhesive materials used. The actual weight, reduced to a unit area basis, becomes a significant loading factor in subsequent vibratory tests.

3.1.1 Illustrative Example

Full-size Honeycomb Sandwich Section; Beam size 1.5" width x 12" span (= 18 sq. in. in flat surface area)

2 Face Sheets, 0.012 thick each,   weight = 0.0432 lb.

Core (density as supplied, 17.1 lb/ft^3),   weight = 0.1775 lb.

Bonding Adhesives FM-1000,   weight = 0.0150 lb.

Calculated Total Weight = 0.2357 lb, or
107 grams

Measured Total Weight =   105 grams

The agreement is satisfactory. The unit weight of 0.0131 lb/in^2 per g (=0.2357/18) compares very favorably with other honeycomb sandwich constructions on record even though a heavy core is used here.

3.1.2 Frequency Correction Factors

From the weight analysis illustrated above, the frequency correction factor may be readily calculated. For the full size section, the correction is $\sqrt{0.0432/0.2357} = 0.428$. This correction factor has been taken as applicable to all beam or plate configurations of this scale (full size). Table III summarizes similar results for all specimens tested.

TABLE III   FREQUENCY CORRECTION FACTORS

Scale	W, Total Weight lb/in^2 per g	$\dfrac{\text{Weight of Face Sheets}}{\text{Total Weight}}$ = Ratio	Frequency Correction = $\sqrt{\text{Ratio}}$
Full Size = 1	.0131	0.183	0.428
5/8	.00841	0.285	0.534
3/8	.00413	0.485	0.696

3.2 Verification of Frequency Correction Factor - Use of Cantilever Beams

Referring again to the frequency equation (Eq. 2, Section 2.5.1.2), it is observed that the calculated frequency corrections of Table III can be verified experimentally if a simple configuration such as a cantilever beam is used for which the value of the lumped constant C is obtainable from many sources (References 9 and 13). However, two spans were employed in each of the three section sizes for added validity in test results. With three samples in each case, a good average is derived from a total of 18 beams. It is unnecessary to relate the modeling ratios to the spans which were chosen merely to change the response frequencies.

3.2.1 Cantilever Beam Tests

The clamped end of a cantilever beam was mounted on the table of an electro-mechanical vibrator whose frequency can be accurately controlled with its input force to the beam monitored by an accelerometer. A strain gage attached to the beam provided a direct reading of the dynamic stress, correctable to a maximum stress by the ratio (squared) of the span to the distance between the strain gage and the free end. The test arrangement is shown in Figure 6. Two methods are available to determine the resonance frequency which in this case would be the first mode. The vibratory frequency of the input force required to sustain a maximum response, or to keep the phase angle between these vectors at 90° would be one resonance indication. The second method is to pluck the beam gently and observe with an oscilloscope the timed frequency traces of the decaying strain gage signal.
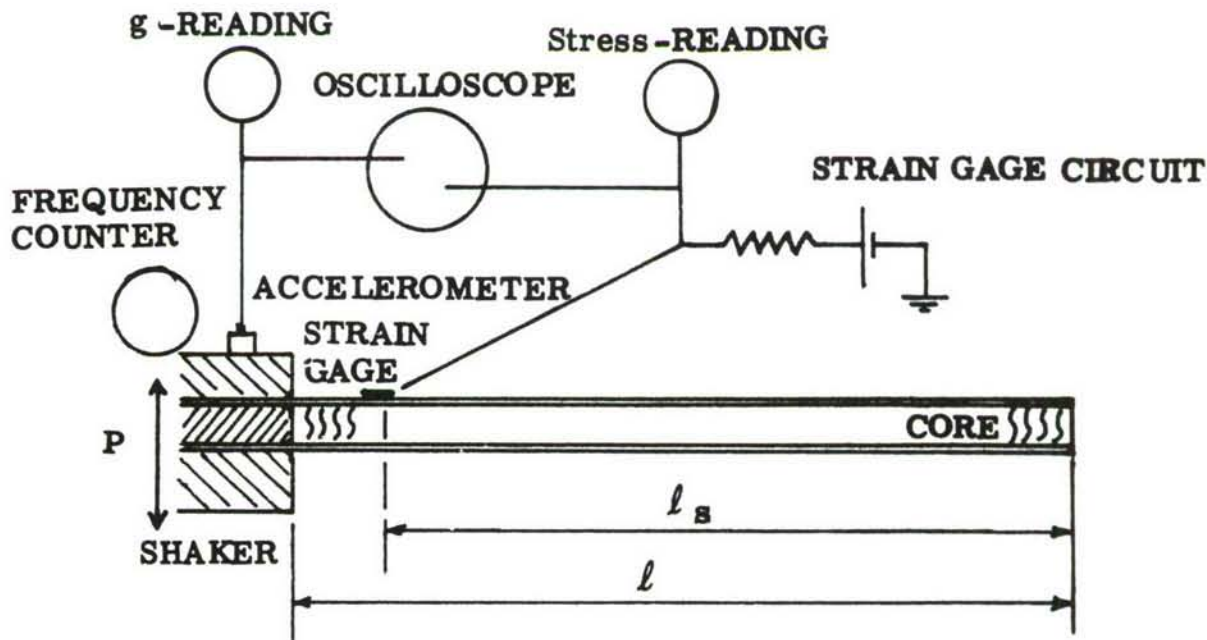
Figure 6. Test Arrangement for Cantilever Beams

3.2.2 Test Results

The results are given in Table IV. On the strength of the agreement between the observed frequencies and the calculated values, a complete verification of the deduced frequency correction factors is achieved. That the calculated frequencies are slightly lower than observed is a natural result of excluding core contribution in the moment of inertia. The differences are barely detectable and do justify the simplified approach. However, it is significant that the differences should occur in the direction cited and not reversed. In the latter case, the beam deformation deviates from pure bending depicted by Figure 54b and approaches the conditions of Figure 54a in Appendix A. This was observed in the case of longer spans with increased dynamic shear forces. As the shear stress exceeded a marginal limit, beam sections began to deviate from the idealized coplanar condition with a reduction in its true moment of inertia and to show a decrease in resonance frequency. The frequency test offers, therefore, a method to determine the maximum safe span which in full-sized sections, appears to be 16" cantilever. The same shear force is generated at longer spans in other end conditions. For all plate sizes selected, this shear force will be found to be well within the respective safe limit.

TABLE IV   RESONANCE FREQUENCY OF CANTILEVER BEAMS

Cantilever Beams		Resonance Frequency, cps			Damping Coefficient c/c_c	
Section Size	Span in.	Calcu-lated	Observed by Excitation	from decay curve	beam	Group Average
Full Size	16	92.9	95.3	95.3	0.0073	0.0063
			96.2	96.2	0.0064	
			90.1	91.0	0.0052	
	24	41.4	38.2	38.2	0.0118	0.0118
			40.9	40.4	X	
			41.5	40.8	X	
	12*	165.6	164.7	169.0	0.0042	0.0042
5/8	12	131.5	130.0	131.3	0.0057	0.0056
			135.0	135.5	0.0063	
			127.0	128.6	0.0050	
	16	73.7	75.4	75.6	0.0094	0.0093
			76.8	76.8	0.0097	
			75.8	76.4	0.0089	
3/8	10	149.9	151.2	151.6	0.0058	0.0058
			152.8	152.6	0.0048	
			150.8	151.8	0.0066	
	14	76.3	76.3	77.8	0.0085	0.0081
			77.8	77.6	0.0080	
			76.3	76.4	0.0079	

*Cut from 24" beams

3.3   Extension of Cantilever Beam Tests to Damping Correlations - A Size Factor

In ascertaining the resonance frequency by the second method discussed in the preceding section, the decay trace provides a conveniently concurrent basis for the calculation of the lumped system damping coefficient ratio, c/c_c. The results indicate that there is a significant variation between sizes. The simple assumption of unchanged damping coefficient ratios in dynamic modeling appears to be faulty and the lumped parameter represented in Equation 1 (Section 2.5.1.1) is, therefore, preferred at equalized dynamic stress. This requires that the damping coefficient ratio associated with each specimen, full-size or scaled models, be accurately determined before a lumped parameter is applied in fatigue tests. The following analysis correlates damping changes to model sizes or scales.

3.3.1   System Damping

A comprehensive and illustrative study on system damping by Kerr and Lazan is available in Reference 14 from which some necessary data were re-introduced here. The results using cantilever beams will be applied to clamped beams and plates, to illustrate the adaptability to panels of somewhat complicated sections.

Figure 7, replotted from Reference 14, shows the results of system damping D in terms of work done per cycle (in.lb/cycle) plotted against the maximum bending stress. Relevant mathematical equations for the damping work in a lumped but equivalent system are given in Reference 15 and are written below.

$$D = \int_0^{\frac{2\pi}{\omega_r}} P \frac{dy_o}{dt} \, dt = \pi P y_o \qquad (3)$$

$$\text{Also,} \quad D = \int_0^{\frac{2\pi}{\omega_r}} c \left\{ \frac{dy}{dt} \right\}^2 dt \; \propto \; \pi c \, y_{max}^2 \, \omega_r \qquad (4)$$

Where P represents the input force applied at the clamped end,

y_o the amplitude of P, a sinusoidal function

ω_r the resonance frequency,

c the damping coefficient

y the amplitude at any section, and

y_{max} the maximum amplitude at the free end.
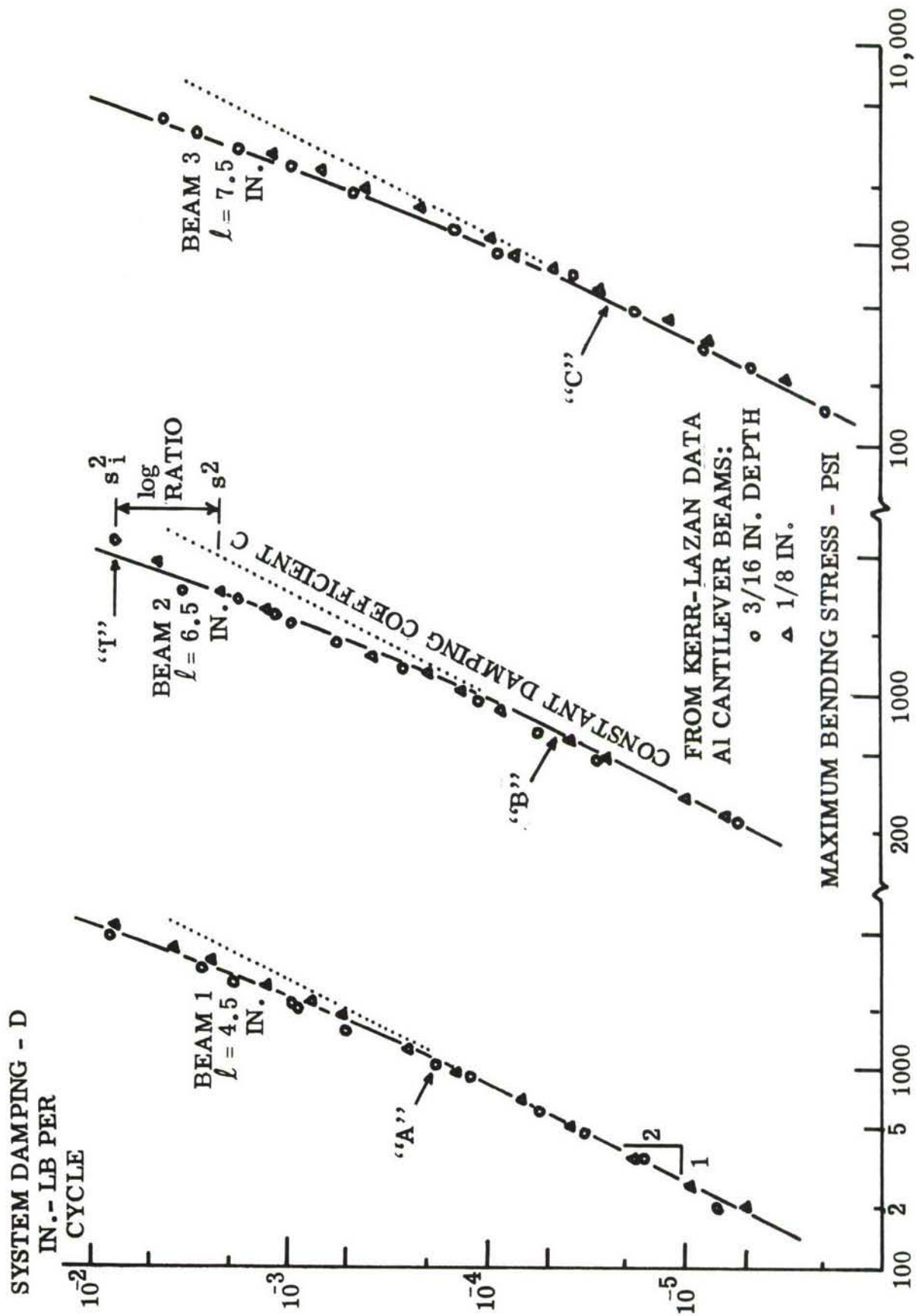
Figure 7. System Damping in Cantilever Beams

22

On the assumption that the maximum amplitude, or deflection, has a linear relationship to the maximum bending stress, it becomes evident that Equation 4 may be represented by a straight line with a slope of 2 as plotted in Figure 7. The data, therefore, indicate that (1) significant points A, B, and C may be located where the specified linear relationship between deflection and stress begins to weaken, and (2) below these points the damping coefficient c is constant but assumes increasing values as A, B, or C is exceeded. Furthermore, in replacing the amplitude (y_{max}) by stress (σ_{max}), a modification is introduced equivalent to dividing the abscissa dimensionally by h/ℓ^2. Thus the thickness difference is effectively removed from consideration, resulting in a single curve in each case with a common parameter c. This dimensional change is also reflected in the ordinate scale. Thus by comparing the damping work at points A, B, and C it will be found that the readings become exactly in inverse proportions to ℓ^4, a condition that is also indicated in Equation A5 Appendix A, where $(\lambda \ell)^4$ is a constant in a particular mode for a given beam or plate configuration. A normalization process is, therefore, feasible if the relative abscissa locations at A, B, and C could also be rationalized. This may be directly accomplished in a dimensional analysis of the critical damping coefficient c_c which, as expressed in Reference 15 and many other textbooks, is:

$$c_c = 2\sqrt{\frac{kW}{g}} \qquad (5)$$

where k, the spring constant, carries the unit of force/displacement for a lumped elastic system of total weight W. Inasmuch as transverse deflection due to bending only is considered, the characteristic dimension of k is essentially $w\ell$ EI/$w\ell$ or EI/ℓ^3. Because c and c_c must have the same dimensions and disregarding common constants for the beams concerned, the parameter c governing the abscissa positions of A, B, or C in Figure 7 varies therefore as $(\ell)^{+3/2}$ which the observed data satisfactorily confirmed. For higher stresses such as at point I shown in Figure 7, the increased damping coefficient c_I can be referred to the dotted extension of the linear base line through point "B" and calculated by proportionate increment in D as indicated in the figure. A more significant indication is found in the fact that upon normalization, all data points presented in Figure 7 merge into one curve as shown in Figure 8. Moreover, additional data given by Kerr and Lazan in the same reference for an assortment of beam sections of sandwich construction obeyed the same normalized curve shown in Figure 9, differing only in scales and specific readings. The general shape is therefore accepted in subsequent analysis and extension of linear conditions will be shown as dotted lines for consistency. From the combined location of points such as A, B, or C, a correlation of damping for different sections and effective spans is obtained.

3.3.2 Damping Correlation Tests

In order to apply the Kerr-Lazan curve to current test results, a change in scale expressions is necessary. While retaining the stress expression in psi, but changing the system damping to force input in unit of g's (which is a variable standard to be defined by the system weight
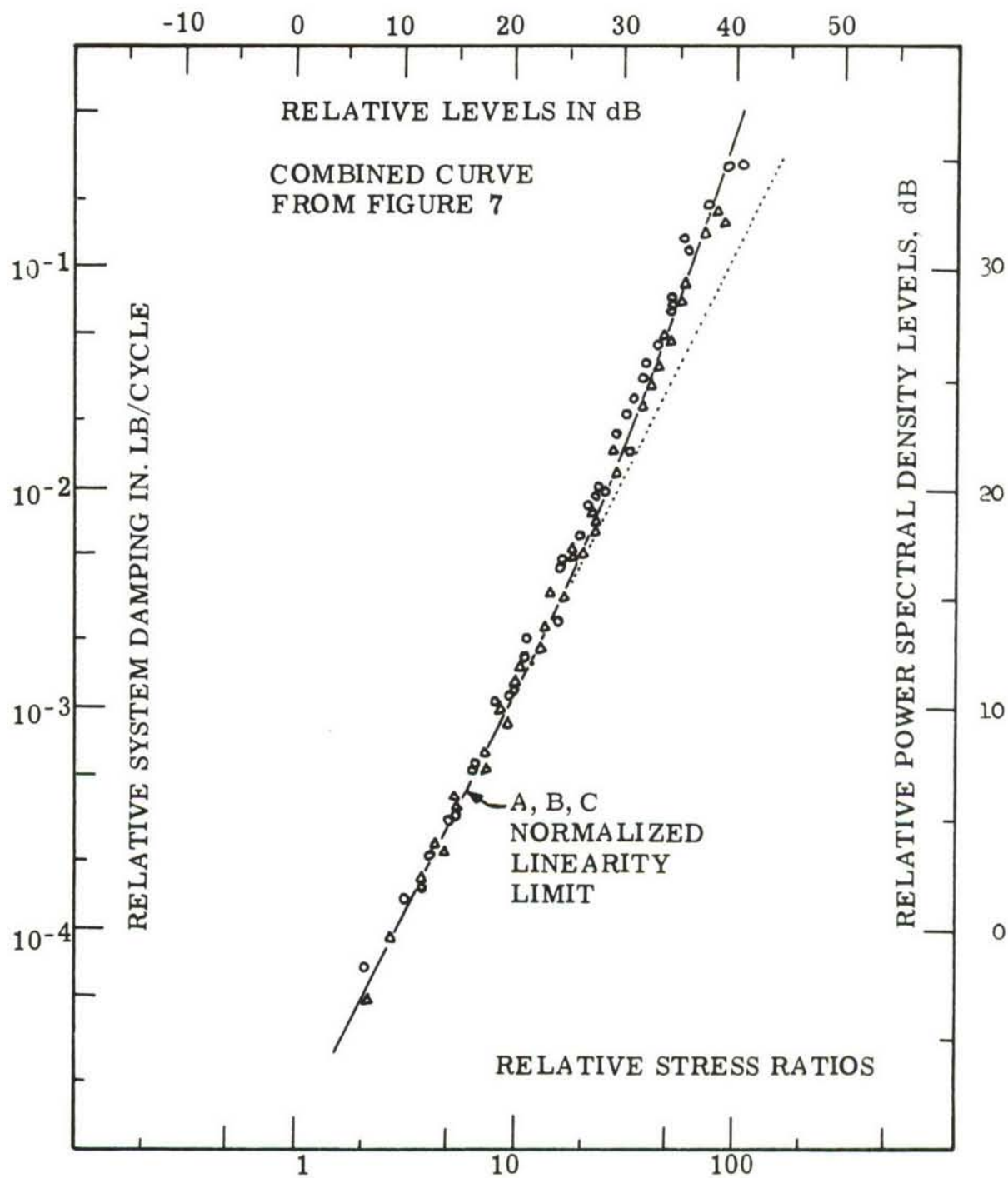
Figure 8. Total Damping in Cantilever Beams

RELATIVE STRESS LEVEL, **dB**

FROM DATA BY KERR-LAZAN, SEE REFERENCE 14:
ASSORTED CANTILEVER BEAMS IN SAME SPAN
ALL AL HONEYCOMB SANDWICH   ○ △ □
AL FACE SHEETS WITH PAPER CORE ▽
AL FACE SHEETS WITH FIBERGLASS CORE ■
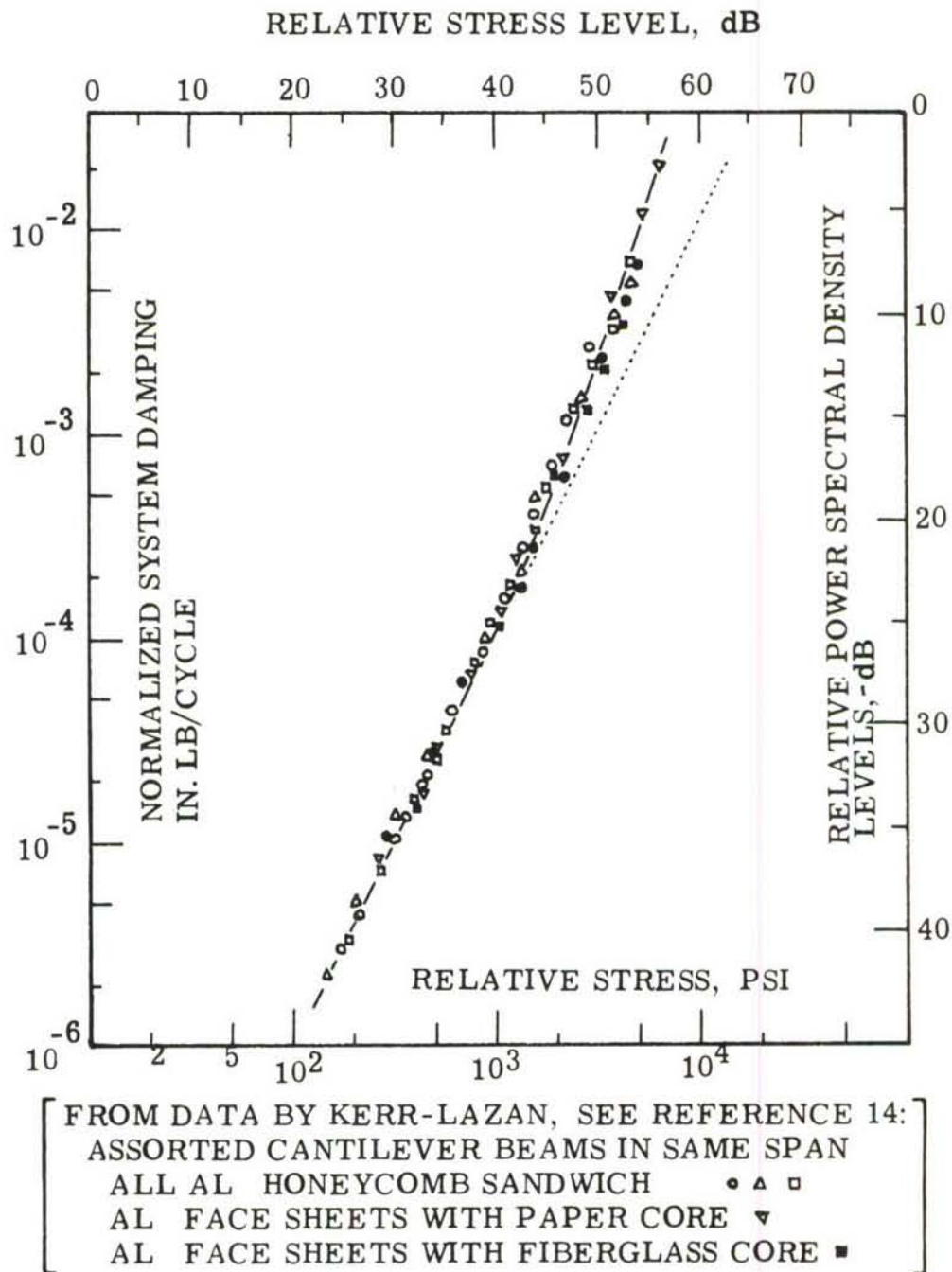
Figure 9. Total Damping in Cantilever Beams

25

per g in each beam) it must be realized that essentially the system damping is being recorded on a unit-displacement basis because the work done is a product of force and displacement. Consequently, the stress correlation in current tests to locate points such as A or B must be reckoned after correction to the same basis of unit displacement. Representative test results as recorded are given in Figure 10 for cantilever beams in the 5/8 size honeycomb sandwich sections at 12" and 16" spans, correlation points are designated as A and B, damping coefficients ratios having been established in decay traces at 0.0056 and 0.0094 respectively.

Observe that following the changes of c introduced in 3.3.1, the damping coefficient ratios 0.0056:0.0094 should be in the same proportion as $(12:16)^{+3/2}$. A close agreement is obtained numerically. For stress correlation of points A and B, it is necessary to convert the respective readings at 4700 and 9000 psi to a unit displacement basis.

The cross-sections being the same, the comparative ratio becomes 4700: $(9000)(12/16)^4$ or 4700:2860 which is also in reasonable agreement numerically with $(12:16)^{-3/2}$. For input correlation, the original factor of l^4 is now effectively cancelled, leaving a direct comparison of total input force which is proportional to the span and actual damping coefficient ratio, or $(l)(c/c_c)$. Thus for the experimental input readings 0.55 and 1.2 in Figure 10, the ratio 0.55:1.2 is found to be quite close to $(12)(0.0056)$: $(16)(0.0094)$. In cantilever beam tests, therefore, a reliable method is available to correlate damping coefficient ratios to size changes.

3.4   Extension of Cantilever Beam Tests to Fatigue Life Observation

3.4.1   Distinctions in Failure Location and Correlation to Sonic Fatigue Strength

Besides verifying the frequency correction factors discussed in Section 3.2, a clear indication is found in the results observed that (1) adequate core rigidity prevailed in all sandwich specimens fabricated and (2) in confining ultimate failures to the face sheets, a uniform tensile stress was obtained corresponding to the material strength with an appropriate stress concentration factor K_t. Without exception, not only were the tensile fractures confined to the locations of maximum bending moment at or within, the clamped section as shown in Figure 11, but the failure stress averaged consistently 30,000 psi (peak) within a range of approximately 20%. Although a failure becomes noticeable only after a time duration has accumulated in the tests, it is the short term fatigue which compares very well with the sonic fatigue strength shown in Figure 4 for simple aluminum plates such as a face sheet. Therefore, insofar as the strength is concerned, there is little difference as a result of the nature of the loading imposed on the material. The stress, as lumped in Equation 1 is indeed the criterion - providing adequate core strength is provided so that failure occurs in the face sheet and not in the core.
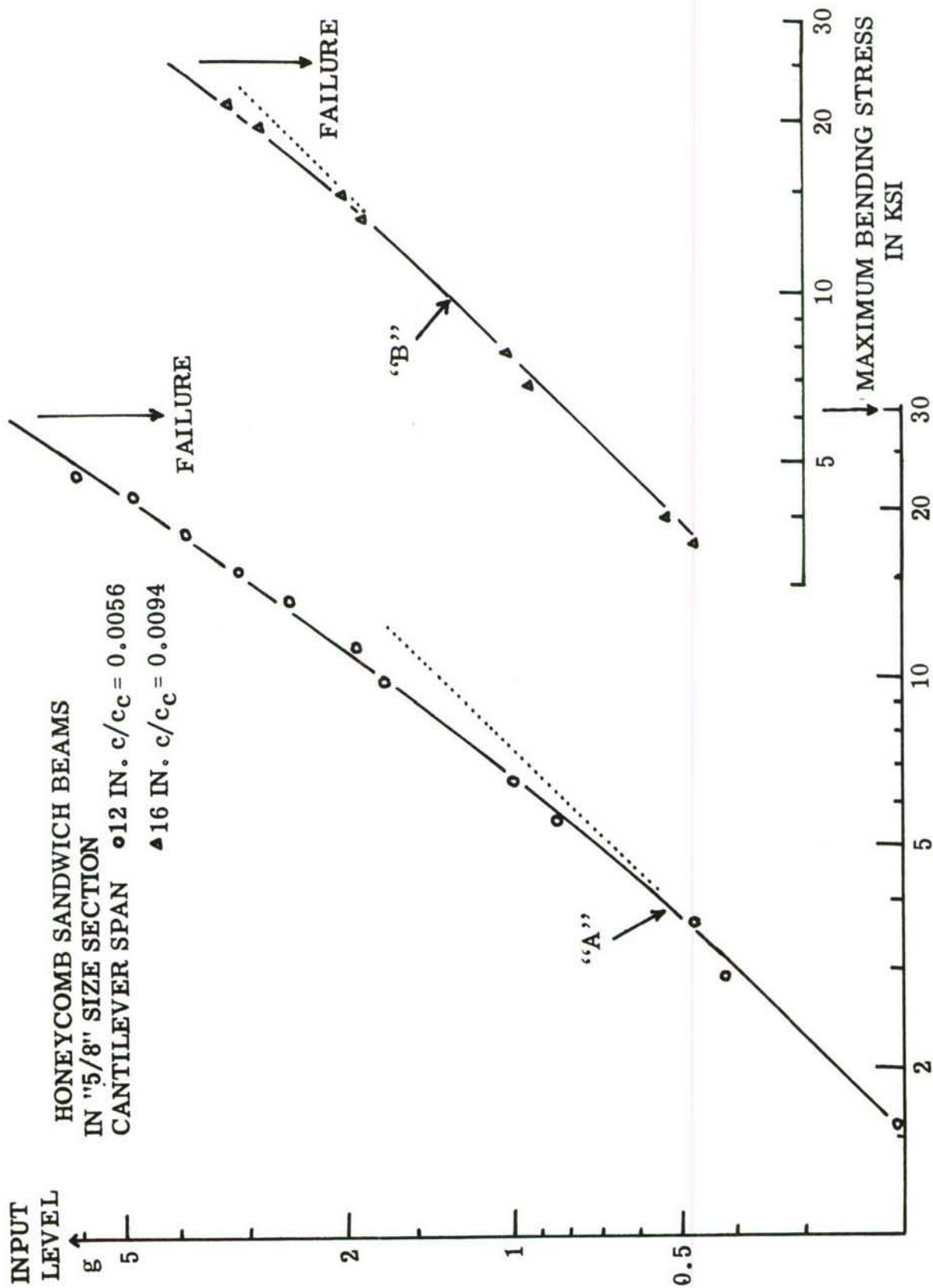
Figure 10. Vibratory Stress in Cantilever Beams

CANTILEVER SPAN ←-- --|-- --→ CLAMPED END

↑→ CLAMPED END
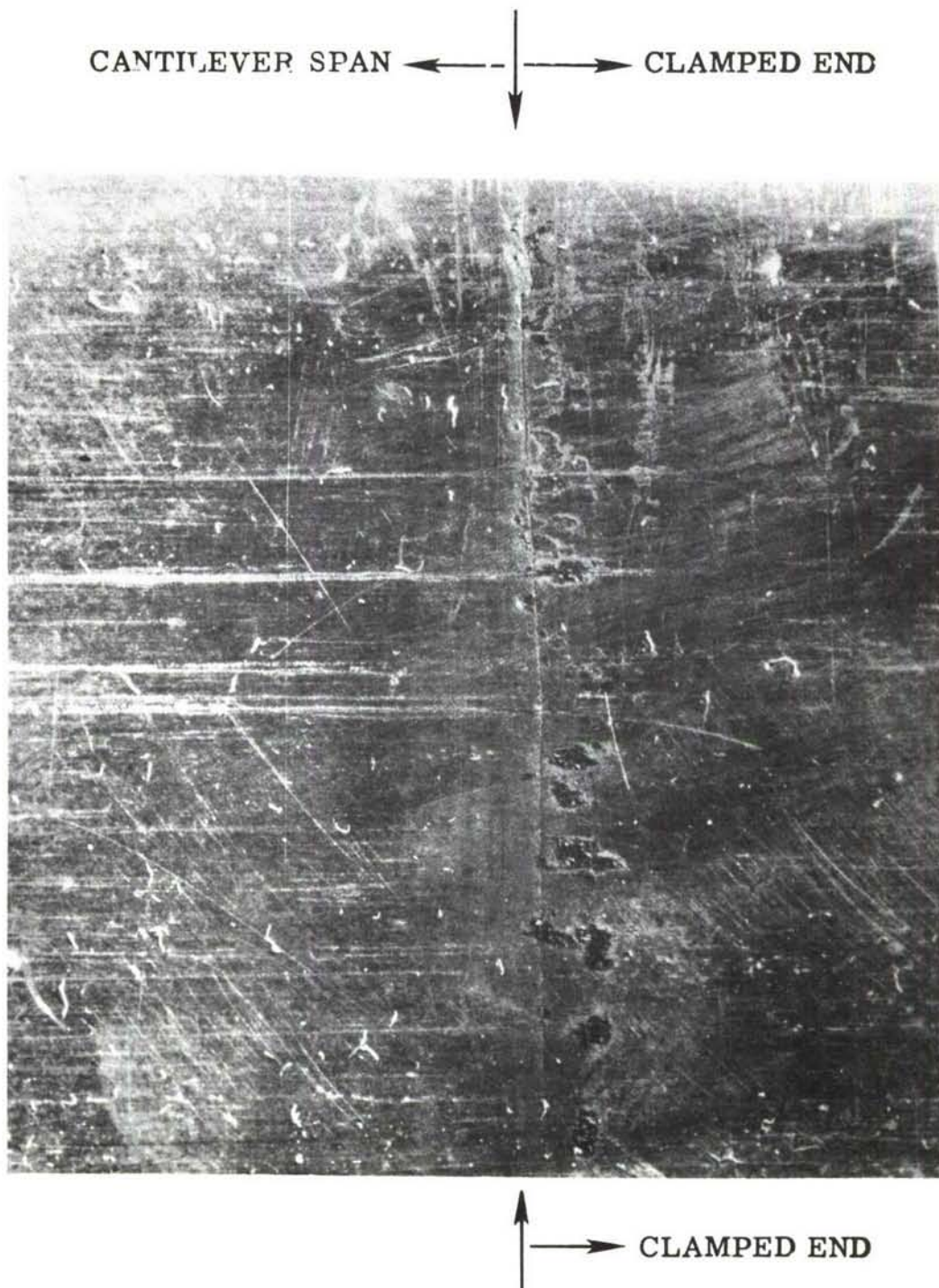
Figure 11.   Face Sheet Fracture in Honeycomb Section

3.4.2   Illustrated Cases of Inadequate Core Stength in Sandwich
        Structures

In addition to the stress criterion of the previous paragraph, a
frequency significance of providing adequate core strength in sandwich
structures can also be experimentally proven. A honeycomb sandwich beam
of the following proportion with a light core was used, Figure 12.

              Face Sheet, aluminum; thickness 0.020"
              Core, aluminum; density 3 lb/ft^3
              Total Weight; .006 lb/in^2
              Cantilever Span 10.5"; Arrangement shown in Figure 12a

The calculated resonance frequency is 222 cps based on a correction
factor of 0.834. The inadequacy of core strength is reflected in the
actual resonance observed at 191.5 cps, and also in the final failure con-
ditions shown in Figure 13. Similar failures of a brazed steel honeycomb
panel also with a light core, subjected to high intensity acoustical loading,
are shown in Figure 14 for comparison. Indeed a modeling of failures between
dissimilar structures is demonstrated.   The significance indicated is
that inadequacy in core rigidity is not permissible in sound sandwich
structures.

3.4.3   Significant Differences in Honeycomb Sandwich Failures

In the case illustrated in the preceding section, based on the peak
loading observed immediately before the failure was initiated, the calculated
maximum bending stress in the face sheets is 8740 psi. The potential strength
is not, therefore, fully utilized. More significant, however, is the fact
that the ultimate load was not sustainable as it continued to decrease sharply
before a failure could be identified as such. The decrease in load is attrib-
uted to a rapid deterioration of damping for which a change from 0.0096 to
0.0078 was observed well in advance of any indication of the impending
failure. The nature of a core failure appears to be inherently catastrophic.

In contrast to the above, by confining failures to the face sheet in a
sound design, more bending resistance must be temporarily carried by the
core for increased system damping. This is indicated in Figure 15 for a
current beam specimen where the top curve is a normal decay trace and the
lower curve is derived from the same strain gage after the occurrence of a
failure. There is a slight change in frequency but the damping coefficient
ratio is raised many times over from 0.0079 to 0.12. Although such an
increment cannot be reckoned as a general rule, the fact remains that a face
sheet failure will not become catastrophic and allows ample time for inspection
and repair. A design standard based on full utilization of face sheet
strength seems to be the proper approach. In actual applications, investiga-
tion of core strength should be conducted for each of its two lateral axes.
In this report, transverse bending along the ribbon direction only has been
investigated.
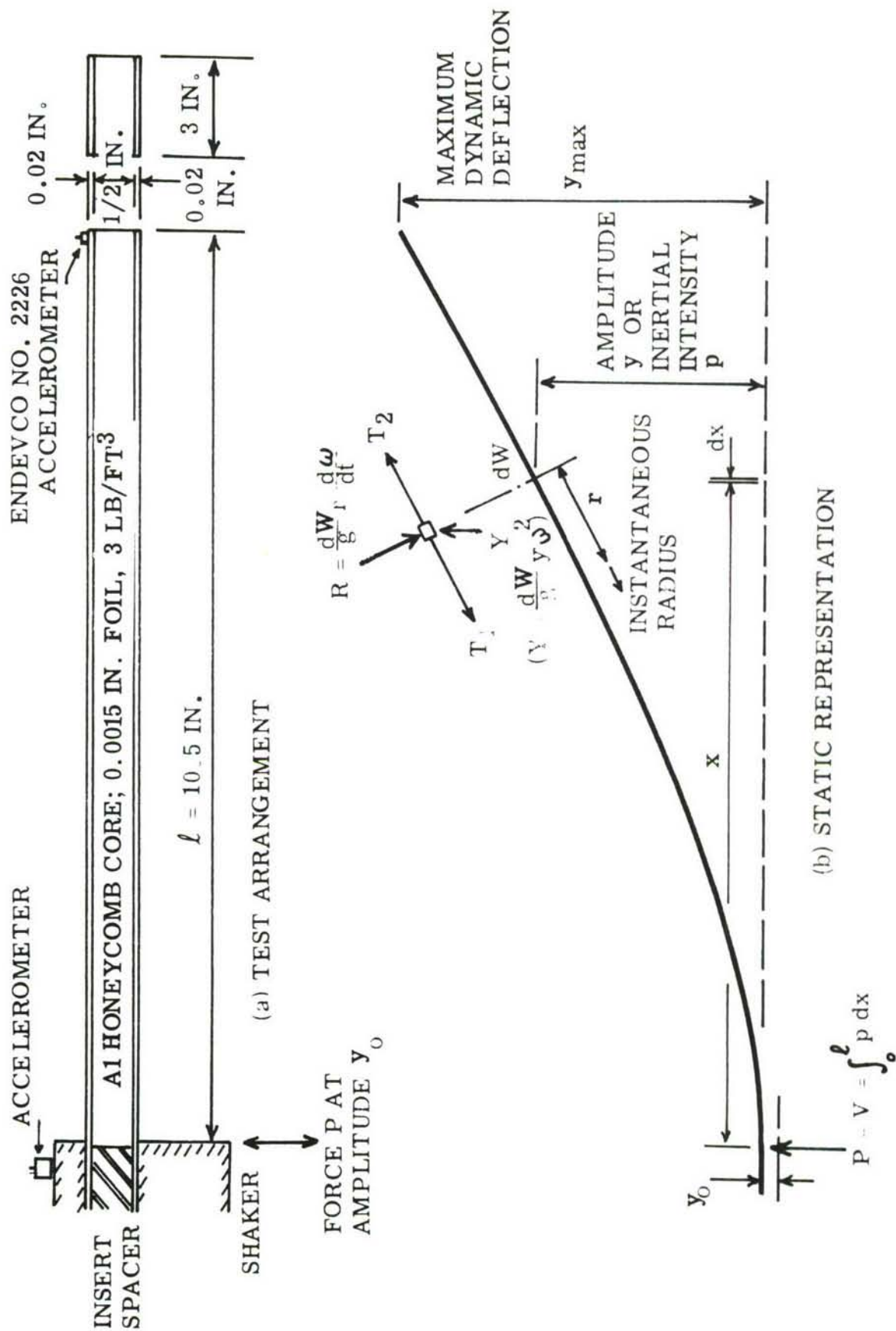
Figure 12. Cantilever Beam Test Arrangement and Static Representation

END INSERT
USED AS
SPACER

FRACTURES IN MIDSECTION
OF CORE EXTENDING OVER
ENTIRE WIDTH OF BEAM

VIEW AFTER REMOVAL OF END INSERT

Figure 13. Core Failure In Honeycomb Section

31

SQUARE PLATE AT 157 dB, NAA TEST DATA DL60-108
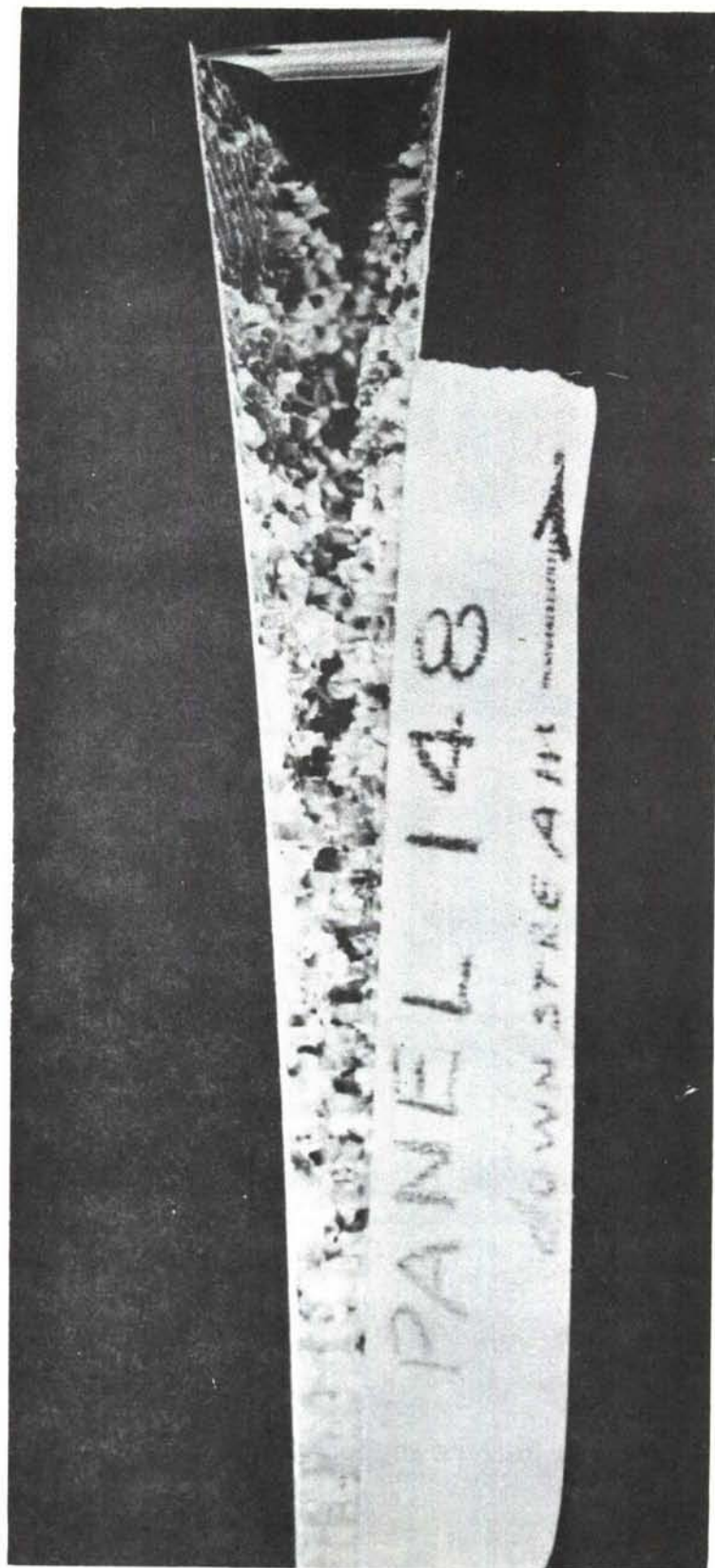
Figure 14. Core Failure In Brazed Steel Honeycomb Panel

(A)

(B)
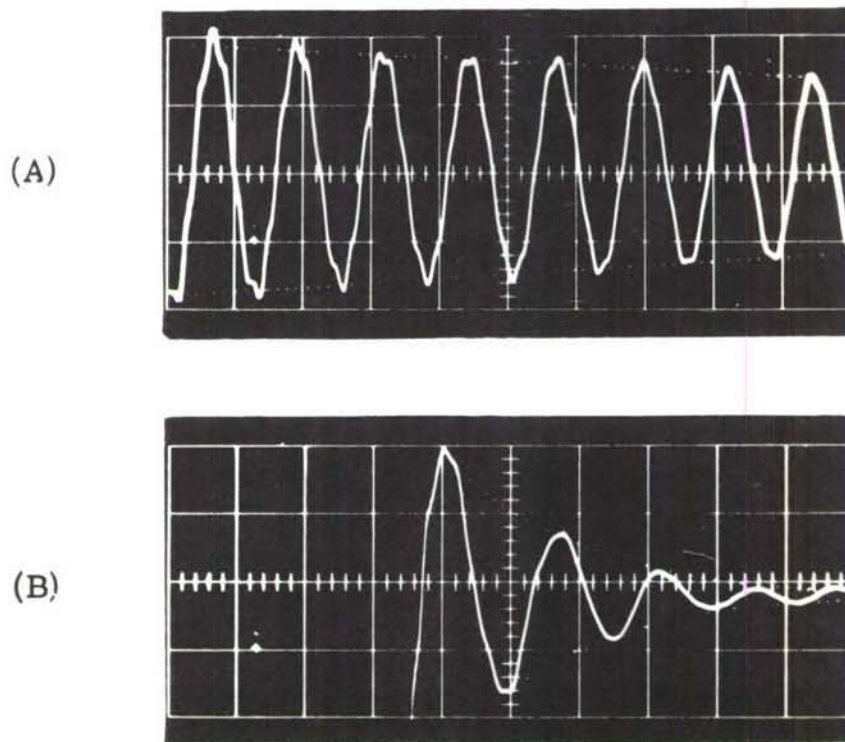
(A) NORMAL DECAY TRACE, - CANTILEVER BEAM
    76.3 **cps**, $c/c_c = 0.0079$

(B) DECAY TRACE FROM SAME SOURCE AFTER FACE
    SHEET FRACTURE
    67.2 **cps**, $c/c_c = 0.120$

Figure 15. Sample Excursion Traces

33

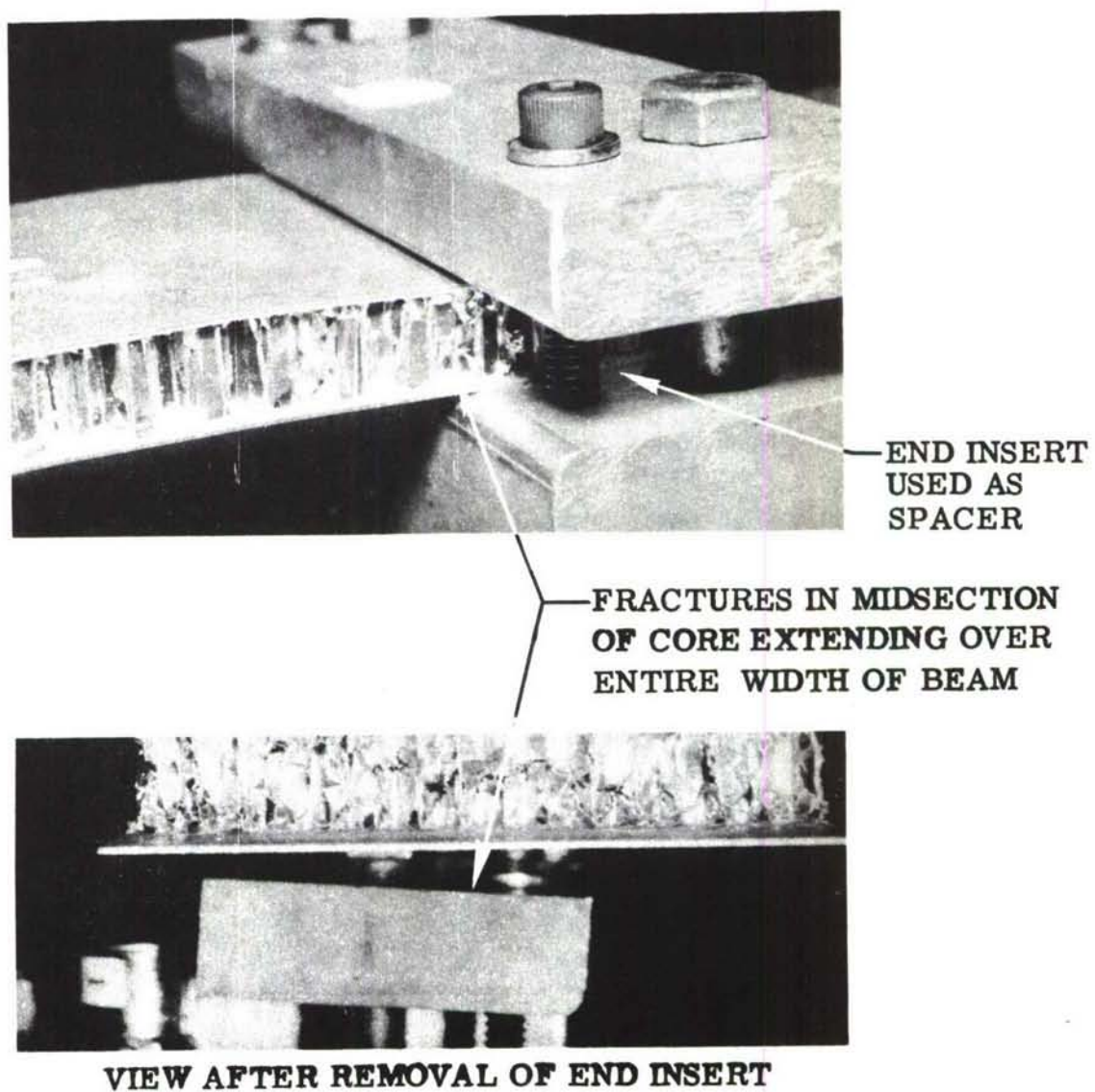## 3.5 Crack Propagation and Resonance Frequency in Fatigue Failure

The consistency in the behavior of all eighteen cantilever beams is summarized in Figure 16 where the frequency change of each beam is plotted versus the input levels. The frequency change is expressed on a percentage basis of the normal beam frequency. In the resultant curve there seems to be a significant point where the crack in a face sheet may be, in fact, initiated. As the crack propagates beyond this point, the change in resonance frequency occurs at a different rate. This point is designated in Figure 16 as the knee, a mere 1 to 1-1/2 percentage below the normal resonance. It is noteworthy that a recommendation of the same percentage change in frequency as a safe limit is contained in Reference 14 based on different test procedures. Of primary importance is the indication in Figure 16 that a fatigue failure is completed within an intensity range of input forces equivalent to a level change of 5 dB only, reckoned from the initial crack at the 'knee' in the failure history curve to an ultimate realization of the accomplished fracture. Therefore, it appears quite necessary to rely on cantilever beam tests to establish an accurate reference of the fatigue strength. Furthermore, the composite failure history curve also sustains the uniformity in damping correlation obtained by merging all response points such as 'A', 'B', 'C', Figure 7, at one location as indicated in Figures 8 or 9.

Similar to the established damping criterion, the input force on a unit displacement basis is normalized upon the displacement parameter $w \ell^4/I$ modified by $(c/c_c)^{-1}$ due to the dynamic amplification involved. The joint parameter becomes $w \ell^4/Ak^2 (c/c_c)$ as numerically illustrated in Table V. In Figure 16, proper scales of the input levels apply to respective sections at indicated cantilever spans. Table V shows the calculated scale ratios required for corresponding failure curves to merge together. The data were actually fitted at slightly different ratios prior to the above deduction. For beams of the same sections w and A will be common. By substituting ℓ^3 by its proportionate quantity $(c/c_c)^2$ introduced in Section 3.3.1, the input parameter is reducible to $(\ell) (c/c_c)$ presented in Section 3.3.2. Figure 16 includes data from beams other than the indicated spans but corrected by the required parametric ratio, c/c_c's as tabulated in Table IV.

3.6 Nonlinear Response

3.6.1 Similarity of Cantilever Beams to Other Elastic Units

On the question of nonlinear response in an elastic plate element subjected to transverse bending variations, theoretical analysis is referred to References 15, 16, 17, and 18 and to References 19, 20, and 21 for experimental investigations. The presence of an induced axial force is generally attributed to be the basic cause of nonlinearity. In a cantilever beam such a force does not appear to exist because one end is always free while the other end only is constrained. Nevertheless, it can be shown that there are induced stresses of varying magnitudes at different beam sections which influence the bending stresses and promote a nonlinear relationship to changes in transverse loading intensities. As sketched in Figure 12b for
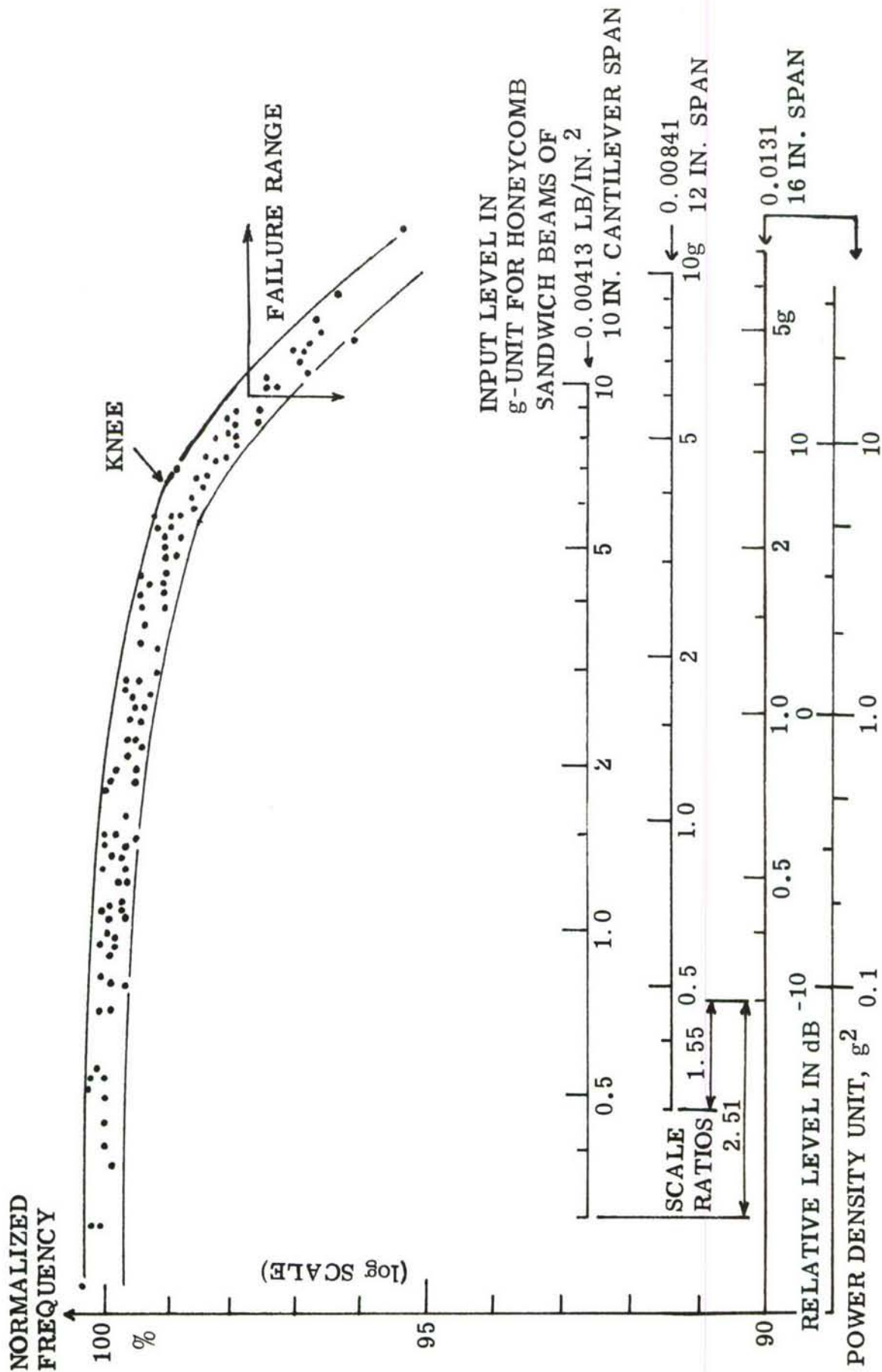
Figure 16. Frequency Change and Fatigue Failure in Cantilever Beams

TABLE V INPUT PARAMETER IN CANTILEVER BEAMS

Section Size	Input Parameters					Lumped Parameter $w\ell^4/Ak \cdot c/c_c$ × 10^{-6}	Relative Ratio	
	w lb/in	ℓ in.	k in.	A in.²	c/c_c		Calculated	Observed (Fig.16)
Full Size	0.01965	16	0.496	0.036	0.0063	23.1	1.00	Reference
5/8	0.00841	12	0.319	0.024	0.0056	12.3	1.87	1.55
3/8	0.00413	10	0.193	0.020	0.0058	8.6	2.67	2.41

the cantilever beam section dx, weight dW, at instantaneous amplitude y, the dynamic forces acting on the rigid body system may be represented by vectors T_1 and T_2, the resultants of uniform sectional stresses, and vectors Y and R the inertial vectors for converting the system to a static balance such that vectorially $T_2 + T_1 + R = Y$. It is observed that T_1 is always greater than T_2 and becomes a maximum at the clamped end. The induced stress modifies the bending displacement y and causes a nonlinear change in bending stress much in the same manner as an induced stress at constant magnitude (under a given load) influences nonlinear response of beams and plates. Due to the varying nature of T_1, which is proportional in magnitude to the displacement y, the characteristic elastic shape in cantilever beams remains, however, unaffected dynamically and a constant resonance frequency is maintained.

3.6.2   Experimental Data for a Clamped Clamped Beam, Damping Characteristics

In contrast to a cantilever beam, the dynamic elastic shape will be greatly modified in a clamped clamped beam if the axial tensile stress induced by forces similar to T_1 approaches a magnitude that can no longer be neglected in comparison to the vibratory bending stress. An example of such a case can be found in Reference 20 from which the pertinent data are replotted in Figure 17 on the same scales as Figure 9 for direct comparison of the observed nonlinear changes attributable to variations in the damping coefficient c. The increase in damping can also be investigated from the two factors defining the damping work done. Representing the displacement factor, the bending deflection coefficient ϕ_2 is given in Reference 22 as a variable dependent of u, a complex function of the induced axial tensile stress. Representing the forcing intensity, an equivalent bending stress coefficient ψ_2 may be used. Both coefficients are plotted in Figure 18a and equal to unity in linear cases when $u = 0$. As nonlinearity becomes more pronounced, the coefficients ψ_2 and ϕ_2 assume divergent values. Because the damping work can also be expressed as the force per unit displacement, in the ratio of coefficients ψ_2 over ϕ_2, a change in damping coefficient c is inherently indicated which is given in Figure 18b. In the nonlinear response of Figure 17, the function u reaches a probable high of 6. From Figure 18, this would correspond to a doubling of coefficient c or c/c_c for a reduction of 6 dB in dynamic amplification ratio. In addition to a change in damping, there is also a simultaneous change in elastic shape and a resultant increase in resonance frequency in nonlinear response which must be taken into further consideration.

3.6.3   Resonance Frequency and Amplified Amplitude or Maximum Dynamic Stress Variations

In Section 3.3.1, Equation 3 may be interpreted as an expression of constancy in the ratio D/y_0 for a given input force P regardless of response nonlinearity in the amplified amplitude y_{max}. By multiplying both sides of Equation 4 by ω_r, an expression of damping power is obtained, $D\omega_r \propto \pi c\, y_{max}^2\, \omega_r^2$. Rearranging and extracting D/y_{max} as a related constant if c is unchanged,
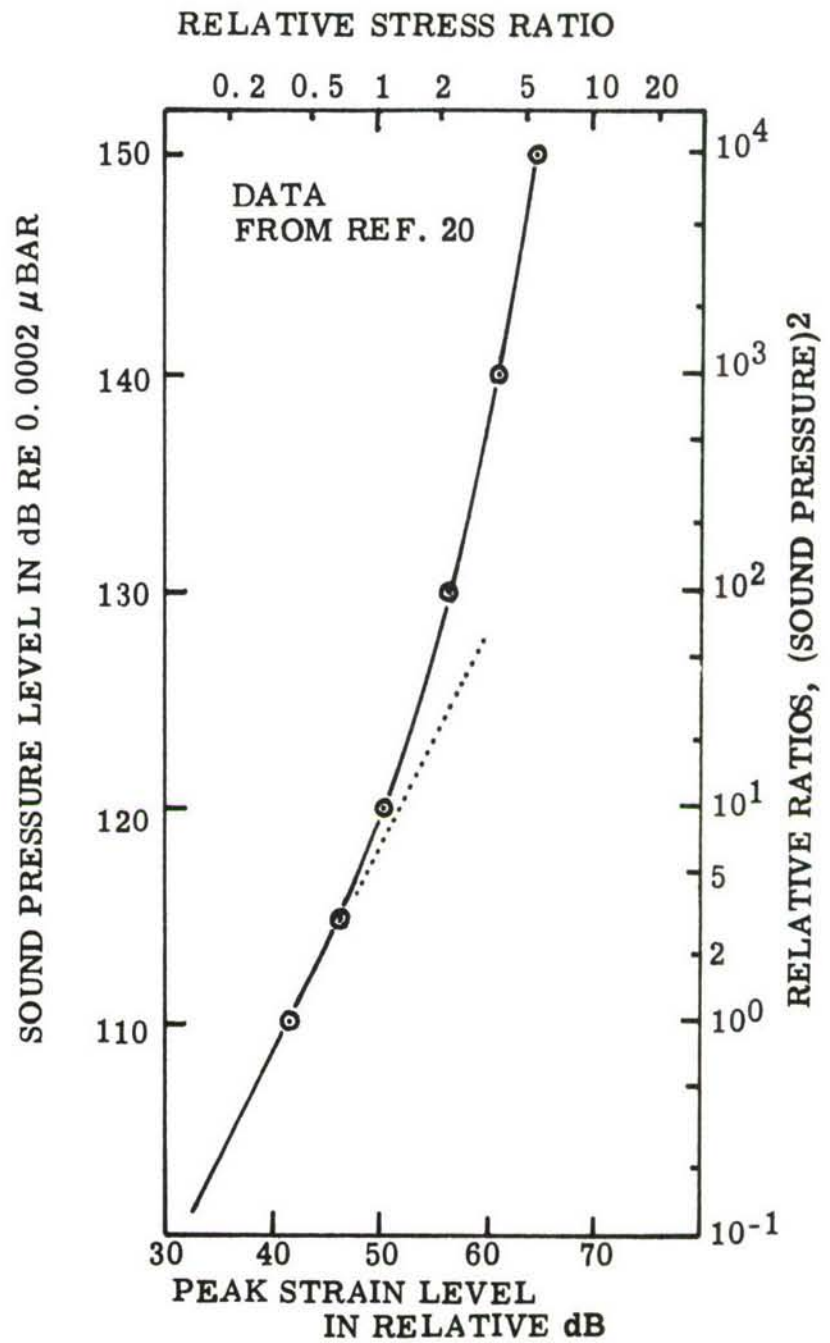
Figure 17. Flexural Response to Acoustical Forces on Beams
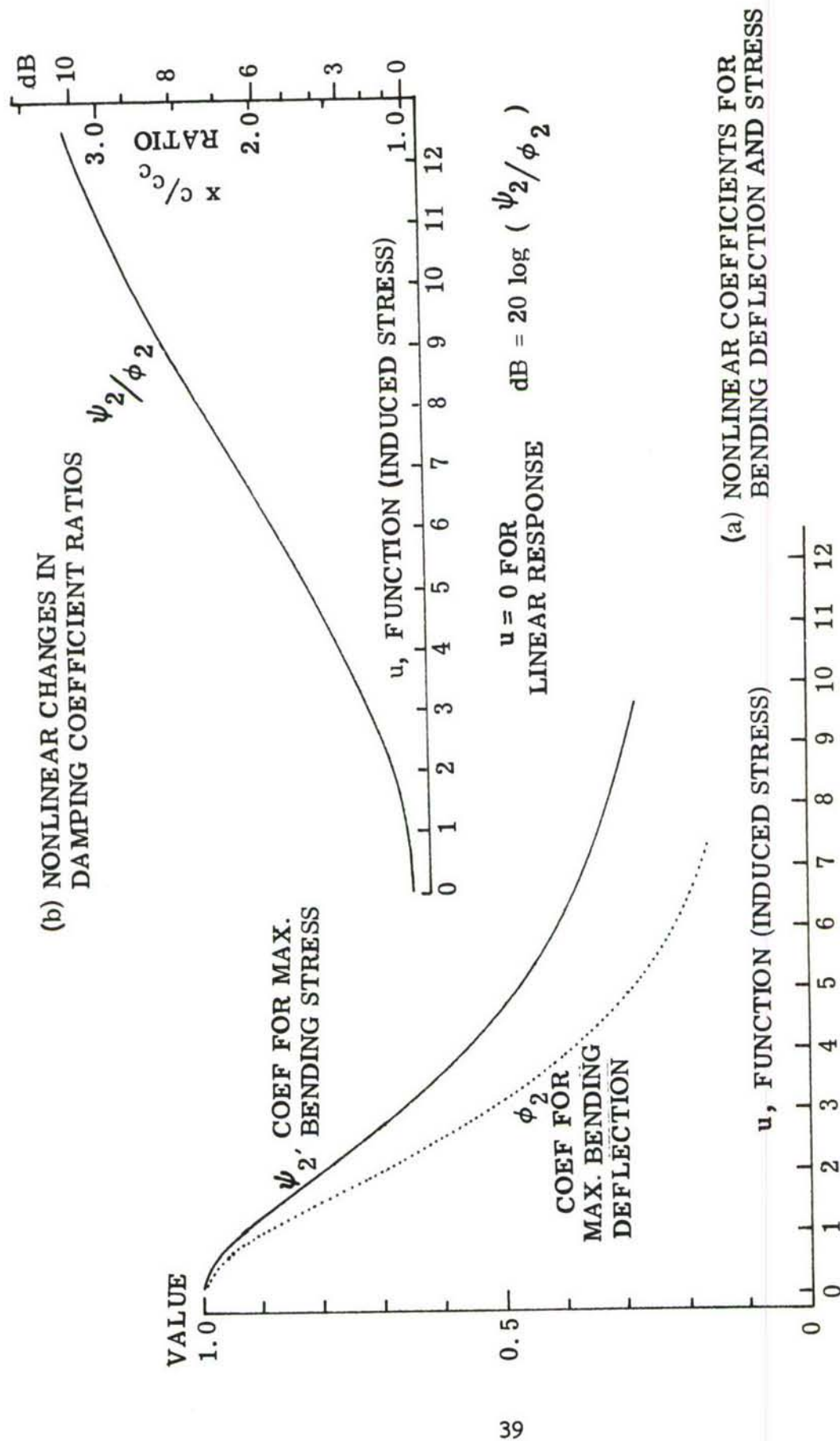
Figure 18. Damping Factors in Nonlinear Response of Clamped Clamped Beams

39

$$P\omega_r \propto y_{max} \omega_r^2 \qquad (6)$$

it is, therefore, observed that for a given damping coefficient c, the input power is proportional to $y_{max} \omega_r^2$. In such a fictitious nonlinear response at frequency ω, the input power will be $P'\omega$ which must be equal to $P\omega$, or $y\omega^2$ where ω is the nonlinear resonance frequency, P' the nonlinear input force and y the maximum nonlinear response amplitude. The generalized solution is therefore -

$$y\omega^2 = \text{Constant, or}$$

$$\sigma\omega^2 = \text{Constant where } \sigma \text{ is the maximum dynamic stress.}$$

A graphical representation of the above equality is given in Figure 19 (from Reference 19) where O_s is an amplitude or stress corresponding to y_{max}, and O'_r the nonlinear amplitude or stress corresponding to y at frequency ω. The line joining O_s and O'_r will be dictated by the numerical relationship $y\omega^2$ that requires a 4 to 1 amplitude change or -12 dB when $\omega = 2\omega_r$. In conjunction with such necessary amplitude change, an apparent change in spring constant is indicated for which a familiar modification in the forcing function attributed to Duffing is -

$$P = ay + by^3, \text{ where a and b are two constants.}$$

With this modification, Chu and Herrmann (Reference 23) calculated the frequency changes which can be plotted as the accented curve in Figure 19, P varying sinusoidally. Sound pressure levels corresponding to P may be indicated along the ordinate scale at ω_r.

The increase in damping coefficient ratio presented in Section 3.6.2 must now be incorporated. An illustrative example is provided in Figure 20, utilizing data from Reference 20. The necessary correction is resolved as the tabulated change in damping obtained from a reduction of amplification ratio or a relative decrease in dB of sound pressure levels for constant damping along the 12 dB per octave rule indicated above. These differences may be compared with the expected reductions in amplification ratios, converted to relative levels in dB in figure 18b.

3.6.4   Sinusoidal Versus Random Excitation Tests

In Figure 19, the amplitude at the point O'_r drops very sharply to the linear resonance curve that peaked at point O_s. If the frequency is then reduced from ω to Ω, a sudden increase of amplitude to point O_r will be
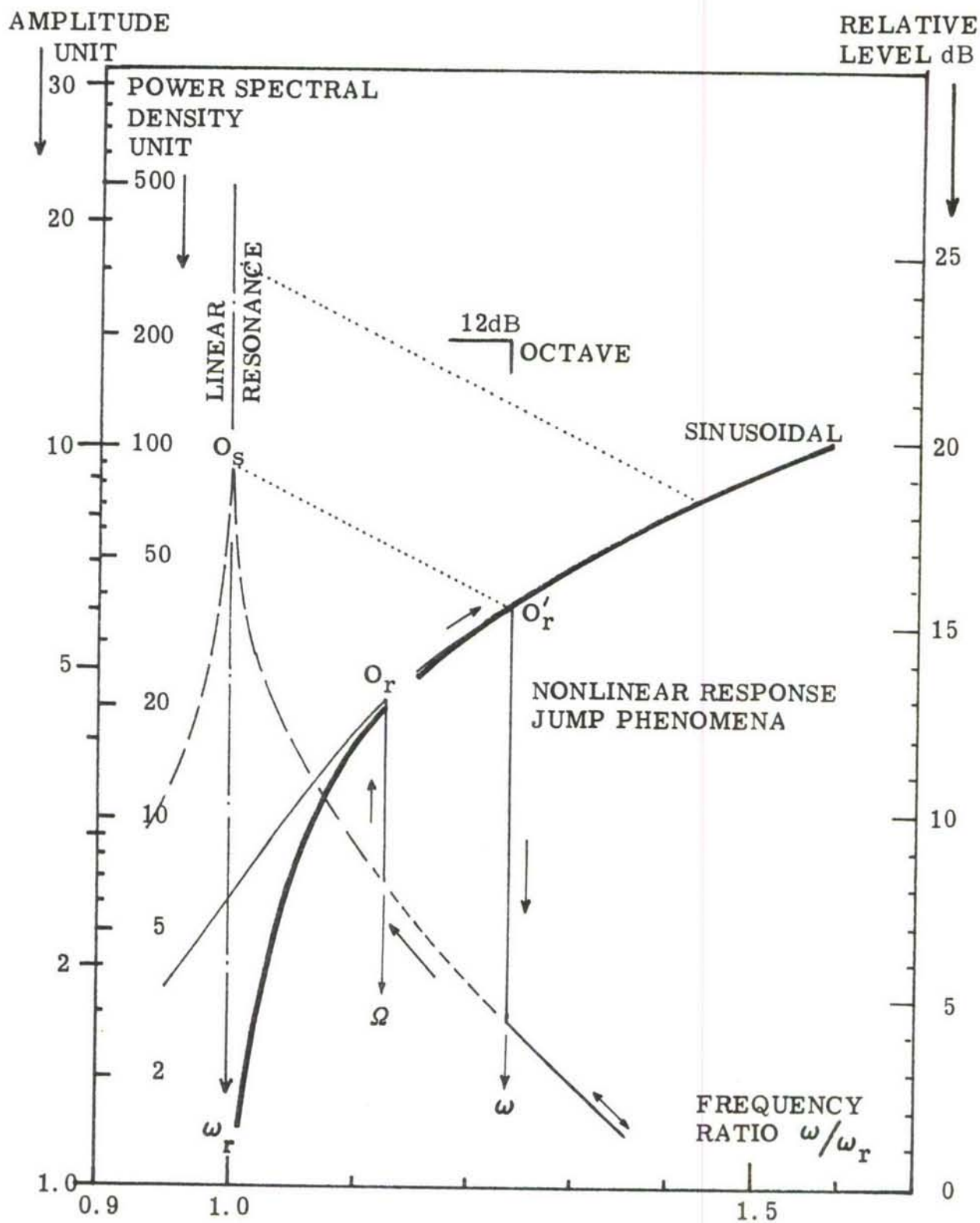
Figure 19. Typical Nonlinear Characteristics in Hard Springs
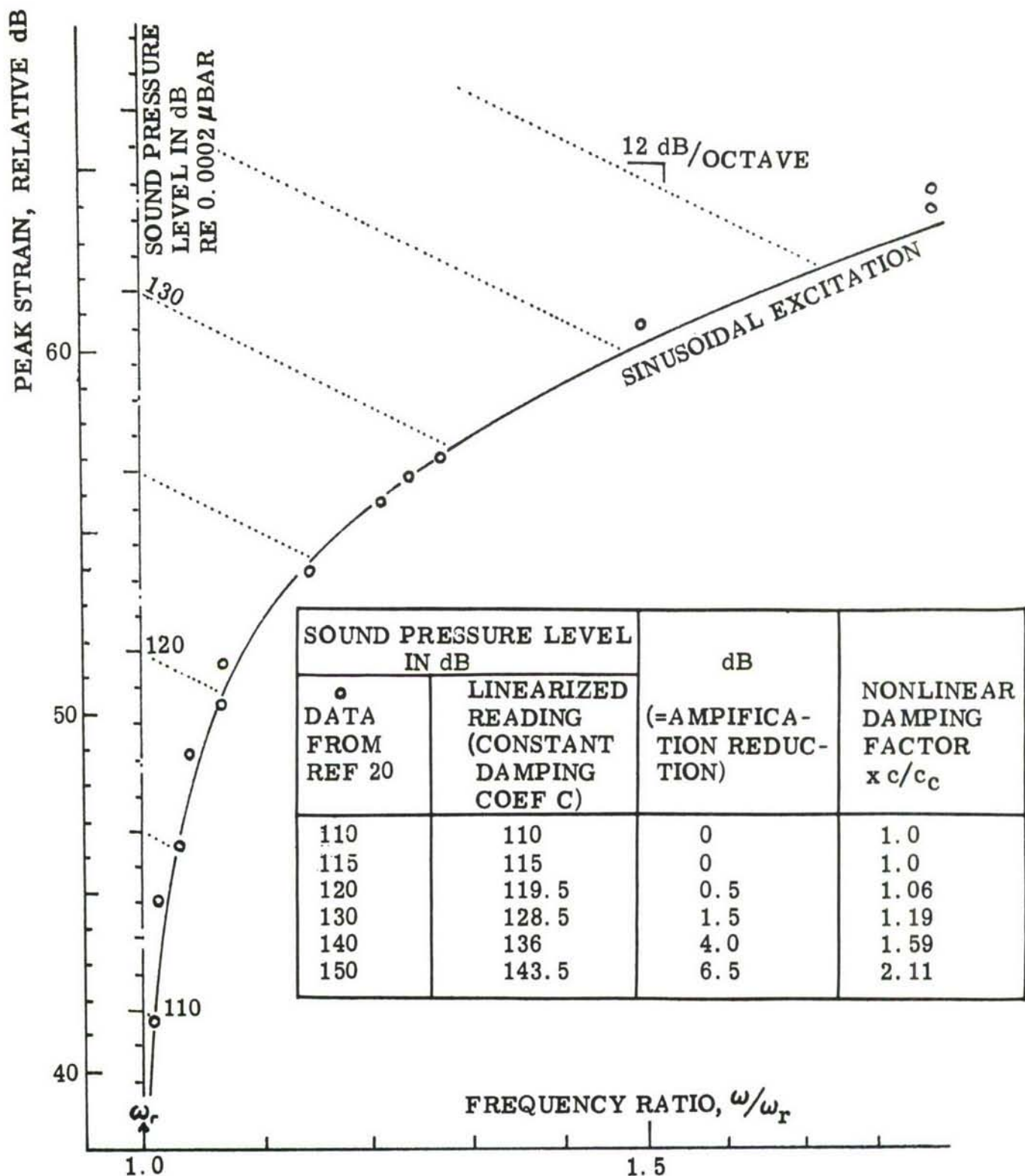
Figure 20 Damping Factor in Nonlinear Response

SOUND PRESSURE LEVEL IN dB		dB	NONLINEAR DAMPING FACTOR $x \, c/c_c$
DATA FROM REF 20	LINEARIZED READING (CONSTANT DAMPING COEF C)	(=AMPIFICA-TION REDUC-TION)	
110	110	0	1.0
115	115	0	1.0
120	119.5	0.5	1.06
130	128.5	1.5	1.19
140	136	4.0	1.59
150	143.5	6.5	2.11

observed. This is discussed in Reference 17 and attributed to phase angle changes in Reference 19. For random excitation and response, the frequency Ω becomes the more significant because the net damping power, represented by the integrated area under the resonance curves, excludes the area between Ω and ω. A separate curve for random excitation can be formed, after an appropriate number of points like 0_r have been obtained first in sinusoidal excitation tests. Inasmuch as the basic nonlinear forcing function represented by Equation 6 in the preceding section is generally applicable without restrictive conditions, the resultant random frequency curve shown in Figure 21 may be employed under all conditions such as illustrated for the best fit with data points from Reference 1. The use of sinusoidal excitation is recommended as an essential step by virtue of a definitive indication in the locations of frequencies Ω .

3.6.5 Nonlinear Effect Due to Deficiency in Core Strength

As indicated in Equation A6 of Appendix A, the frequency of a beam or plate element of honeycomb sandwich construction can be evaluated on the basis of complete adequacy in core rigidity, subject only to a weight correction factor demonstrated in Section 3.2 and verified in the tabulated results of Table IV, Section 3.2.2. In the case of marginal rigidity at a shear stress that is still within the strength of the core, the expectation is a degradation in resonance frequency as shown by the three beams in the full size sections at 24" cantilever span. While the change in frequency is barely detectable, the extent of nonlinearity in amplitude or stress response to load changes is much more severe. This offers another reason for the advisability of testing with sinusoidal excitation forces. For these beams, the results are shown in Figure 22, plotted in the same manner as Figure 10. The correlation point B is calculated as before (Section 3.3.1) in addition to a reference check point S. Through these two points the linear response line (dotted) passes. The accented solid line, transferred from an established curve would represent the anticipated primary response curve if the core rigidity remained adequate. The actual response in this case involves, therefore, secondary nonlinearity. The area between these curves indicates the effect due to core deficiency. In comparison, the observed stress response for beams at 16" span in the same sections passes through the calculated linear check points and the correlation point A without any indication of secondary nonlinearity. As a further proof, a 12"-span was cut from the outside end of each of two 24"-beams. The observed frequencies of these shortened halves reverted to slightly above the theoretical frequencies. See Table IV. By reducing the dynamic shear force, the shear stress is held within a safe limit and perfect adequacy in core rigidity is again maintained. Incidentally, the test also shows that the damage was localized to the clamped area and did not extend to the free ends where the shear forces were less.

Figure 21.   Linearized Random Response Characteristics

44

Figure 22. Vibratory Stress in Cantilever Beams

45
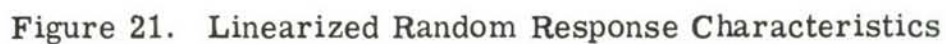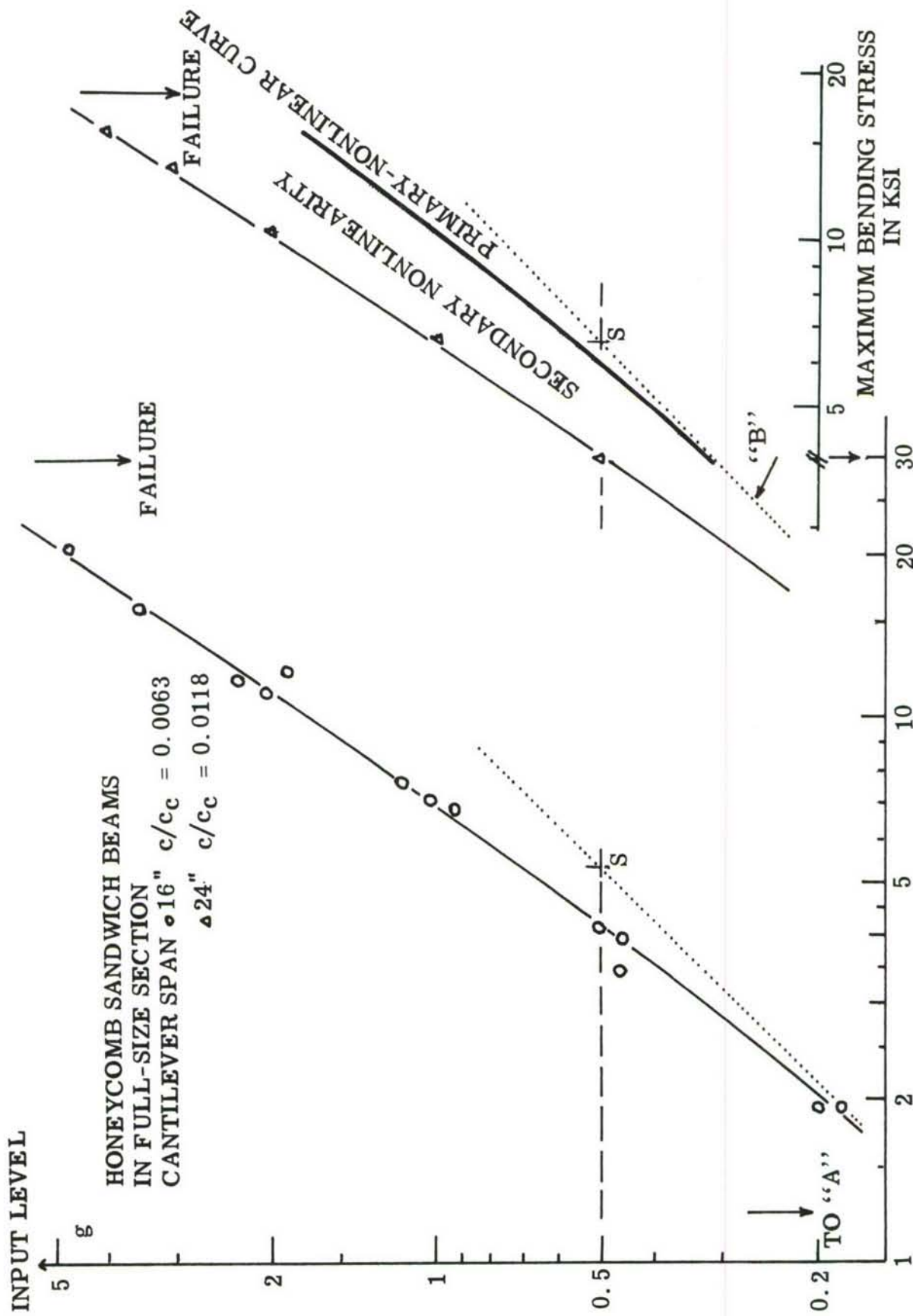
3.7   Honeycomb Sandwich Panel Tests

3.7.1   Full size specimens, 41" x 28" plate dimensions

3.7.1.1 Calculated Frequencies

The calculated resonance frequency on the basis of Equation 2, Section
2.5.1.2 is shown in Figure 23 for various modes defined by mode numbers m
for the longer side b, n for the shorter side a and the boundary conditions
C for clamped, and S for supported edges. Thus 1,1S would be the expected
first mode. In practice, supported edges are not physically achieved
unless accompanied by a slight yield in the clamping plates in which case
the effective dimensions extend to bolt hole centerlines. Figure 23 shows
the clamped mode frequencies in solid lines, supported mode at clamped
dimensions in dotted lines and extended dimensions (+2 inches to both b and
a) in broken lines. Mode number's m are plotted as ordinates for all fre-
quency curves at parameters n for each of the boundary conditions specified.
The theoretical resonance frequencies of Fig. 23 were defined from the data
of Fig. 5 using the techniques of Appendix A of Reference 33.

3.7.1.2 Test Arrangement

The test arrangement is shown in Figure 24 for the specimen mounted
on one side of a duct through which acoustical forces at controlled inten-
sities are propagated. The input sound pressure level was sensed with
three microphones spaced apart at less than 1/4 of the minimum acoustical
wave-length when sinusoidal signals were being used. If a truly progressive
wave is generated, identical sound pressure levels should be indicated. In
general, this condition is likely unobtainable and significant changes in
sound levels are expected because of reflected waves at the duct termination.
Due to the fact that the pressure trough would be quite sharp, its effect on
pressure distribution upon the specimen surface may be neglected. For the
effective pressures acting as if uniformly distributed on the specimen, the
highest reading of the three microphones was therefore used. When specimen
vibrations contain higher harmonics resulting in significant distortions
in sound waves as indicated by the microphones, the corrected harmonic
amplitude at the excitation frequency indicates the true effective pressures.

The strain gage circuit was the same as used in cantilever beam tests,
and gage locations in accordance with the designations of Figure 24a. Read-
ings were directly recorded as bending stresses in psi rms or peak.

When the acoustical excitation is by random signal, the three micro-
phone outputs are more or less even. Any one signal, microphone or strain
gage, may be selected to feed into a spectrum analyzer for a continuous
record and to feed into a probability density analyzer for indications
pertaining to amplitude distributions.

46
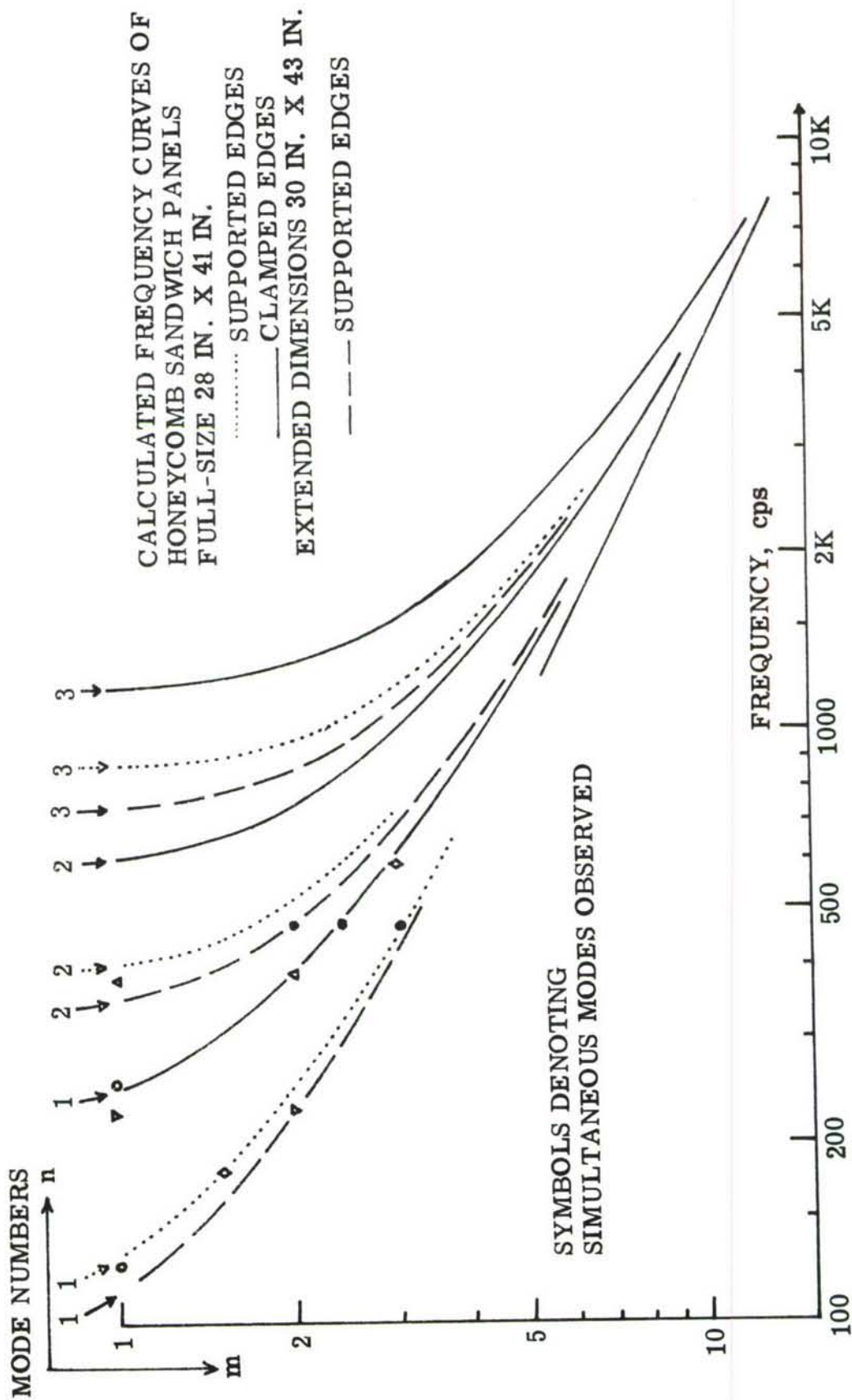
Figure 23. Resonance Frequencies of Honeycomb Sandwich Panels

47
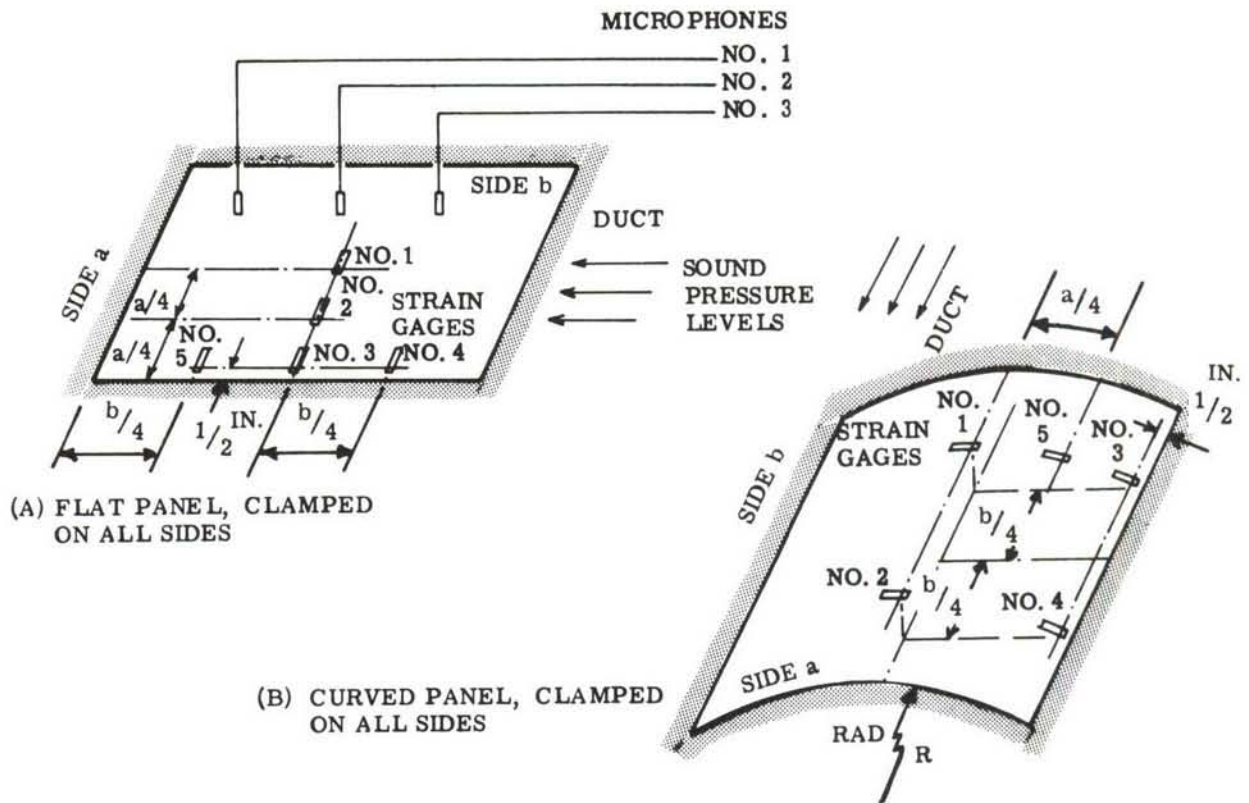
Figure 24. General Test Arrangement

3.7.1.3 Modes Observed

The following analysis will indicate that the modes observed in each specimen are neither simple modes defined in singular combinations of m, n nor restrained in one of the classical boundary conditions. However, multiple numbers in both m and n were identified for many modes existing simultaneously at harmonically related frequencies. Thus the application of Fourier's series in the analysis becomes completely relevant. While the combined constraint can be created through the elastic properties of the supporting elements, the harmonic relationship of the frequencies is

greatly influenced by the overall aspect ratio of the original panel. The choice of a ratio so close to $\sqrt{2}$ was unfortunate. The significance of $\sqrt{2}$ as an aspect ratio is given in Appendix C. The unfortunate result (from a test viewpoint) of the many harmonic modes obtainable is that it becomes virtually impossible to excite single pure modes. However, the subsequent stress analysis shows that for such a panel aspect ratio a significant reduction in stress is realized. This of itself could be of substantial benefit in structural design. Unfortunately, this indication of potential benefits accruable from panel aspect ratio of $\sqrt{2}$ was obtained at the expense of relinquishing fatigue data for these panels. If an aspect ratio of 1.8 had been used, the interaction of these harmonically related modes would have been extensively reduced and the first mode response would have been enhanced.

Examples of mode analysis are given in Figure 25 and 26 for full-size specimens. Figure 25 shows the observed waveforms at 385 cps at an acoustical excitation level of 138 dB re 0.0002 μbar, analyzed into two predominant amplitudes at frequencies of 385 cps and 770 cps. Each of which can be further divided into component modes, - 1,2S or 2,1C at 385 cps and 3,2S or 4,1S at 770 cps. Figure 26 shows the waveforms at 470 cps at the same excitation level, analyzed into three predominant amplitudes at frequencies of 470 cps, 940 cps and 1410 cps. The component modes are 2,2S and 2.5,1C at 470 cps, 2,3S and 3,2C at 940 cps, and 5,2C at 1410 cps. Observed frequencies falling between the theoretical values of m, n modes in Figure 23 were assigned the fractional m value corresponding to their m, n location on the figure (e.g. 2.5,1C). Note that to be sustained, these modes require a higher order m, n mode with m an integer for excitation (e.g. the 5,2C mode at 1410 cps excites the 2.5,1C mode at 470 cps). In these multiple numbers for either m, n or both occuring at the same frequencies, phase angles would be constantly but regularly varying as displayed in the oscilloscope pictures in both figures. A summary of all modes detected in this manner is tabulated in Table VI from the two panels tested. Inasmuch as the calculated frequencies curves are verified, the third panel was not needed in model analysis.

3.7.1.4 Damping Coefficient Ratio and Frame Vibrations

The multiplicity in the number of modes excited at any one instant gives considerable complexity in the decay trace. This complexity does not permit a simple and accurate indication of the damping coefficient ratio. The mode multiplicity is further complicated by the frame vibrations which appeared to be in resonance at about 128 cps, investigated through a separate strain gage attached thereto (see Section 3.7.2.3). No coupling effect between the frame system and the panel system was observed, however, in spite of the fact that at an excitation frequency of 128 cps, the first panel mode with supported edges was excited in coexistence with the first clamped mode at the second harmonic

138 dB AT 385 cps :
FULL SIZE HONEYCOMB SANDWICH PANELS

STRAIN GAGES

MODE ANALYSIS

STRAIN GAGES   1ST HARMONIC, 385 cps
NO. 3 NO. 2

NO. 1   1, 2S + 2, 1C

2ND HARMONIC, 770 cps

4, 1S + 3, 2S

AMPLITUDE ANALYSIS

GAGE NO.	RELATIVE %		O A	PSI RMS	
	HARMONICS			HARMONICS	
	1ST	2ND		1ST	2ND
1	100	200	90	40	80
2	100	260	90	32	+84
3	100	280	50	17	-47

Figure 25.   Waveform Analyses in Complex Modes

50

138 dB AT 470 cps :
FULL SIZE HONEYCOMB SANDWICH PANELS

NO. 2

NO. 1

NO. 3
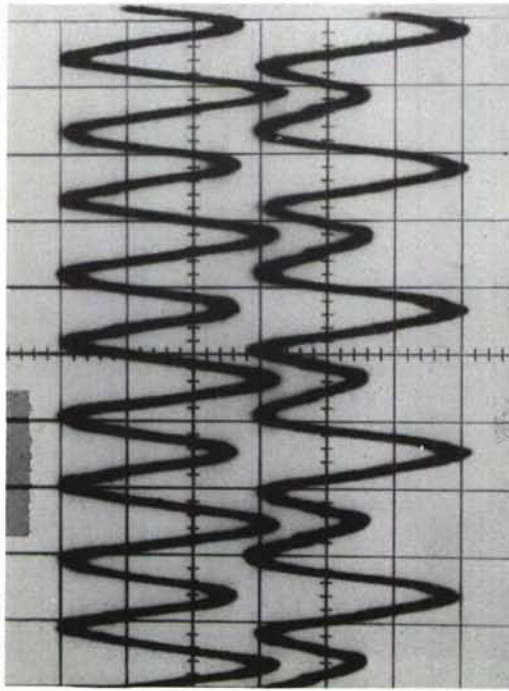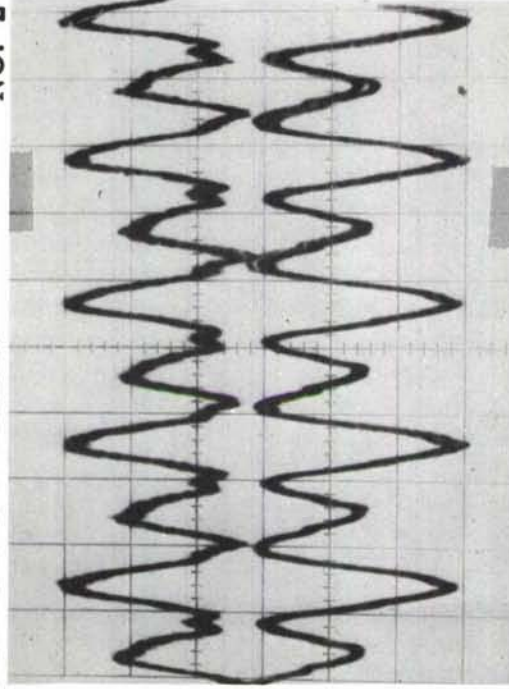
NO. 1

STRAIN GAGES

MODE ANALYSIS
1ST HARMONIC, 470 cps

3, 1S + 2, 2S
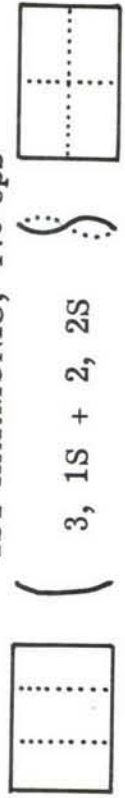
2ND HARMONIC, 940 cps

2, 3S + 3, 2C
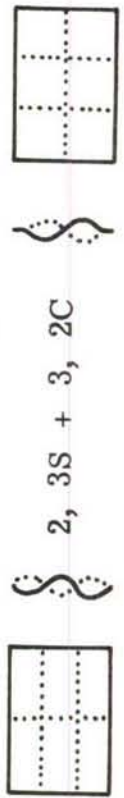
3RD HARMONIC, 1410 cps

5, 2C AT LOW AMPLITUDES

AMPLITUDE ANALYSIS

GAGE NO.	RELATIVE %			PSI RMS		
	HARMONICS		O A	HARMONICS		
	1ST	2ND		O A	1ST	2ND
1	100	154	160	87	134
2	100	206	62	27	+56
3	100	355	90	24	-87

Figure 26. Waveform Analysis in Complex Modes

51

TABLE VI   MODE COMBINATION IN FULL-SIZE SPECIMENS

		FREQUENCY SCALE	100	150	200	250	300	400	500 cps
SPECIMEN NO.1 / HARMONIC ORDER	EXCITATION RANGE	1st		1,1S	1.5,1S	1,1C 2,1S	1.5,1C 2,1S	1,2S 2,1C	2,2S 2.5,1C 3,1S
		2nd		1,1C		3,1S	2,2S	3,2S 4,1S	2,3S 3,2C
		3rd							5,2C
		4th			3,2C 2,3S 4,1C	3,2C			
SPECIMEN NO.2 / HARMONIC ORDER	EXCITATION RANGE	1st		1,1S 1.5,1S	2,1S		1.5,1C		2,2S 3,1S
		2nd		1,1C 1.5,2C	1,2S 2,1C		3,1C		2,3S 3,2C 4,1C
		3rd		3,1S					
		4th		3,1C					

order of excitation. It is to be recalled that as a second order excitation, the latter mode is self-excited and extracts no damping power from the input energy (see Reference 15). The energy summation of all modes must, therefore, be identical to the damping energy in whichever fundamental mode $[1,1S$ or $1,1C]$ exists individually without complications. Because of the displacement reduction in $1,1C$ mode, the damping coefficient c (but not necessarily the coefficient ratio to critical c/c_c) becomes larger in the $1,1S$ mode.

Representative oscilloscope displays of frame vibrations, occurring at the same time as panel vibrations in complicated modes, are shown in Figure 27. By extracting an imaginary decay trace appropriate to the frame frequency as shown at the top of Figure 27 and superimposing the same over the original traces, not only are the multiple panel modes easily revealed, some phase reversals required in the frame trace can also be observed. These reversals do not occur when the frame drives the model panels at second or higher harmonic orders (see Section 3.7.2.3). It appears, therefore, that the frame and panel are essentially two separate elastic systems in simultaneous resonance without interference or amplitude reinforcement. Both amplitudes are 90° in phase to the common forcing vector whose energy is shared by the two systems. If the respective phase angles are 90° and 270°, then the amplitudes are merely opposed or reversed without upsetting the input energy distribution. The conclusion is that a sub-structure need not be specifically designed to have a drastically different resonance mode. The mounting of an electronic package or black box at the area of maximum amplitude is, however, a different problem where the input to the black box itself may become excessively large.

3.7.2   5/8-Size Specimens, 23.75" x 16.25" Plate Dimensions

3.7.2.1 Calculated Frequencies

The calculated resonance frequencies are given in Figure 28 in identical manner as described in Section 3.7.1.1. Because the specimens are modeled in the same aspect ratio these curves take the same forms as Figure 23 except for numerical changes in frequencies . In extending the boundaries to bolt-hole centerlines for supported conditions, 2 inches are added for each side, modifying the aspect ratio differently to result in a slightly altered frequency curve shown in broken lines.

3.7.2.2 Test Arrangement

The test arrangement is identical to that given in Section 3.7.1.2.

3.7.2.3 Modes Observed

The modes observed are identified through the waveforms of strain gage signals displayed on an oscilloscope and analyzed into component modes pertaining to each harmonic order. An example is shown in Figure 29. Like the full-sized specimens, each order is again a combined mode. Table VII lists all modes so recognized which are represented by the data points from two panels plotted onto Figure 28, the calculated frequency curves. The third specimen was not tested.

STRAIN GAGES NO. 1

FULL-SIZE HONEYCOMB
SANDWICH PANEL NO. 1

NO. 3   10 M SEC

NO. 1

NO. 2 NO. 3

NO. 1

STRAIN GAGE LOCATIONS

NO. 2
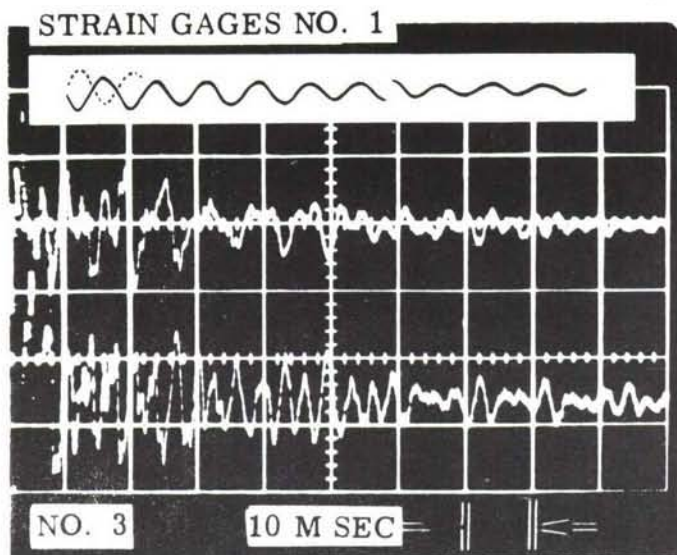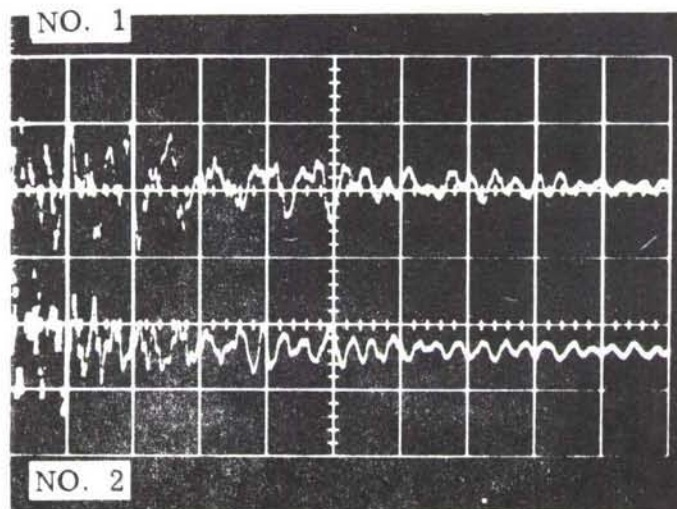
ARTIFICIAL DAMPING
SIGNALS AT SUPPORT
FRAME FREQUENCY SHOWN
AT THE TOP AND BOTTOM
FOR REFERENCE. NOTE
PHASE REVERSALS REQUIRED
TO FIT STRAIN SIGNALS

NO. 3

NO. 2
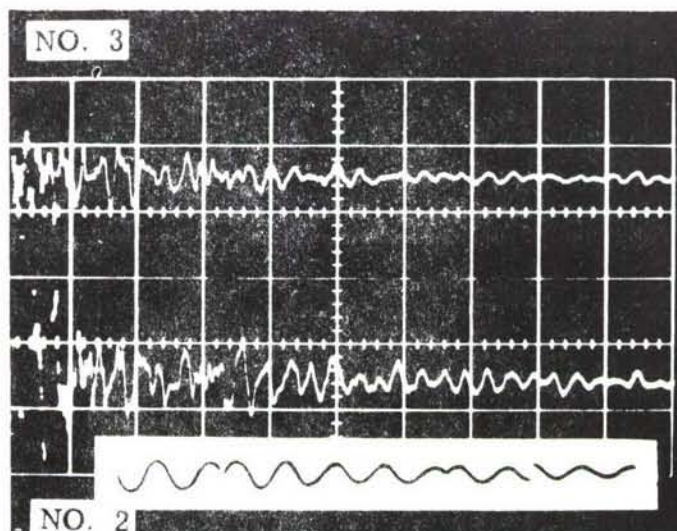
Figure 27. Decay Signals From a Honeycomb Sandwich Panel
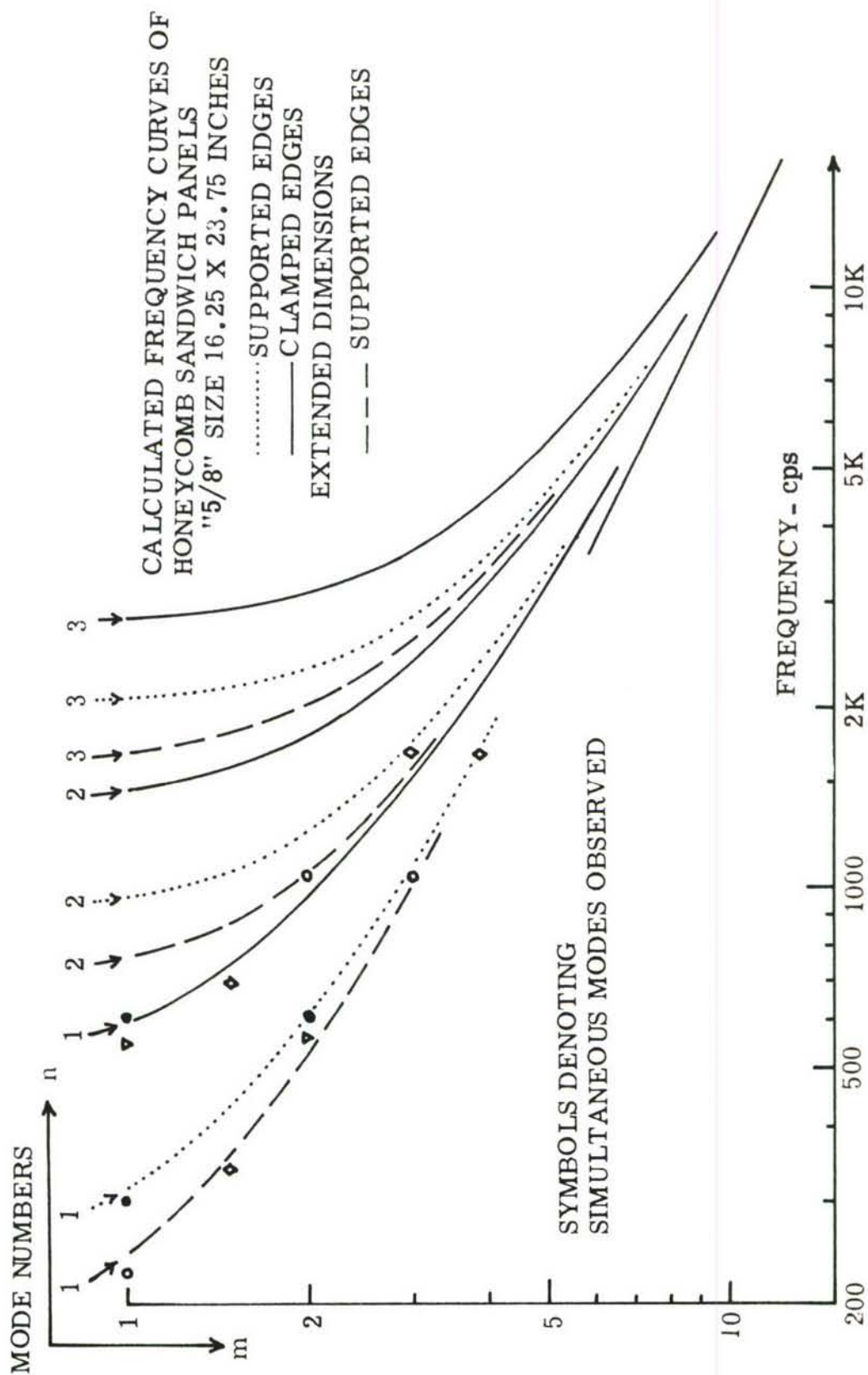
Figure 23. Resonance Frequencies of Modeled Honeycomb Sandwich Panels at "5/8" Size

55

HONEYCOMB SANDWICH PANEL NO. 2, "5/8" SIZE

EXCITATION LEVEL 150 dB
at 528 cps

STRAIN GAGES

No. 4

NO. 4

NO. 1

No. 1

ANALYSIS: HARMONIC   1ST   4TH   5TH
FREQUENCY   528   2112   2640 cps

1, 1C   4, 1C   3, 3S

MODES   2, 1S   OR   2, 3S   OR   5, 1S   OR

OBSERVATION   GAGE READING COMBINED MODE IN ALL CASES

PHASE OSCILLATIONS DUE TO
VARIATIONS IN MODE NUMBERS
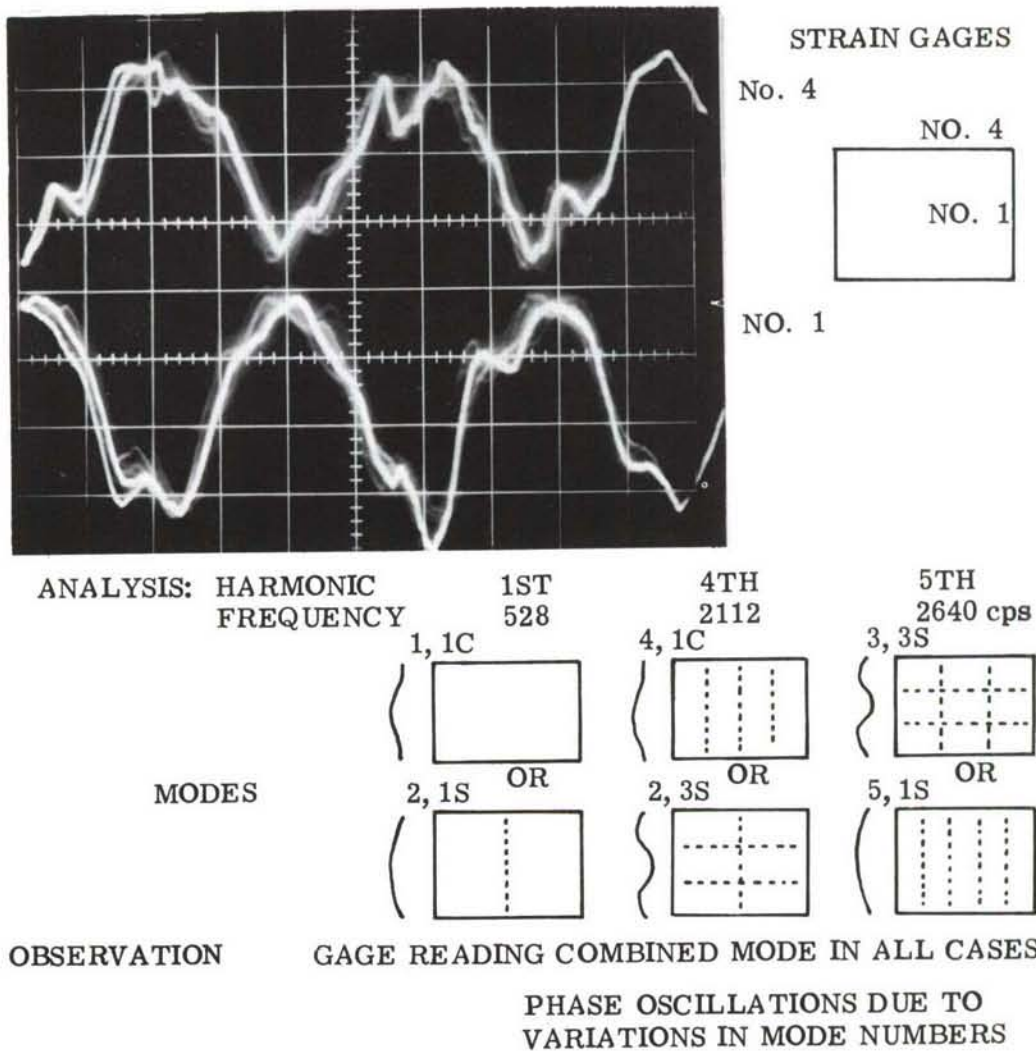
Figure 29.   Sample Response Waveform and Analysis From a
Honeycomb Sandwich Panel

TABLE VII   MODE COMBINATION IN 5/8-MODEL SPECIMENS

FREQUENCY SCALE (cps)

	100	150	200	250	300	350	400	500
SPECIMEN NO. 1 — HARMONIC ORDER / EXCITATION RANGE								
1st	Frame Vibrations		1,1S					1.5,1S
2nd		1,1S	1.5,1S					1.5,2S
4th		1,1C 2,1S	1.5,2S				4,1S 3,2S 2,2C	
5th			3,1S 2,2S				4,1C 3,2C 4,2S	
6th		2,1C						
SPECIMEN NO. 2 — HARMONIC ORDER / EXCITATION RANGE								
1st	Frame Vibrations			1,1S	1,1S	1.5,1S		2,1S 1,1C
2nd		1,1S		1,1C 2,1S	1,1S / 2,1S	1.5,1C		
3rd		1.5,1S					2,2S 3,1S	
4th		1,1C 2,1S					4,1C 2,3S	
5th		1,5,1C				4,1S 3,2S 2,2C	5,1S 3,3S	
7th		2,1C						
8th		2,2S 3,1S						

57

By comparing Tables VI and VII together, it is noted that the same modes are duplicated or successfully modeled. For example, the combination of 1,1S and 1,1C mode in the full-sized specimens is also observed in the 5/8-size specimens in spite of the fact that in the latter panels frame vibrations were excited by the acoustical forces, exciting in turn these same panel modes of higher harmonic orders. The presence of frame vibrations is indicated by a separate strain gage attached to a frame member whose signal is shown in Figure 30. The lower curve shows the predominant frame frequency, idealized into the artificial trace at the top of the figure, which reveals the true panel modes at the 2nd and 4th harmonics when it is superimposed onto the panel trace. It proves to be difficult, however, to extract appropriate decay curves for damping coefficient ratio calculation.

A further significance derived from Tables VI and VII is seen in the mode parameter product m · n for supported component modes. This will be discussed in a subsequent section (5.3)

3.7.3   3/8-Size Specimens, 14.25 x 9.75

3.7.3.1   Test Arrangement

In view of the size reduction, it became expedient to use a different mounting which closely simulated fully clamped boundary conditions. The size of the opening, or the frame size, exposing the panel to acoustical forces was slightly larger than the honeycombed section, extending the true panel size to 14.25" x 11". The test arrangement is sketched in Figure 31, employing acoustical forces generated through electro-dynamic speakers.

3.7.3.2   Calculated Frequency & Damping Coefficient

The frequency is calculated on the same basis as before, e.g., 1,1C mode at 1000 cps. The observed decay curve is shown in Figure 32, obtained when the electrical input to the speaker was instantaneously removed. The observed frequency is 990 cps and the decay rate corresponds to a damping coefficient ratio c/c_c of 0.015. The slight modulation is probably caused by the heavy frame structure which is smoothed out and averaged for damping calculation.

At this frequency range, it would be difficult to subject this panel to the same acoustical environment as the larger panels. Because the frequency correlation has been obtained and very little increment in stress could be realized in this arrangement, further tests with 3/8 panels were not conducted.

3.7.4   Mode and Response Correlation between Models

Apart from the general indications in Tables VI and VII that similar modes were indeed obtained in the modeling experiments, detailed considerations in fatigue analysis requires specific correlation in the respective stresses and in the respective modes generated. Therefore, for each combination mode, the stress component due to each individual mode must be
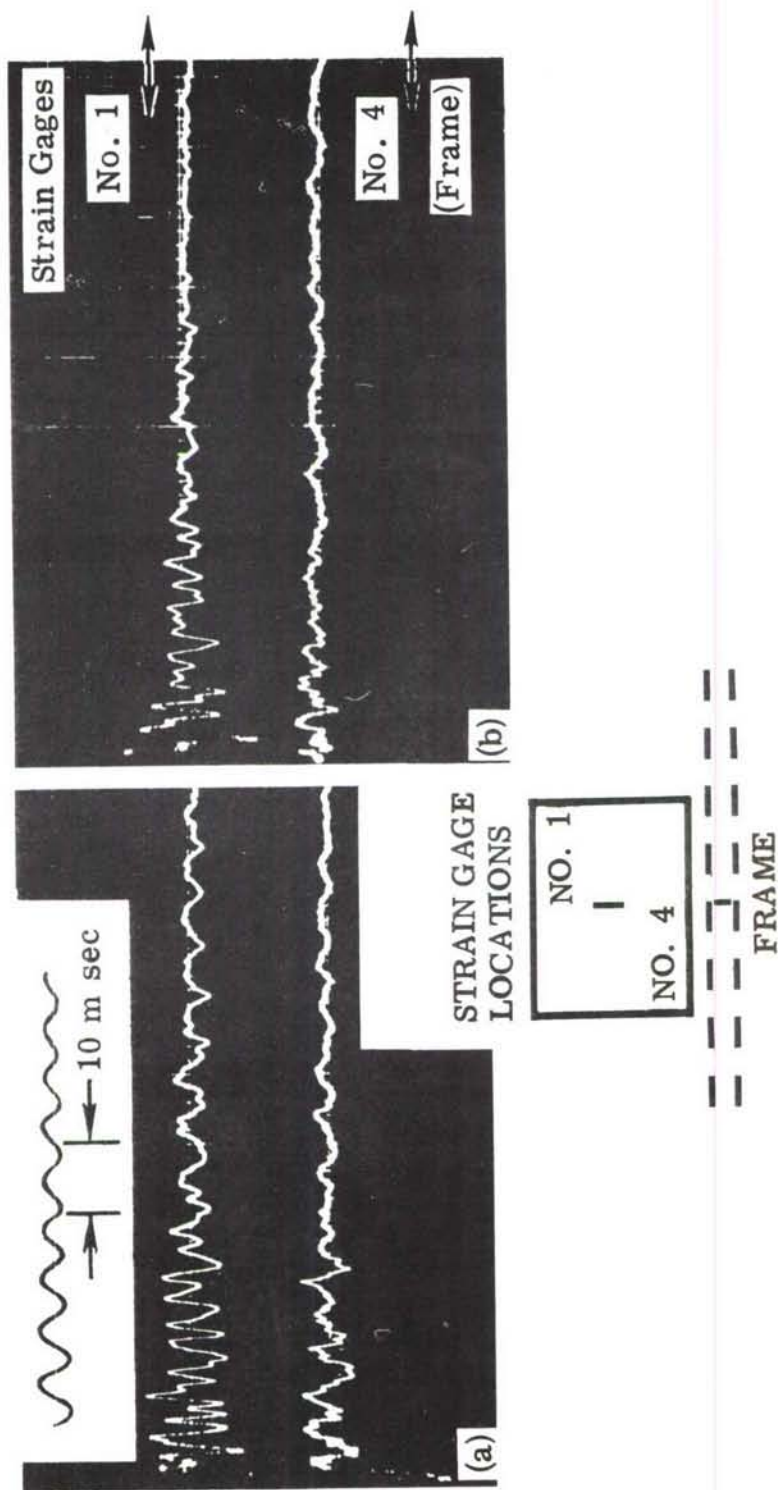
Figure 30. Detection of Frame Vibrations

16 ELECTRO-DYNAMIC SPEAKERS

TEST PANEL CLAMPED TO A BAFFLED FRAME

2 STRAIN GAGES USED

± PSI

2 MICROPHONE STATIONS
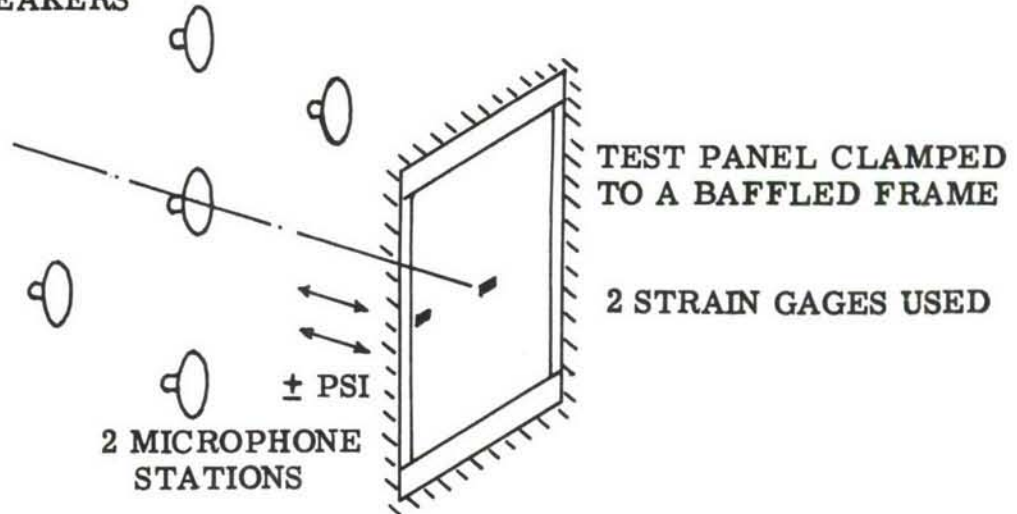
Figure 31. Test Arrangement for "3/8" Size Honeycomb Sandwich Panel Models

0.002 SEC

FREQ. = 990 cps
c/c_c = 0.015
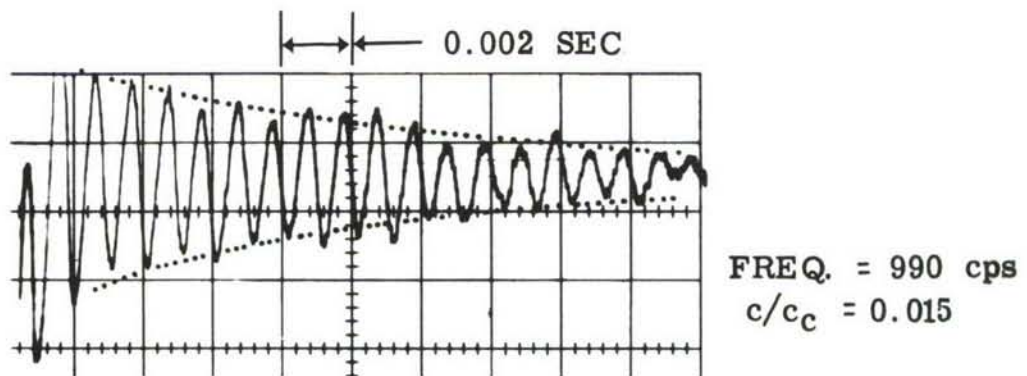
Figure 32. Decay Signal From a Modeled Honeycomb Sandwich Panel at "3/8" Size

ascertained in order to differentiate between the cumulative damage in each case. The basic considerations as indicated by Equation 2 (Section 2.5.1.2) for frequency correlation and Equation 1 (Section 2.5.1.1) for stress correlation will be applied in the following cases.

3.7.4.1 Combined Mode: 1,1C and 2,1S

Full-Size Panel	5/8-Size Model
Tested at 142 dB, 227 cps	Tested at 150 dB, 528 cps

Freq. Equation:
$$f_{m,n} = \frac{C_{m,n}\sqrt{12}\ k}{a^2}\sqrt{\text{Weight Ratio}}$$

Modeling Requirement: $C_{m,n}$ = common constant for each component
(W.R. = weight ratio)

Modeling Parameters

k_1 = 0.496 inch	k_2 = 0.319 inch
a_1 = 28 inch	a_2 = 16.25 inch
$\sqrt{WR_1}$ = 0.430	$\sqrt{WR_2}$ = 0.534
f_1 = 227 cps observed	f_2 = 528 cps observed

Calculated frequency ratio, $\dfrac{f_2}{f_1} = \dfrac{0.319\ (0.534)\ (28)^2}{(16.25)^2(0.496)(0.430)} = 2.37$

Observed frequency ratio, $\dfrac{528}{227} = 2.32$

These ratios hold true for all other modes at higher harmonic orders. Observe that the weight ratio factors cannot be retained at a fixed magnitude. Whereas the frequency ratio ceases to follow inversely as the apparent geometric scale factor of 8 to 5 in this case, the inclusion of the weight ratio correction is clearly indicated as a necessary modeling parameter.

Stress Analysis, full-size panel 142 dB	Stress Analysis, 5/8 size model 150 dB
Center of Plate, Sinusoidal response, rms = 1100 psi	Center of Plate = 3300 psi, rms
	1st order response = 3100 psi
Linear Conversion to 150 dB, = 2760 psi	(best sine wave fit from Figure 29)

Stress Equation: $\sigma = \dfrac{\beta\ p\ a^2 d\ (A.R.)}{6\ A\ k^2}$ (Modeling Basis; See Appendix A)

Modeling Relationship: β = common constant

p = common pressure intensity

A = common area, as fabricated

Modeling Parameters

d_1 = 0.502 inch	d_2 = 0.324 inch
k_1 = 0.496	k_2 = 0.319
a_1 = 28	a_2 = 16.25
$(AR)_1$ = yet unknown	$(AR)_2$ = yet unknown
σ_1 = 2760	σ_2 = 3100

Assume $\dfrac{(AR)_2}{(AR)_1} = \dfrac{(c/c_c)_1}{(c/c_c)_2} = \left(\dfrac{a_1}{a_2}\right)^{3/2}$ from cantilever tests

$$= \left(\frac{28}{16.25}\right)^{3/2} = 2.26$$

Calculated stress ratio $= \dfrac{\sigma_2}{\sigma_1} = \dfrac{(16.25)^2(0.324)(2.26)(.496)^2}{(.319)^2(28)^2(.502)} = 1.18$

Observed stress ratio $= \dfrac{3100}{2760} = 1.12$

Note that if the model stress was left uncorrected into a sinusoidal wave, the observed stress ratio would be 1.20. In any event, the deviation from full agreement is within 5% which is only 1/2 dB off. Therefore, either reading may be used for subsequent analysis into its component stress due to vibratory excursions in either 1,1C mode or 2,1S mode at the same frequency. The locations of the strain gages permit response observation in n-modes only which, in this case, are stronger than corresponding m-modes of the same order along the other principal axis. If a single m,1C mode prevailed, the edge stress should be almost twice the stress at the center. As this is not so observed, a simultaneous mode m,1S must also be in existence where the stress would be zero at the edge and high at the center; hence the necessity of the following analysis as illustrated.

Thus the given conditions, observed with a model specimen, are:

Excitation Frequency and Intensity: 528 cps at 150dB or 0.13 psi peak

Center Stress: 3100 psi rms in combined 1,1C and 2,1S mode

Edge Stress: 1350 psi rms, responding to 1,1C only, zero in 2,1S mode

Let σ_c represent the edge stress due to a component load intensity p_c at 528 cps, and $(AR)_c$ be the resonance amplification factor at a damping coefficient ratio $(c/c_c)_c$.

With $\beta/6 = 0.0726$, (from Reference 24; See Appendix A)

$a = 16.25$ in., the clamped span

$A = 0.024$ in^2

$k = 0.319$ in.

$d = 0.325$ in.

Then $\sigma_c = 1350 \times 1.414 = 1910$ psi peak

And $p_c\ (AR)_c = \dfrac{(1910)(0.024)(0.319)(0.319)}{(0.0726)(16.25)(16.25)(0.325)} = 0.752 \pm$ psi peak

Possible answers are paired below:

1,1C MODE - Response & Amplification Ratio

$(AR)_c$	100	80	60	50	40	30	20
p_c	0.00752	0.0094	0.0125	0.015	0.0188	0.025	0.0376

At the same time, the center stress could be determined by changing $\beta/6$ from 0.0726 to 0.0349 for a component magnitude of 650 psi rms, leaving a difference of 2450 psi rms as the other component in m,1S mode.

Let σ_s represent the center stress due to component load intensity p_s at 528 cps, and $(AR)_s$ be the resonance amplification factor at damping coefficient ratio $(c/c_c)_s$.

Then $\sigma_s = 2450 \times 1.414 = 3460$ psi peak; $\beta/6 = 0.0506$ (From Ref. 22; See Appendix A)

Based on $a = \dfrac{23.8 + 2}{2} = 12.9$ in.

And $\bar{p}_s\ (AR)_s = \dfrac{(3460)(0.024)(0.319)(0.319)}{(0.0506)(12.9)(12.9)(0.325)} = 3.11 \pm$ psi peak

Possible answers are paired below:

2,1S MODE - Response & Amplification Ratio

$(AR)_s$	100	80	60	50	40	30	20
p_s	0.0311	0.0388	0.0519	0.0620	0.0778	0.104	0.155

Though these component modes are considered in different boundaries, the actions are necessarily simultaneous. For this reason a uniform amplification ratio prevails in addition to the known condition $p_s + p_c = p = 0.130$. It appears, therefore, that the following combination is the only solution applicable to the conditions at 150 dB.

$$p_c = 0.025 \text{ psi}, \ (c/c_c) = 0.015$$

$$p_s = 0.104 \text{ psi}, \ (c/c_c) = 0.015$$

While it appears that the damping coefficient ratio in a supported system should be much lower than that in a clamped plate, the observation is made that in this case the supported constraints can be realized only at the expense of elastic deformation in the form of twisted clamping plates or distorted frames, resulting in additional damping work required and a relatively higher lumped coefficient ratio. By considering this clamped plate in 5/8 size to have the same damping ratio as a 3/8 size specimen (Section 3.7.3.2), a slight error of little significance is probably incurred.

3.7.4.2 Simple Mode, 2,1S Predominating

Apart from the combined mode discussed above, there are many other modes of higher complexities but inducing much lower stresses. Agreement in modeling parameters is nevertheless obtained as illustrated below.

Observed data corresponding to 140 dB excitation levels are as follows:

Full Size Panel

Specimen #1 at 185 cps
    Center stress = 270 psi
    Edge stress = 170 psi

Specimen #2 at 195 cps
    Center stress = 350 psi
    Edge stress = 110 psi

5/8 Size Model

Excited by frame vibrations at the 4th harmonic order of direct excitation frequency.

Specimen #1 at 125 cps, 4th harmonic = 500 cps for partial resonance only and low amplitude center stress = 40 psi

Specimen #2 at 133 cps, 4th harmonic = 532 cps for full resonance center stress = 430 psi edge stress = 60 psi

64

The difference between this mode and the previous mode is the relative weakness in 1,1C mode and the enrichment in many other modes at still higher orders. For simplification, idealization to a simple 2,1S mode may be made by transferring and adding the observed edge stress, which would have been zero, to the center for the maximum plate stress. The full size panel average of 450 psi rms as compared to 490 psi in modeling relationship follows very much the same ratio as 2760 to 3100 in the previous illustration. However, important significance is indicated in the frequency changes and the stress magnitude attained.

In the modeled specimens, this mode was generated in self-excited vibrations for no energy loss with the mode frequency remaining the same as before. The slight frequency variation (528 to 532) is of an experimental nature or due to differential temperature changes. The input energy at a different frequency was largely consumed in frame vibrations so that by extrapolation to the previously illustrated level at 150 dB the indicated stress at 1550 psi was well below the directly excited response. In the full-sized panel, the mode frequency was 227 cps, where in combination with 1,1C mode, the energy absorbed by the edge constraints was partially compensated between the two modes resulting in lowered damping work necessary. However, as a directly excited and predominantly 2,1S mode, the additional force required to overcome damping is available only at a reduced frequency. The observed reduction to 185 or 195 cps is expected from the generalized relationship $P\omega$ = constant and the average at 84% of the theoretical mode (227 cps) is compatible with other results under similar environment. (See Section 5.1 and Fig. 50).

It is interesting to note that the idealized center stress for any m,1S mode can be obtained from any combined m,1C mode by adding together the component stress readings at the center and at the edge for a given excitation level. This condition was indeed supported by the results of such a summation in the data obtained. As one component appears to improve nonlinearly with soft spring characteristics, the other component must vary with hard spring characteristics in order to maintain the sum at an appropriate level. The equalivent total response remained in fact linearly dependent on the excitation pressures applied.

3.7.4.3 Simple Mode, 3,1C Predominating

This mode at 550-600 cps is observed with full-size specimens sub-harmonically generated as a second order within an excitation frequency range of 263 to 286 cps. The modeled panels in the same mode would be at 1500 cps, too high to be excited as a dominating component. All observed stress readings at the center gages are in agreement and indicating 240 to 250 psi at 140 dB. The average edge stress of 400 psi serves to substantiate the clamped boundaries on the basis that the aspect ratio of the middle element in this 3,1C mode would be in excess of 2.5, and the bending stress coefficients for the center and edge locations would approach one to two as the readings so indicated. To calculate these stresses, due to a self-excited mode, a determination of the effective forcing intensity is required in addition to a still unknown damping coefficient. However, by assuming that the maximum displacement y is related through the factor $y\omega^2$ = constant

(see Section 3.6.3) the amplitude of the self-excited mode at twice the frequency at full power may be reckoned at 1/4 as large, i.e. the equivalent intensity p' equals 1/4 p. Using a bending stress coefficient of 0.73 from Appendix A corresponding to b/a ≈ 2.5 for the center element in this case, the stress equation is:

$$\sigma = \frac{(0.73)(12.4)(12.4)(.505)(AR)p}{6\ (0.024)(0.496)^2} = 400\ (1.414)$$

With p = 0.041 psi at 140 dB, p' = 0.010; the amplification ratio (AR) is 35.5 which appears to be within the proper range as estimated in the combined mode illustrated elsewhere. It is demonstrated that in higher modes, the stress is always so significantly reduced that its damage contribution becomes increasingly less and less.

4.   EXPERIMENTAL OBSERVATIONS IN CURVED PLATE MODELING

4.1   An Investigation of Boundary Conditions and Resonance Response

To analyze the vibratory motions of a curved plate such as ABCD shown in Fig. 33 as a representative element in a fuselage section (see Ref. 26) a ring section may be used in the same analogy as a beam is to a flat plate.

SECTION 1-1

SHOWING i NUMBER OF
COMPLETE WAVES PER
CIRCUMFERENCE,   AND $\ell = \pi R /_i$
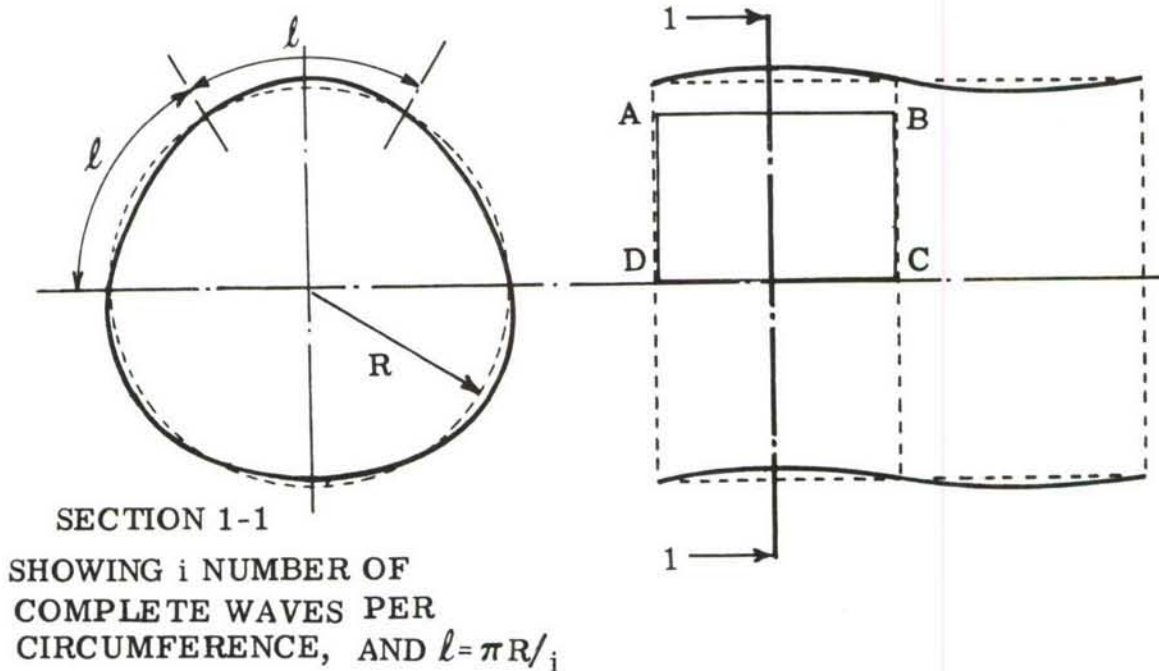
Figure 33. Outline of Cylinder (Fuselage Section)
Vibration in a Breathing Mode

For ring modes, the resonance frequency equation as given in Reference 15 is

$$f_r = \frac{1}{2\pi} \sqrt{\frac{EI}{\rho A R^4}} \sqrt{\frac{i^2 (1 - i^2)^2}{1 + i^2}} \qquad \text{cps} \qquad (7)$$

If the number i of complete waves per circumferential length is large, it is permissible to simulate ring segments as stiffened flat beams either in 1/2-wave lengths or full-wave lengths with   respective end conditions as specified in Table VIII. The observation is that the stiffening effect prevailing at increased modal frequencies may also be expressed as an increased moment of inertia or as a shortened effective span. To account for the boundary conditions of a complete plate, additional stiffening due to axial constraint   must be added. For the observation of dynamic effect between two axially adjacent elements , a preliminary test was undertaken with a two-panel configuration to determine the extent of possible interactions.

67

TABLE VIII   EQUIVALENT BEAMS IN RING FLEXURAL MODES

Equivalent Beam Considerations for Same Resonance Frequencies

Ring Flexural Mode Frequency = f_r Parameter No. i	Simply-Supported Beam at Span ℓ		Clamped - Clamped Beam at Span 2ℓ	
	Frequency Ratio — Beam Frequency = f_s — $\dfrac{f_r}{f_s} = \dfrac{i^2-1}{i\sqrt{1+i^2}}$	Remarks — $\ell = \dfrac{\pi R}{i}$ — $f_s = \dfrac{\pi}{2}\sqrt{\dfrac{EIg}{\rho A \ell^4}}$	Frequency Ratio — Beam Frequency = f_c — $\dfrac{f_r}{f_c} = \dfrac{1.765\,(i^2-1)}{i\left(1+i^2\right)^{1/2}}$ — $I = I_c$	Remarks — $\ell = \dfrac{\pi R}{i}$ — $f_c = 3.5608\sqrt{\dfrac{EI_c g}{\rho A (2\ell)^4}}$
2	0.671	Equivalent beam is under a combined loading of transverse forces and bending couples, — Increased deflections indicated by the reduced frequencies.	1.1840	Equivalent beam is under a combined loading of transverse forces and bending couples, — Increased deflections indicated by the reduced frequencies.
3	0.843		1.4875	
4	0.910		1.6057	
8	0.977		1.7240	
16	0.994	Bending couples now vanishing. Ring in flexural modes approaches flat beams of same I, simply supported at nodal points.	1.7540	Bending couples now vanishing. Ring in flexural modes approaches flat beams clamped a full-wave apart. For same frequency, make $I_c = (\text{Freq. Ratio})^2\, I$
24	0.997		1.7593	
32	0.999 −		1.7628 −	
64	0.999 +	No stiffening effect	1.7628 +	Approached constant stiffening effect

68

4.1.1 Curved Plate in Two-Panel Configuration

The center clamp was one inch wide and solidly clamped on both sides of the specimen plates. The aspect ratio of each element as a divided half of the full plate was maintained at b/a = 1.525 with b = 24.5, 15.25, and 9.15 in. respectively for the scaled models arbitrarily selected as full-size, 5/8, and 3/8 sizes. As one-half of the plate, or one element panel, was lightly but sharply struck once, strain gage signals from corresponding locations in each half were displayed simultaneously on an oscilloscope to show the characteristic waveforms. The samples given in Figs. 34 and 35 are for full-size and 5/8 size specimens respectively. The indicated frequencies of 271 and 446 cps are found to be within 3% of the expected scale ratio at 5 to 8. The use of 3/8-models was terminated because the frequency would be too high and stress level too low for meaningful fatigue tests.

Besides indicating the stiffening effect, the real significance lies in the modulation between the two elements or in the transfer of dynamic energies between the two panels having nearly equal but not identical modal frequencies. The true decay rate follows the envelope shown in each figure yielding a damping coefficient ratio of 0.0016 for the full-size specimens and 0.0017 for the 5/8-models. In spite of the extremely low damping, the observed stress in each case under the maximum acoustical forces available was not high enough to warrant continued tests in this configuration. However, within the frame work of the discussion of frequencies and length factors in Paragraph 5.1, the results do indicate a consistency in damping ratios which in conjunction with high frequencies point to the fact that for the curved elastic element, the length factor is significantly reduced (because of the high frequencies) and approaches simply supported boundaries (because of the low and uniform damping). Furthermore, in the transfer of energy between the two halves, a modification in fatigue contribution appears to be taking place due to the indicated manner of stress variations. These may possibly be additive to the Rayleigh distribution that was the basis of fatigue cummulation used in the Miles-Miner (References 6 and 8) theories. In order to attain test objectives directly, the center clamp was, therefore, removed resulting in enlarged test specimens at the dimensions given in Table II (Section 2.7). After this change was made, the two original halves of the 5/8 scale plate vibrated in phase as shown in Fig. 36, modulated jointly at a frequency equal to that expected of a flat plate. The enlarged full size plate on the other hand, was excited in a higher mode such that the two previously divided halves remained out of phase. In this case, however, the energy transfer previously evident with the center clamped installed was clearly not shown in Fig. 37. The modulation was common to both halves and was again due to the flat plate mode.

NATURAL FREQUENCY AT 271 CPS
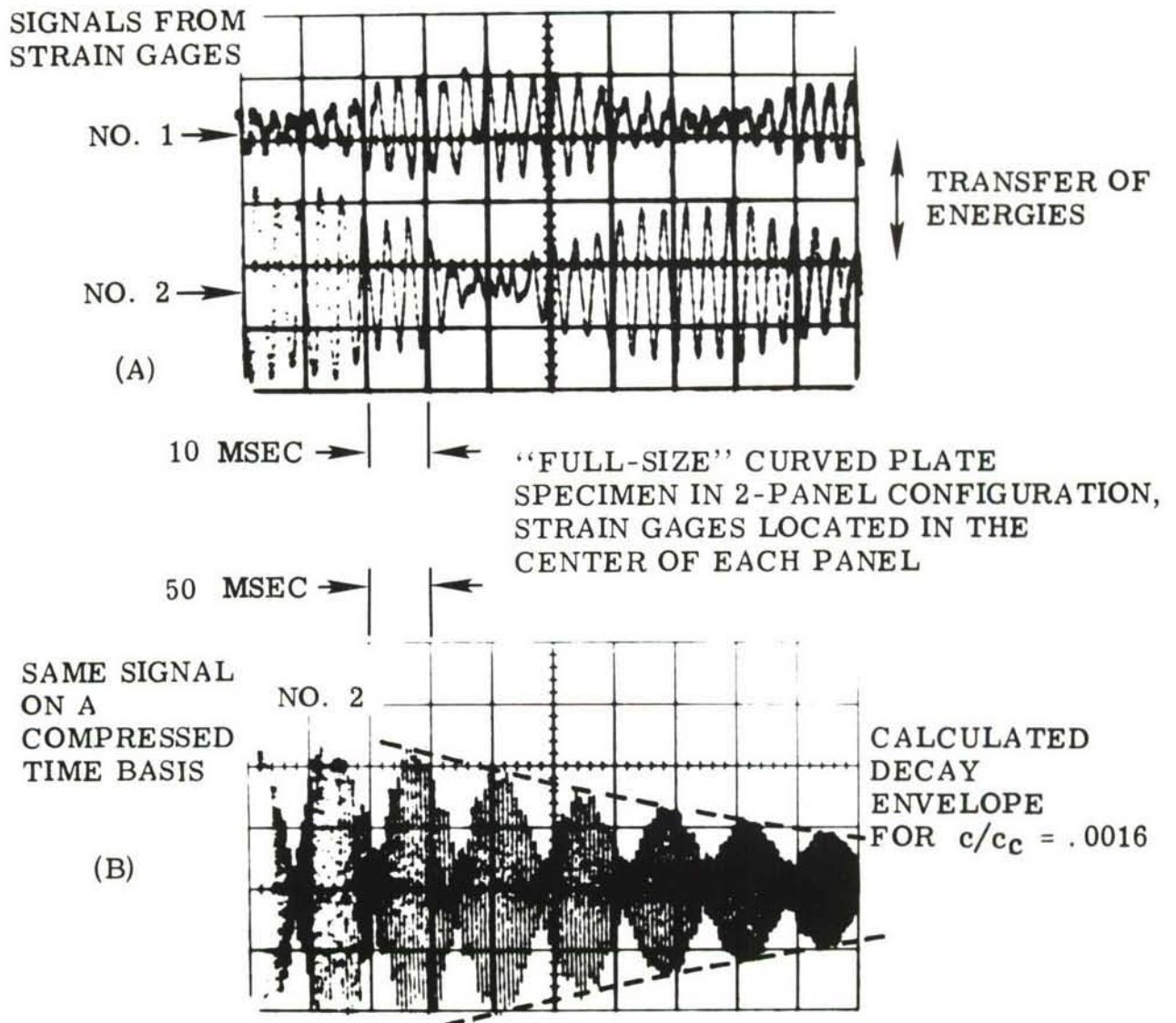
Figure 34. Decay Signals From a Curved Panel

CURVED PANEL, "5/8" SIZE IN 2-PANEL CONFIGURATION

FREQUENCY = 446 cps

STRAIN
GAGES

NO. 1 →

NO. 2 →

TRANSFER OF
ENERGY

DECAY ENVELOPE FOR
c/c_c = .0017

← 10 MILLISEC

TWO PANEL
CONFIGURATION

NO. 3 →

NO. 4 →

TRANSFER OF ENERGY
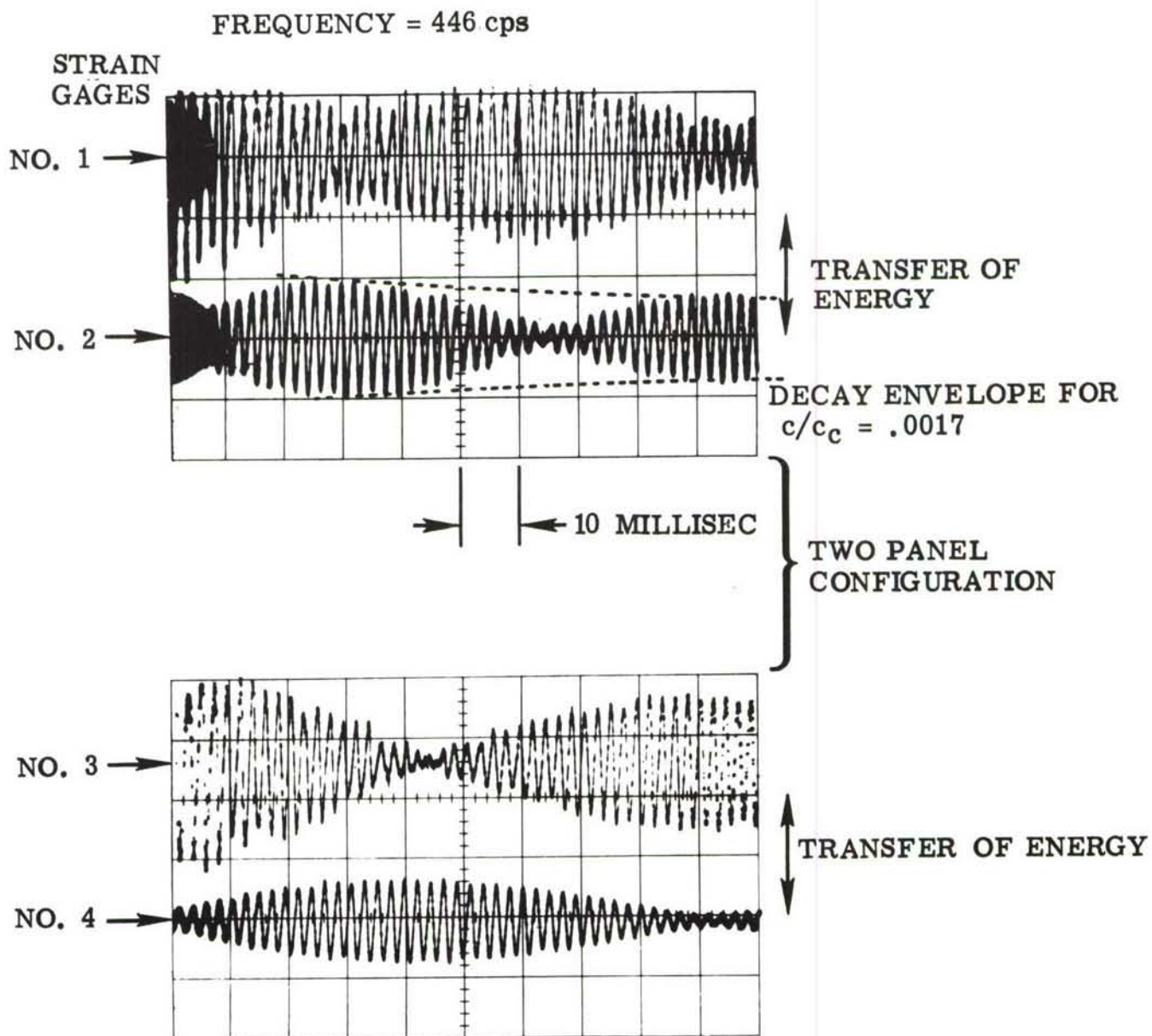
Figure 35.   Decay Signals From a Curved Panel

71
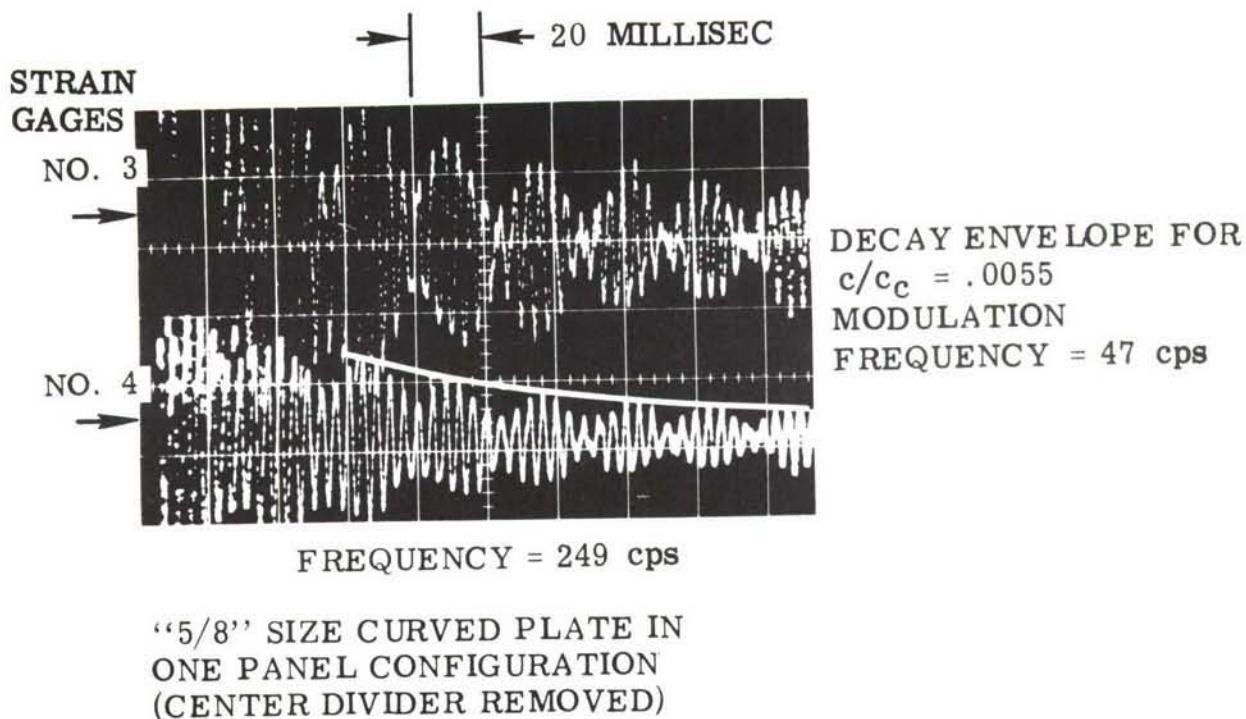
Figure 36. Decay Signals from a Curved Panel

4.1.2   Curved Plate In 1-Panel Configuration, Test Arrangement

The curved plates now measure 33 x 24.4 x .040 inches in full size
with a 36" radius on the 24.4" side, 21 x 15.25 x .024, and R = 22.5" in
5/8-size, and 13 x 9.15 x 0.024, R = 13.5 in 3/8 size. Observe that the
aspect ratios vary slightly which must be accounted for in all frequency
correlations. The test arrangement was essentially the same as for flat
plates with the exception that more strain gages were used as indicated in
Fig. 24b.

SIGNALS FROM STRAIN GAGES

(A)

← 50 MILLISEC

→ NO. 1

CALCULATED
DECAY ENVELOPE
FOR c/c_c = .0016

→ NO. 2

NATURAL FREQUENCY AT 252-266 cps

← 10 MILLISEC

(B)

PHASE OPPOSITION
AT NATURAL
FREQUENCIES

MODULATION AT
30 cps

"FULL-SIZE" CURVED PLATE
SPECIMEN, CENTER DIVIDER
CLAMP REMOVED

Figure 37. Decay Signals from a Curved Panel

73

4.1.3 Frequency Correlation in Curved Plate Modeling

The observed frequencies of the curved plates in each size are summarized in Tables IX and X together with line sketches of the vibrating element(indicated by node lines)in each configuration. From these results, the stiffening effect of curvature is calculated in terms of the ratio of its frequency to that of a flat plate of the same linear dimensions with equal mode numbers m and n. Significant agreement is obtained in the stiffening effect so defined as well as in frequency dependency on size factors. It is, therefore, indicated that modeling of stiffening effect of curvature has evidently been achieved. In the higher modes, additional comparison of current results from full-size plates with data extracted from Reference 27 is shown in Figure 38, using the product of mode numbers as a lumped argument. It appears from Figure 38 that a key is being obtained in reducing the nonlinear characteristics of stiffness in curved plates to a function of the subtended angle which is shown to be the control parameter identifying each curve. To obtain frequency modeling of curved plates, the subtended an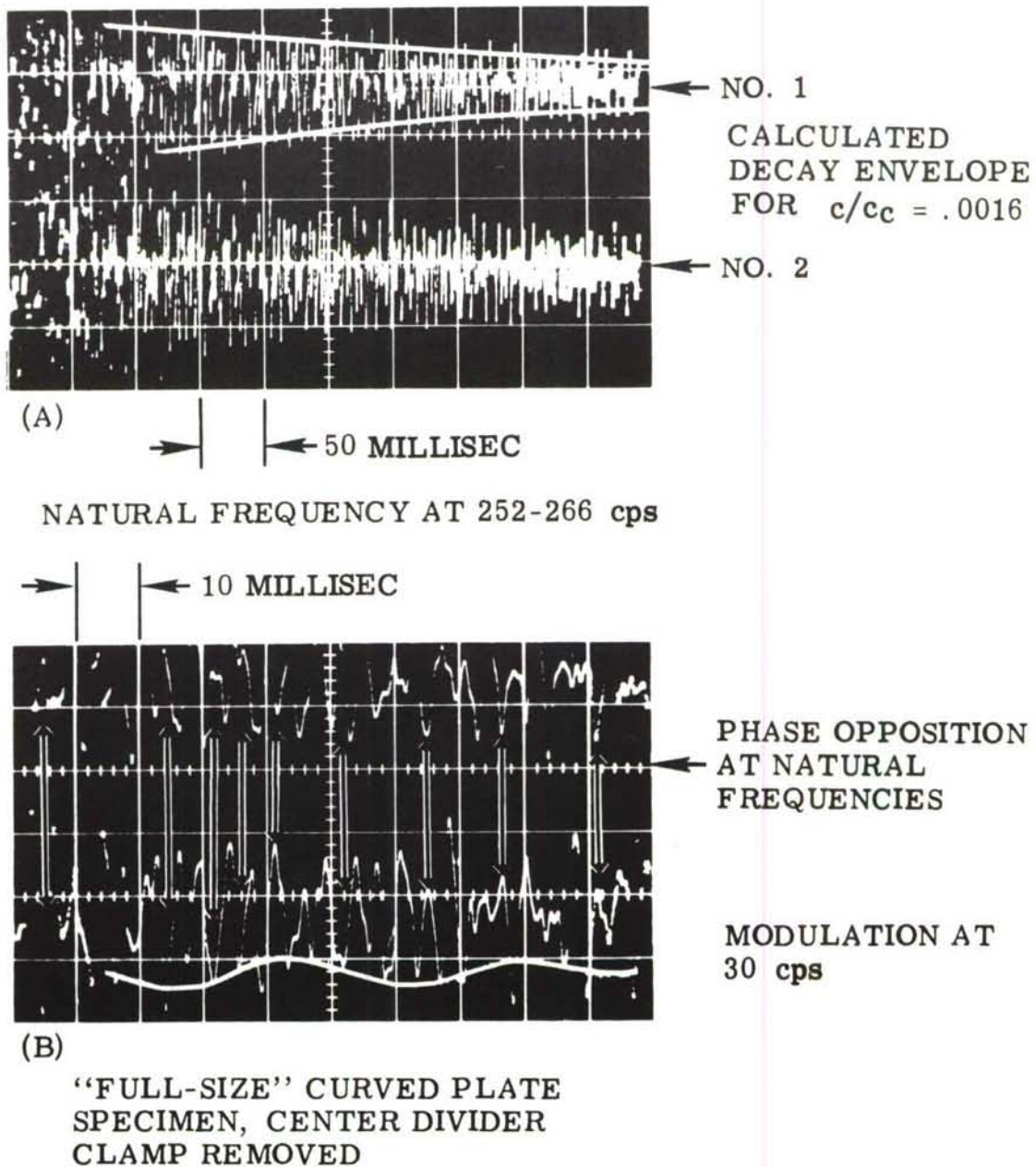gle of the curvature is, therefore, maintained constant. As in the case of flat plates, either true or adequate models may be used in other linear dimensions.

The same stiffening effect of curvature is also illustrated in the curves of Figure 39. In this case the separation distance or ratio between the calculated flat plate frequencies (determined as for Figure 23) for the plate geometric data of Table IX and appropriate curved plate data for the same mode numbers represents the stiffening effect. It is noted that when the flat plate curve for n = 1 is displaced to the right at the designated ratio of first mode stiffening as defined in Table IX so that the 1, 1 point coincides with the observed curved plate 1, 1 frequency, the transposed curve (dotted line-Figure 39) intercepts the accented lines for curved plates. Thus at the point marked F, a common condition exists where the mode could be either 2,1 or 2,3 (See Section 4.3.2) depending on the prevailing stiffening effect over an unstiffened condition at F_1 or F_3. No modes m,n lying above and to the right of this transposed flat plate n = 1 curve could be defined on the curved plates.

TABLE IX FUNDAMENTAL MODES IN CURVED PLATES
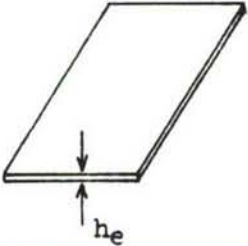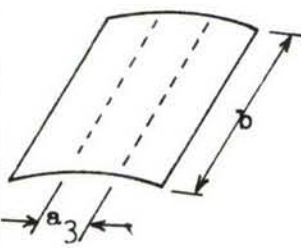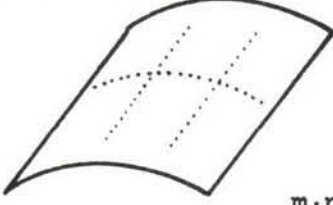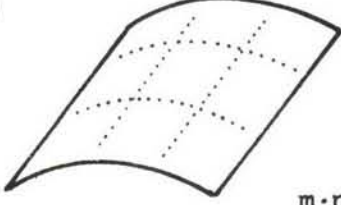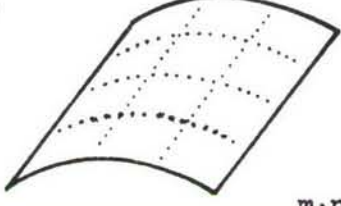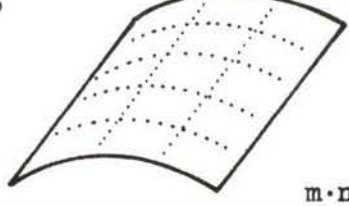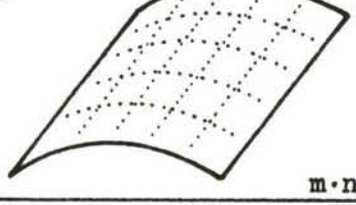
	Nominal Scale Ratio / Item	1	5/8	3/8
	Dimension's, inch Plate Thickness Long side, b Short side, a Radius, R	0.064 33.0 24.5 36.0	0.040 21.0 15.5 22.5	0.024 13.0 9.3 13.5
	Aspect Ratio b/a	1.347	1.355	1.397
Observed Frequencies, cps	Calculated flat plate in clamped edges	(29.2)	(45.3)	(74.5)
	Observed Modulation Rate (beat frequencies on curved plate)	30	50	77
	Curved Plate	153/154	249 258 260	426
	Stiffening Effect = Freq. Ratio	5.11	5.12	5.52
Equivalent Configurations	Flat Plate at Curved Plate Frequency		Maintain same outside dimensions. Increase thickness h to h_e, - $$\frac{I_e}{I} = (\text{Freq. Ratio})^2 = \frac{h_e^3}{h^3}$$	
	Curved Plate at Apparent Flat Plate Sizes		Approximation only: Consider flat plate to have 1,3 mode and determine a_3, distance between displacement nodes. Actual curved element will be bounded by stress nodes at distance a_e. $a_e < a_3$, for a slightly higher frequency.	

TABLE X HIGH ORDER MODES OBSERVED IN CURVED PLATES (FULL SIZE)

Mode Designation m, n		Frequencies		
		Flat Plate cps	Curved Plate cps	Ratio
2,3 m·n = 6		156	260	1.67
3,3 m·n = 9		182	280	1.54
4,3 m·n=12		229	338	1.48
5,3 m·n=15		278	388	1.40
4,5 m·n=20		405	540	1.34
5,5 m·n=25		465	580	1.24
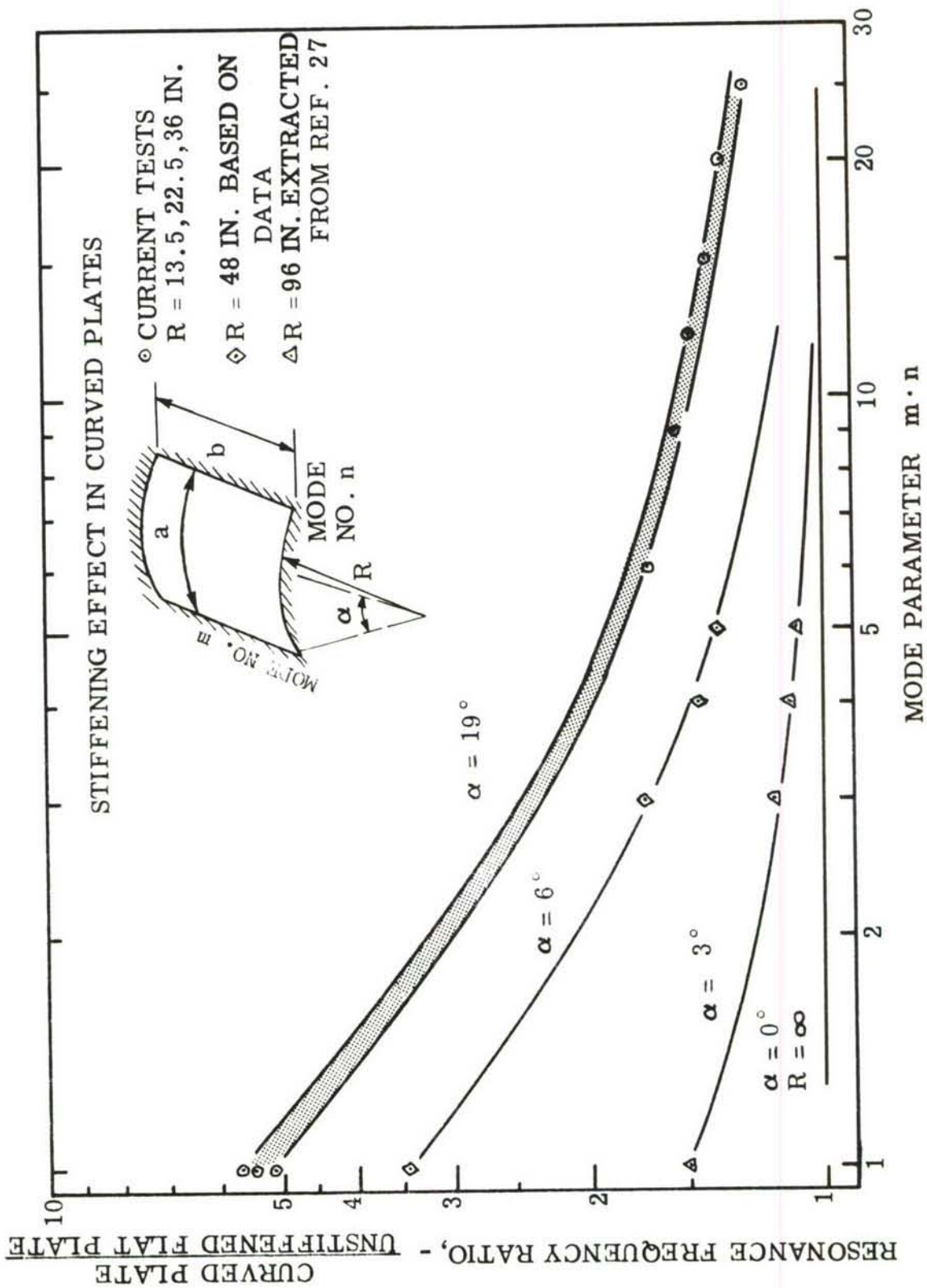
Figure 38. Stiffening Effect in Curved Plates

77
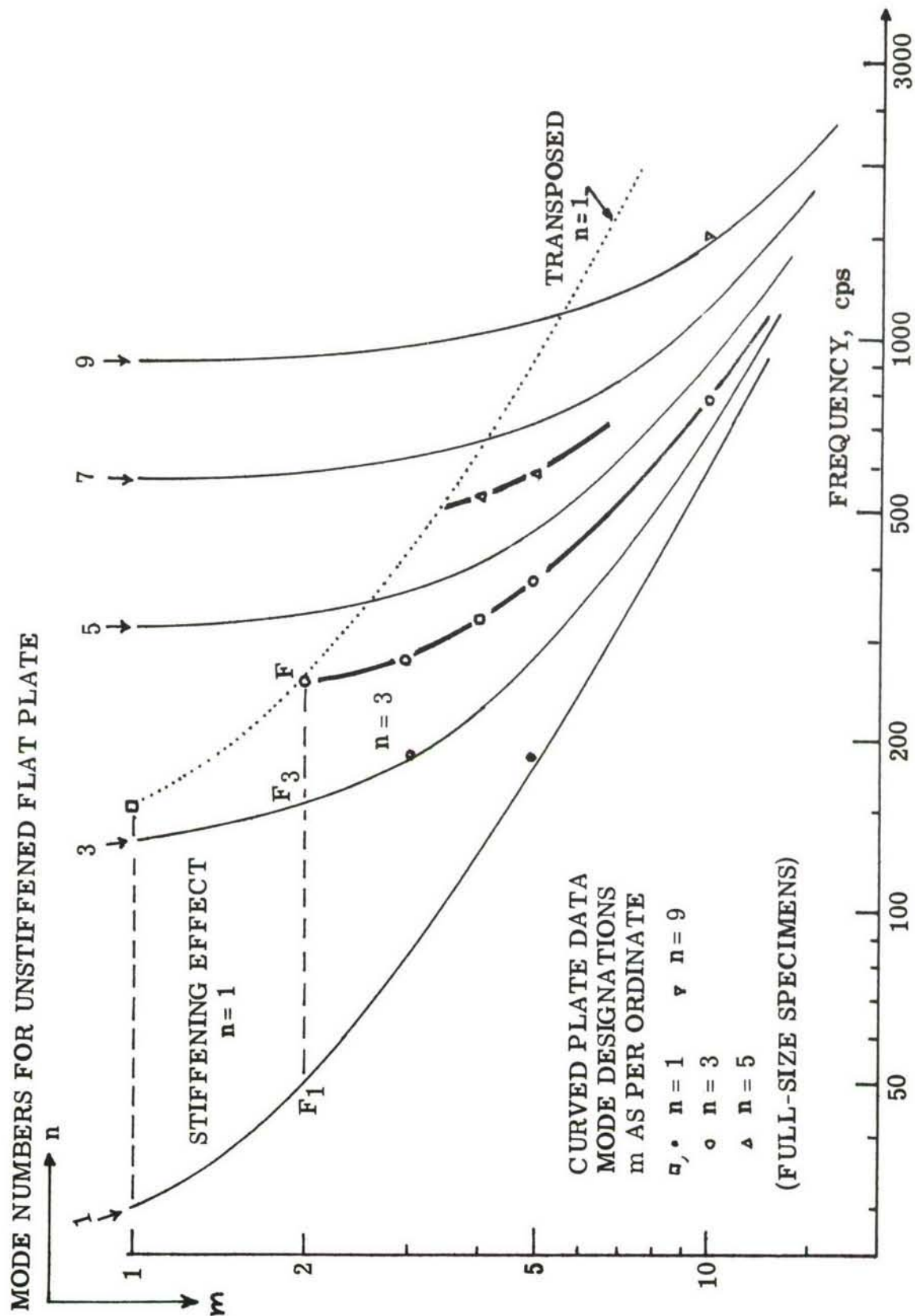
Figure 39. Resonance Frequency of Curved Plates

78

4.2   Damping Analysis in Modeled Plates

Damping coefficient ratios are derived from decay curves as shown in Figure 40 for a full-sized panel and in Figure 41 for a 5/8-model plate. In the tabulated results given in Table XI, a general agreement in first mode damping coefficients is indicated not only between plates of the same size but also between model sizes. The observation is, therefore, that all control length factors which determine the frequencies as well as damping are effectively simply supported (See Section 4.1.1).

TABLE XI   DAMPING CHARACTERISTICS IN CURVED PLATES

Mode / Specimens		1,1		2,3		3,3
		Frequency cps	c/c_c	Frequency cps	c/c_c	Frequency cps
Full Size	No. 1	(152)	---	260	---	282
	No. 2	153	0.0062	258	---	281
	No. 3	154	0.0068	260	0.002	286
5/8 Size	No. 1	249	0.0055	X		480
	No. 2	258	0.0060	X		Note: $\dfrac{480}{282} = \dfrac{249}{152}$
	No. 3	260	0.0064	X	not tested	
3/8 Size	No. 1	426	0.0030	X		
	No. 2	X	X	X		
	No. 3	X	X	X		

CURVED PANEL, FULL SIZE; NO. 2

STRAIN GAGE NO. 1
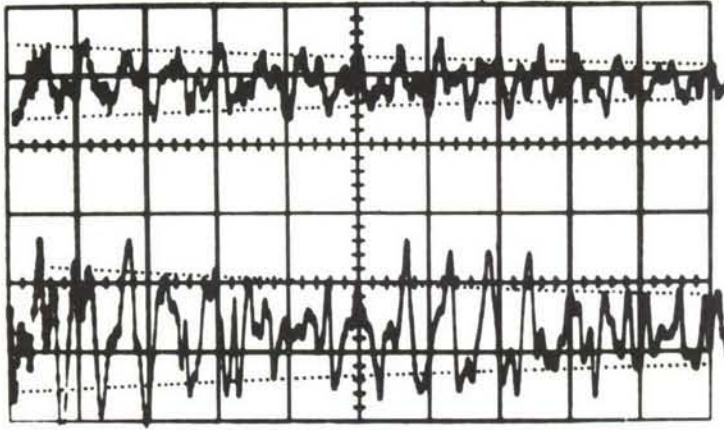
(A)

STRAIN GAGE NO. 3 |←→| 10 MSEC

SHOWING ALL SIGNALS
ARE IN PHASE AT 153 cps

AVERAGE $c/c_c = 0.0062$

FREQUENCY = 153 cps

STRAIN GAGE NO. 1
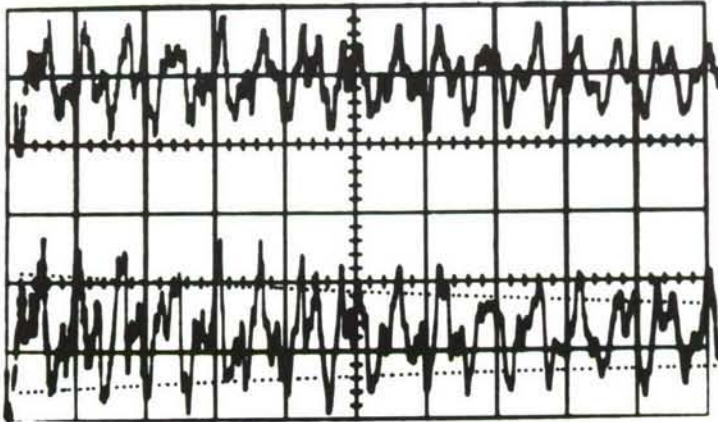
(B)

STRAIN GAGE NO. 2

Figure 40.   Decay Signals From a Curved Panel
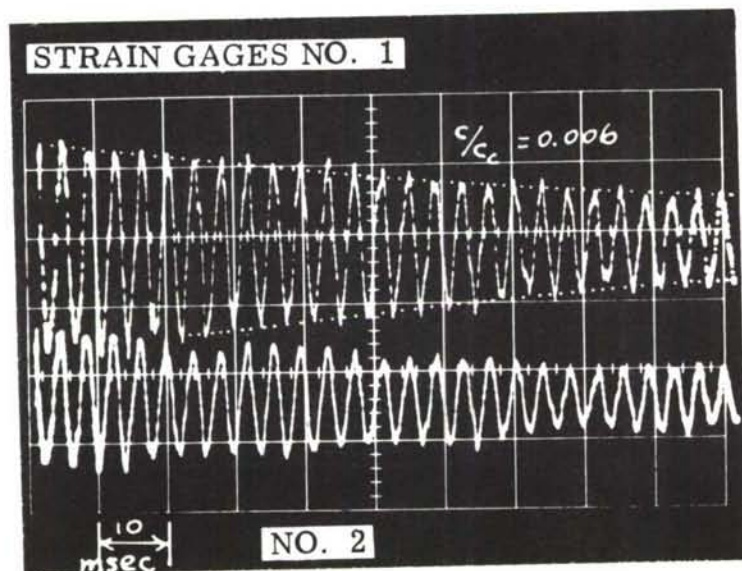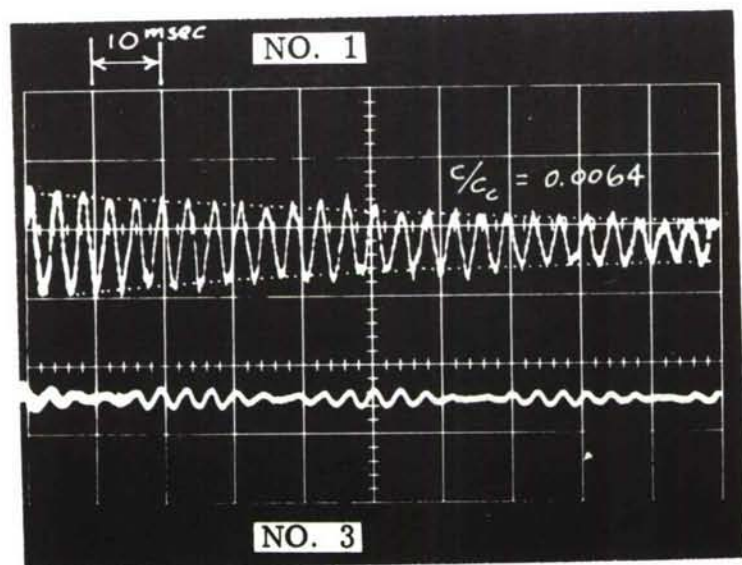
Figure 41.   Decay Signals From a Curved Panel

81

To determine the damping coefficient at a higher mode is an endeavor that has not been extensively covered elsewhere. The effort being presented below appears to yield a reasonable result but limited to only one higher mode. The procedure is shown in Figure 42. The initial step, Figure 42a, is to ascertain the decay envelope (dotted) for the first mode at 154 cps. If repeated blows of identical intensity are applied, then the same decay envelope could be transferred to Figure 42b or 42c at the appropriate time scales as noted, adjusting amplitude scales for a best fit for variances in forcing intensities. The decay envelope at the next significant mode, apparently 260 cps in this case may then be extracted from the outside traces which varied within ±10% of each other for an average c/c_c of 0.002. Compared to the damping coefficient of 0.006 at the fundamental mode, this implies a shortened control length in a numerical relationship that is compatible to the correlation determined for cantilever beams (Section 3.3.1). However, the stiffening effect is different which accounts for the relatively low frequency in the higher mode.

4.3   Stress Correlation Between Models

4.3.1   First Mode Response

The observed data for the fundamental mode are shown in Figure 43 in the form of stress variations at various sound pressure levels for which separate scales are provided for each panel size in order to show the curves in the same figure. A significant difference exists between the respective ratio of the stresses at the edge and at the center. A change in mode shape had occurred which could be attributed to the curvature size. For the apparently different behavior in the modeled plates, additional data must be obtained in an extended dissertation. The following analysis can be based, however, on the center stresses which were the dominant readings in all specimens tested.

In the modal analysis of Table IX it has been shown that the curvature effect is to raise the first mode resonance of a reference flat plate of the same dimensions by a particular stiffening ratio. A simple approach in stress analysis is to calculate the maximum bending stresses in the flat plate and convert it to curved plate stress by considering the same stiffening effect as a corresponding change in the moment of inertia,-stiffened as it were and raised in magnitude by the square of the frequency ratio.

For example, under a static peak pressure p, the equation of bending stress in an unstiffened plate is:

$$S_f = \beta p \ (a/h)^2,$$

and for the stiffened or curved plate,

$$S_c' = \beta p \ (a/h)^2 \ \frac{I_f}{I_c} = \beta p \ (a/h)^2 \ (\text{Frequency Ratio})^{-2}$$

STRAIN GAGE NO. 1
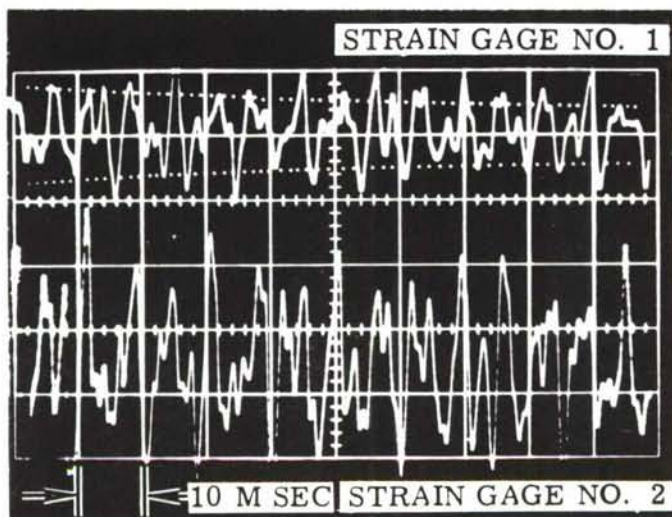
FULL-SIZE CURVED PANEL
NO. 3

FREQUENCY = 154 **cps**
c/c_C = .0068

(A)

MODULATION DUE TO OTHER
MODES, 260 **cps** ETC

10 M SEC STRAIN GAGE NO. 2

STRAIN GAGE NO. 1

(B)

0.1 SEC STRAIN GAGE NO. 2
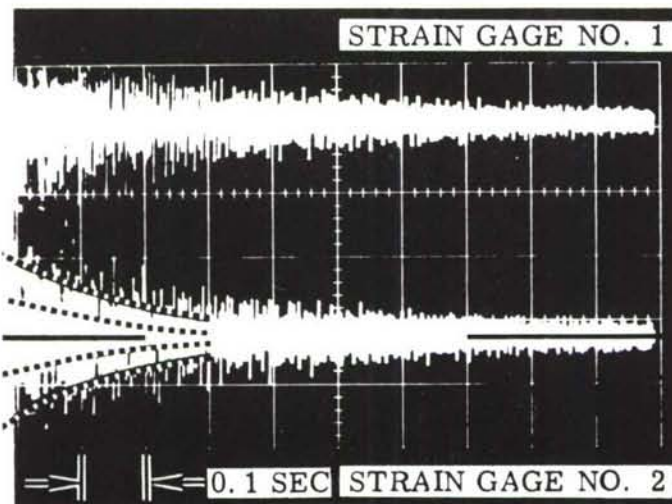
AVERAGE c/c_C = .002
FOR 260 **cps** MODE
(DECAY AMPLITUDE
EXCLUDING 154 **cps**
ENVELOPE)

0.2 SEC STRAIN GAGE NO. 1

STRAIN GAGE NO. 2
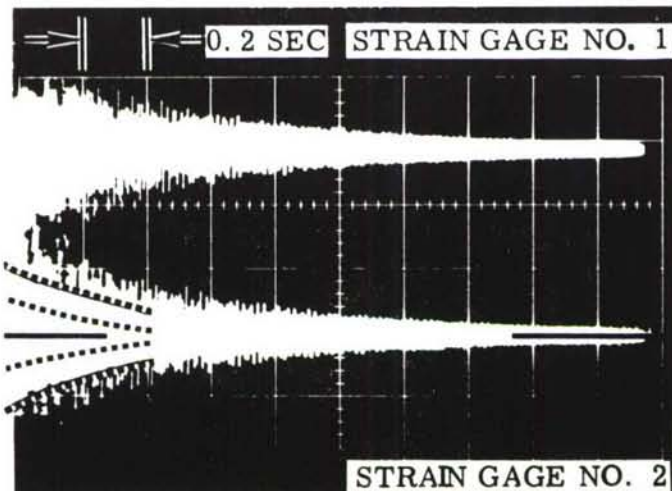
Figure 42. Decay Signals From a Curved Panel
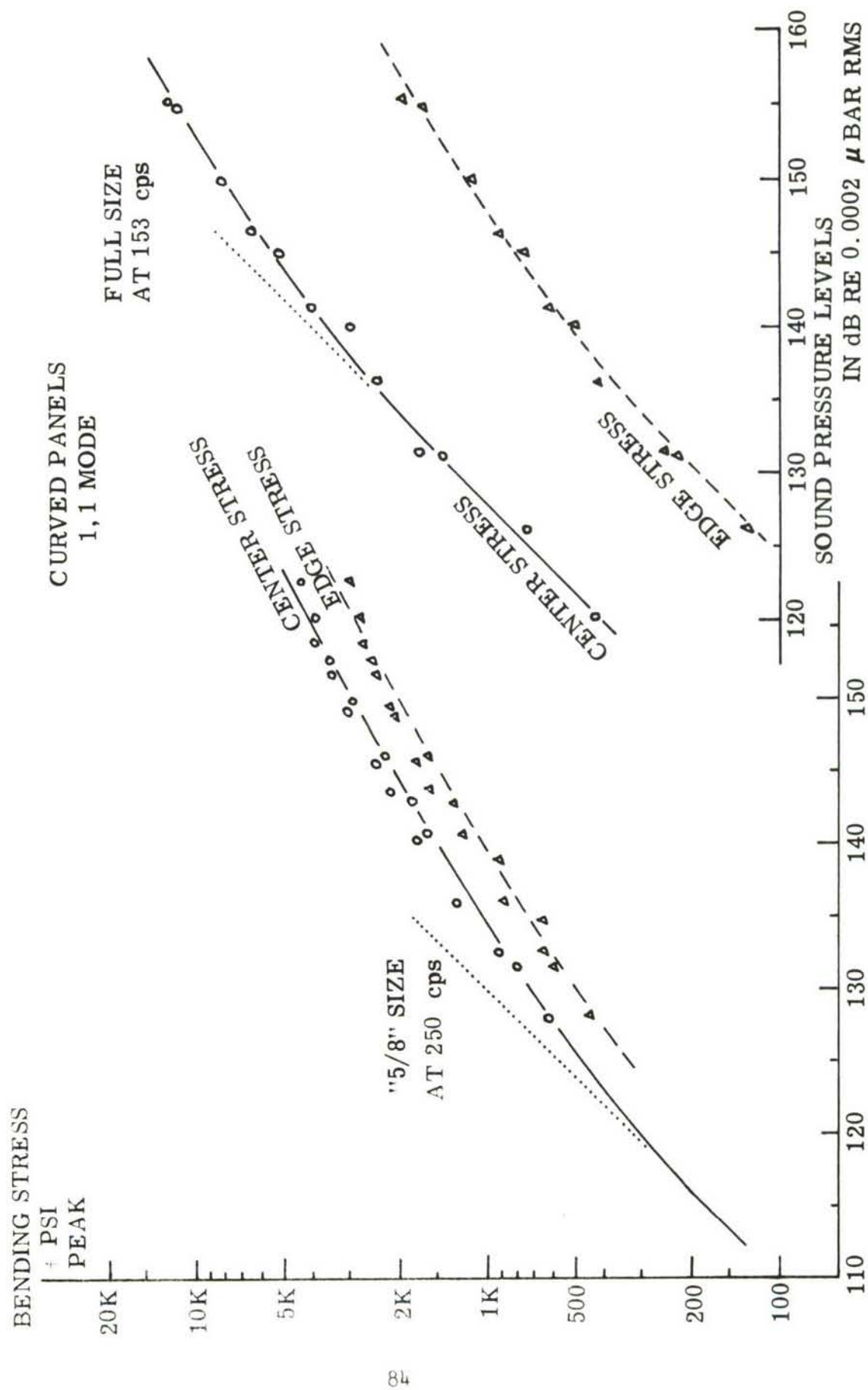
Figure 43. Vibratory Stress in Curved Plates

The peak dynamic stress to which equation (A3) in Appendix A also applies, is simply this same (static) bending stress multiplied by an amplification ratio and becomes a modeling criterion. Thus at 120 dB, p = 0.0042 psi peak for the fundamental mode, the moment coefficeint at the location and orientation of the relevant strain gage is 0.0349 (See Appendix A) and the bending stress coefficient is 0.21 (= 6 X 0.0349).

	Full-Size Panel	5/8-Size Model

Full-Size Panel

β = 0.21
a = 24.5 inches
h = 0.064 inch
c/c_c = 0.0065

Frequency Ratio = 5.1

Calculated Stress = 495 psi

Observed Stress = 450 psi

5/8-Size Model

β = 0.21
a = 15.5 inches
h = 0.040 inch
c/c_c = 0.006

Frequency Ratio = 5.4

Calculated Stress = 455 psi

Observed Stress - 450 psi

The agreement confirms the large reduction of bending stress in a curved plate due to the stiffening effect. At a sinusoidal excitation level of 150 dB, a maximum stress of 10,000 psi is indicated which would be far short of reaching fatigue within a reasonable test period.

4.3.2   Response in a Higher Mode, Full-Sized Panel Only

In the following illustration, it is intended to demonstrate that a calculated stress is in ready agreement with an observed value if the stiffening effect is predetermined.   The fatigue expectancy can then be   simply reckoned on the basis of known material properties expressed in constant amplitude S-N curves.

The observed data in the next higher mode at 260 cps for the full size plate are given in Fig. 44. The mode may be designated either as 2,3 or 2,1 depending on the strength of the principal stress. Referring to Fig. 39, the 2,1 mode would be reckoned along the dotted line curve drawn for the stiffened flat plate as a complete unit. If the elements between node lines are considered individually, the controlling length factor becomes b/2 which is now the shorter dimension. Referred to an unstiffened flat plate, the same mode may also be the 2,3 mode stiffened to the accented solid line for the curved plate. In the latter case, there are two displacement nodes within the outside edges and the middle strip may be singularly considered as a flat plate element stiffened to a lesser degree at a parametric mode number m·n of 6 formulated in Table X and in Fig. 38. The control length becomes merely a fraction of a.

The stress analysis follows, - c/c_c = 0.002 (See Fig. 42 for full-sized specimens only, in 2,3 mode- where the central portion vibrating as an element measures very nearly 7" long on the shorter dimension.)
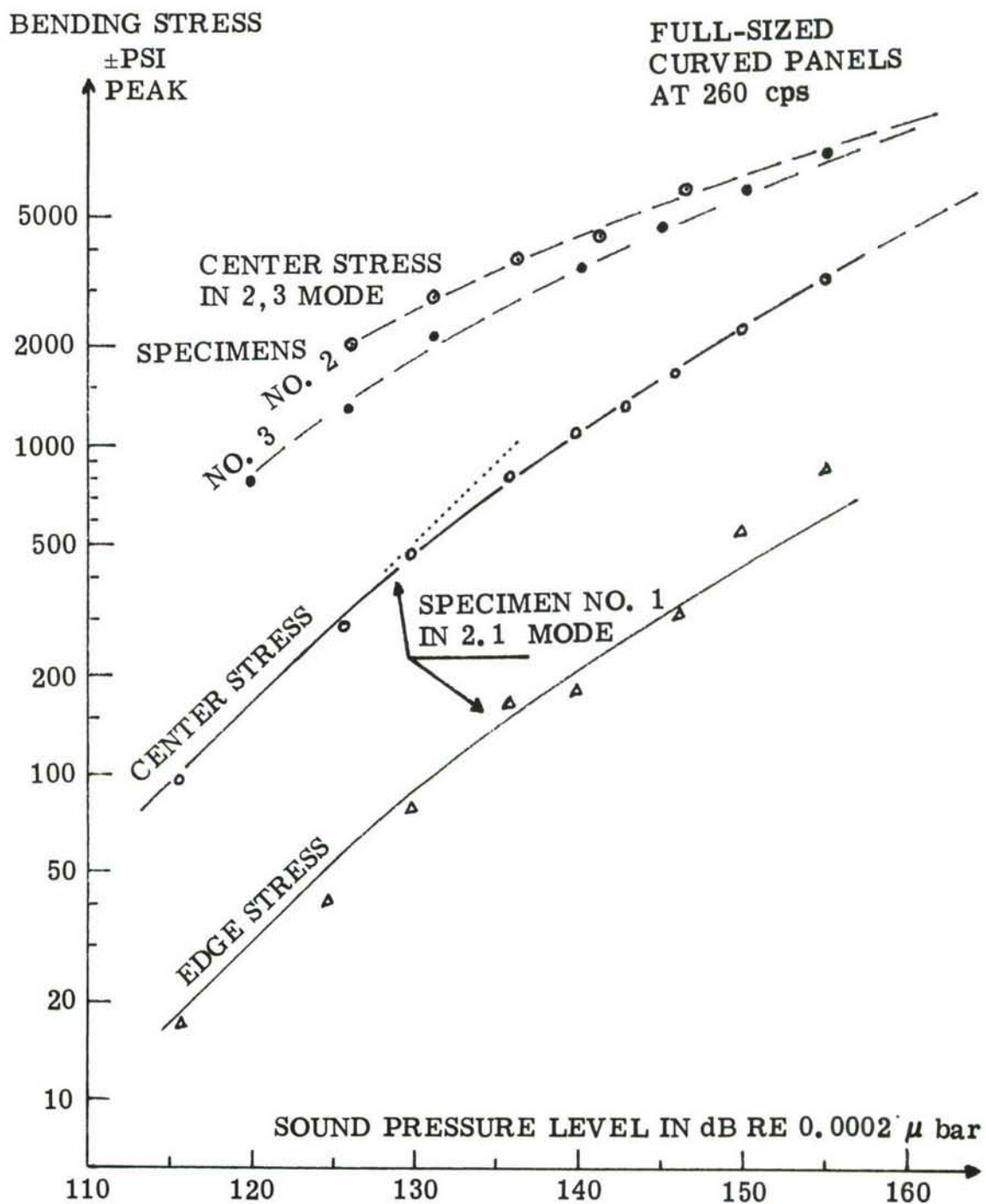
Figure 44. Vibratory Stress in Curved Plates

$S_f = \beta \, p \, (a/h)^2; \; - \quad \beta = .73 \quad a = 7$ displacement node distance

$\quad\quad\quad\quad\quad\quad\quad\quad\quad\quad a_3 = 7 \times .55 = 3.9$ stress node distance

$\quad\quad\quad\quad\quad\quad\quad\quad\quad$ (between the inflexion points of a clamped beam)
The factor 0.55 for determining the inflexion point distance is obtained from
Reference 13. The effective aspect ratio for this mode component is
24.5/3.0 or larger than 6. The bending stress coefficient as listed in
Appendix A is 0.73. Stiffening ratio = 1.67 (from Table X)

At 120 dB sound pressure level,

$S_c = (0.73)(0.0042)(3.9/0.064)^2(1/1.67)^2(1/0.004) = 1020$ psi peak

Against this value, the observed readings from two specimen panels
were 1350 and 760 psi averaging 1055. The analytical value is, therefore,
reasonable.

On the other hand, if the mode was 2,1 the calculated maximum stress
would be: - at a stiffening ratio of 5.1 (from Table IX) in frequencies
and an approximate stress coefficient $\beta = 0.57$ which is averaged from
the nearest end conditions listed in Appendix A.

$S_c = (0.57)(.0042)(16.5/0.064)^2(1/5.1)^2(1/.013) = 470$ psi

Against this, the observed reading from the third specimen was only
160 psi. This is in fact expected because the maximum stress location in
this case would be at the center of the short side and not at the actual
gage location. Using appropriate coefficients from Reference 24 or 25, the
corrected bending stress at the center of the short side should be close to
three times the observed value at the center of the long side. The resulting
stress at 480 psi would then compare very favorably with the calculated
result.

The observation can now be made that in curved plates, an additional
degree of freedom is available in the stiffening effect. In the above
illustration, the 2,3 mode dominated in two specimens and 2,1 mode dominated
in a third. Due to the reduced stiffening, the maximum stress in the 2,3 mode
is higher than in the 2,1 mode as data so indicated. However, as excitation
forces are increased at higher sound pressure levels, the plates would tend
to be stiffer by virtue of inherent hard-spring characteristics; and mode
2,3 improves to 2,1 but the stress either decreases by comparison or changes
nonlinearly. Under this condition no fatigue due to bending stress can occur
within a reasonably long test period.

4.3.3   Changes in Still Higher Modes

Two of the higher modes were observed at 283 and 338 cps for the full-
sized specimens with composite curves shown in Figs. 45 and 46. The results
indicate that as excitation pressures are raised, the maximum stress
increases nonlinearly in a general sense as both the mode complexity and
the stiffening effect vary simultaneously. Thus one mode may appear to be
more linear than another without necessarily having a nonlinear spring rate

BENDING STRESS
±PSI PEAK

FULL-SIZE CURVED PANELS
STIFFENED 3, 3 MODE
AT 283 cps
CENTER STRESS

SOUND PRESSURE LEVEL IN dB RE 0.0002 μ bar
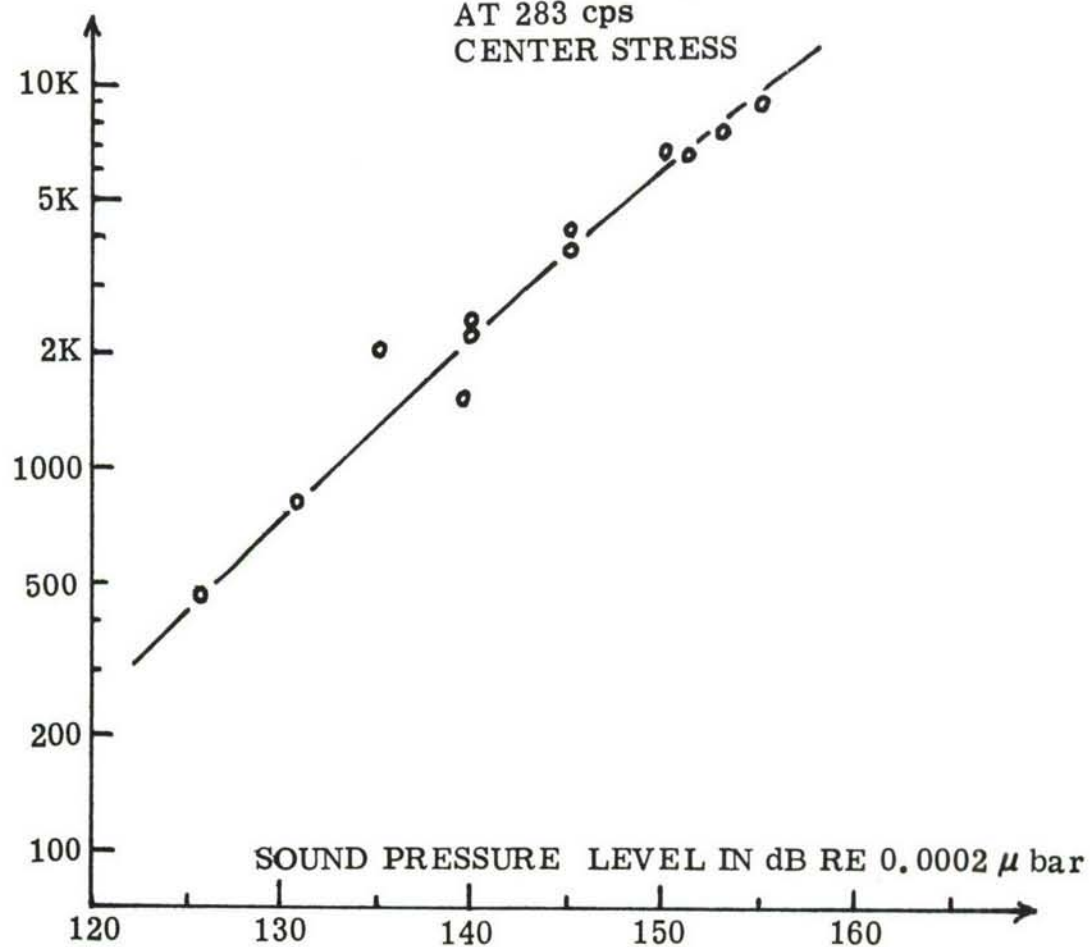
Figure 45. Vibratory Stress in Curved Plates
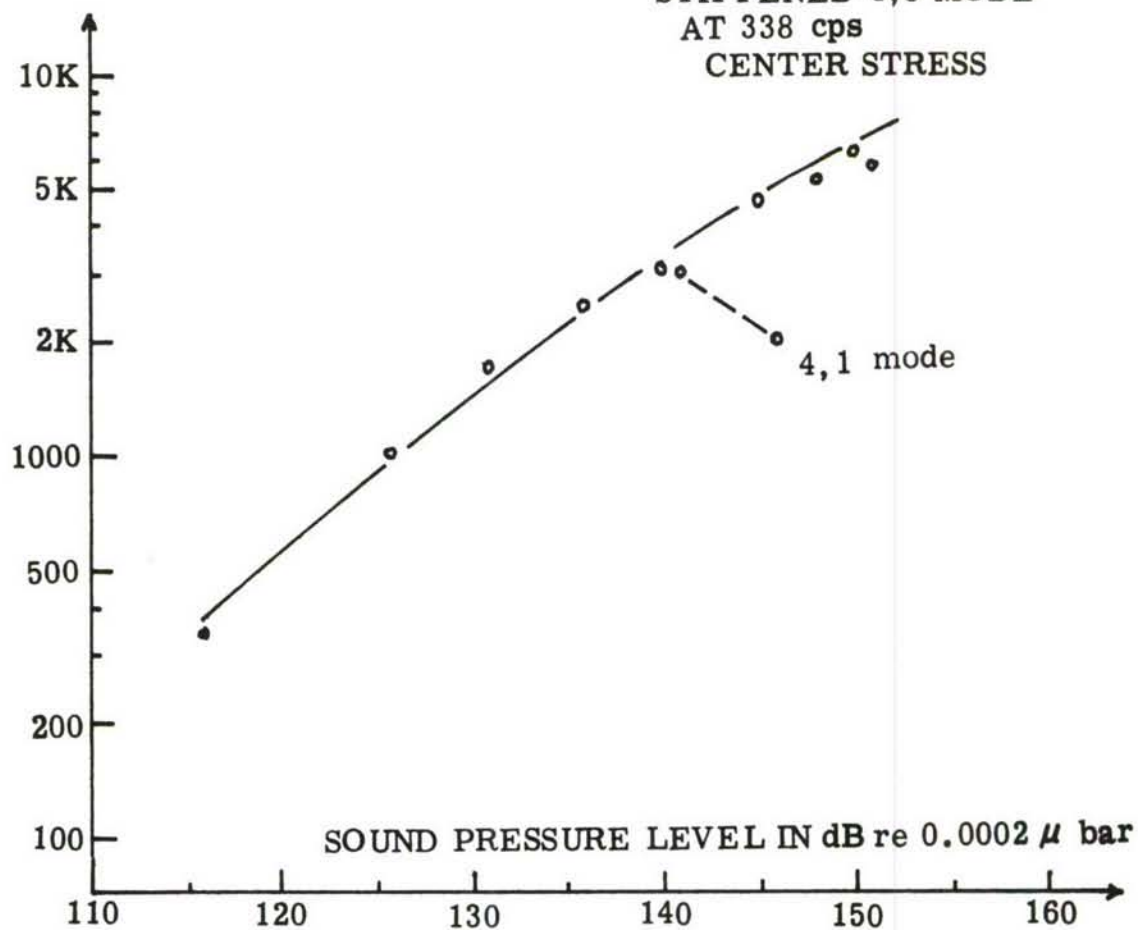
Figure 46. Vibratory Stress in Curved Plates

in either. By superposing Figures 45 and 46 for these two modes over
Figure 44 for another mode, it is observed that the peak amplitudes appeared
to be approaching a common limit at about 155dB.   The implication is
that at high acoustical intensities, many modes exist at the same time, with
amplitudes limited in each component mode and apparent nonlinearities
attributable to the presence of many modes. The possible potential for
mode improvement (i.e., altering the primary response mode) with
increased stiffening effect giving reduced stress is found in one of the
three specimens tested as shown in Figure 46 at 141 dB. In changing from
4,3 to 4,1 mode, the principal component was sub-harmonically excited in
the form of low amplitude modulations carrying highly enriched harmonics
at 4,3 mode frequencies. Indeed in many other modes, frequent up and
down changes in response amplitudes were of this nature.

One other example of such mode improvement is provided in the wave-form
analyses given in Fig. 47 for a full-sized specimen. Depending on the
specific strain gage signal of reference, many concurrent mode components
can be identified. Fig. 47a shows a good resonance condition at 156 dB for
a nominal 5,3 mode at 386 cps, with some second harmonic component at 772
cps but little modulation at 193 cps as a subharmonic. However, at 141 dB
in Fig. 47b, considerable noise is generated at 194 cps due to the un-
stiffened flat plate response in the 4,1 mode. Insignificant strain in-
dications are shown at 194 cps. Returning to 156 dB again, Fig. 47c shows
the enriched harmonics of 193 cps, identifiable as a subharmonic of no
less than five different modes existing simultaneously in the response.

4.4 Response to Random Excitation

With a specimen retained in the test fixture, discrete frequency excita-
tion was replaced by random signals of limited bandwidth. The spectrum
analysis of this signal is shown at the top of Figure 48a which indicates
that the bandwidth extended essentially from 60 cps to 500 cps with a
moderate amount of extraneous high frequency noise presumedly caused by
the accompanying airflow. The amplitude distribution in terms of rms
sound pressures was ascertained by means of a probability density analyzer
in conjunction with an X-Y recorder. The result shown in Figure 49 con-
firms the normal distribution assumed in the theoretical analysis by Miles
and many others whose solutions were introduced in Section 2. The spec-
trum analyses of all five strain gages in use are shown in Figures 48a and
48b recorded through 1/3-octave band filters.

Significant indications in support of the analyses presented in
References 6 and 19 may be obtained from these random response data. For
the condition of equivalent rms stress, the deduced requirement is that a
sinusoidal excitation level should be in excess of the random spectrum
level by ΔdB_1, expressed as

$$\Delta dB_1 = 2 + 10 \log \Delta f, \text{ where } \Delta f = (c/c_c)(2f_r) \text{ for each resonance mode at frequency } f_r$$

The observed results based on the maximum stress are given in Table XII,
along with the calculated results obtained from the above expression for
the two modes indicated.

90
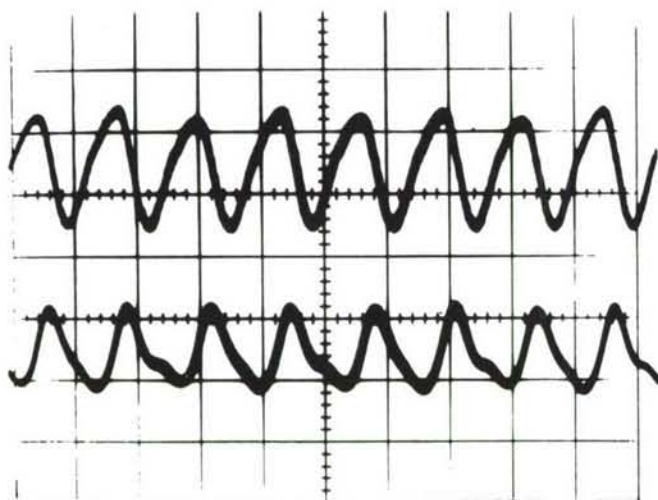
Microphone Signal
156dB At 386 cps
Curved Plate
Response = 5, 3 Mode

Strain Gage No. 5
Showing 2nd Harmonic at 772 cps
For 10, 3 Mode Component

(a)
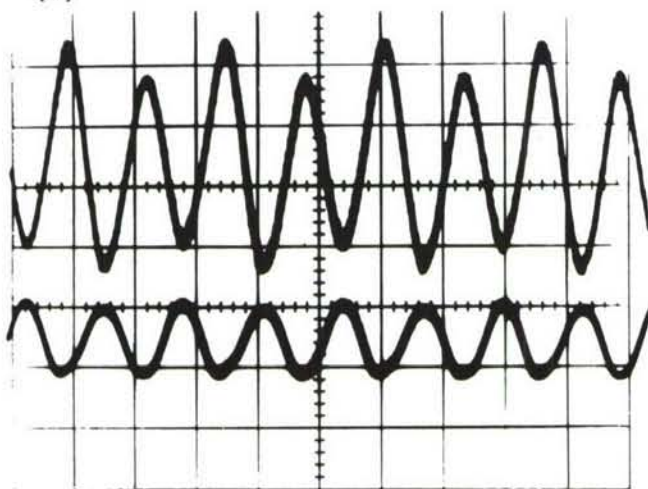
Microphone Signal
141dB At 388 cps

Curved Plate Response = 5, 3 Mode
But Generating Noise At 194 cps

Strain Gage No. 3
Showing Weak Modulation At 194
cps , - A Flat Plate 3, 3 Mode

(b)
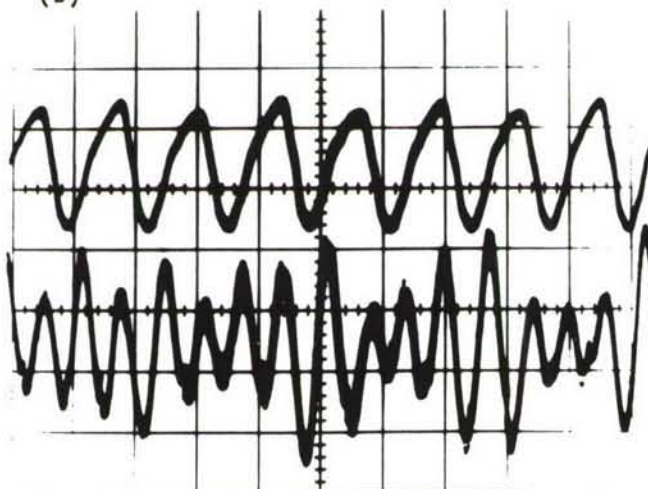
Microphone Signal
156dB At 386 cps

Curved Plate Response = 5, 3 Mode

Strain Gage No. 1
Mode Complexities

Flat Plate 3, 3 Mode At 193 cps
Curved Plate 5, 5 Mode At 579 cps

(Coupled Into 5, 3 Mode With
Phase Oscillations)

Curved Plate 10, 3 Mode At 772 cps
Curved Plate 10, 9 Mode At 1544 cps

(c)

Figure 47.   Characteristics of Response Waveforms
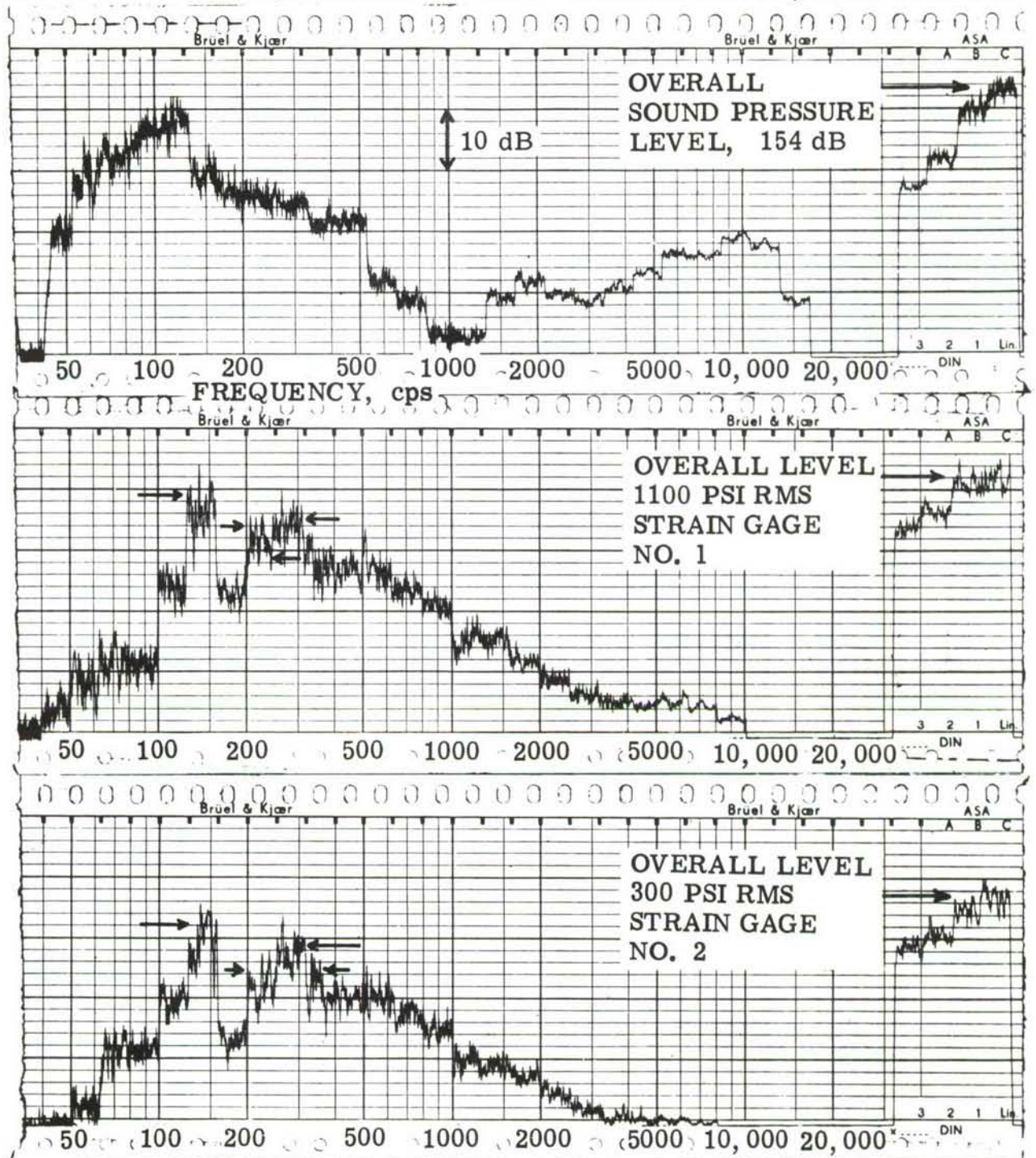
Figure 48a.   Spectra of Random Noise and Response
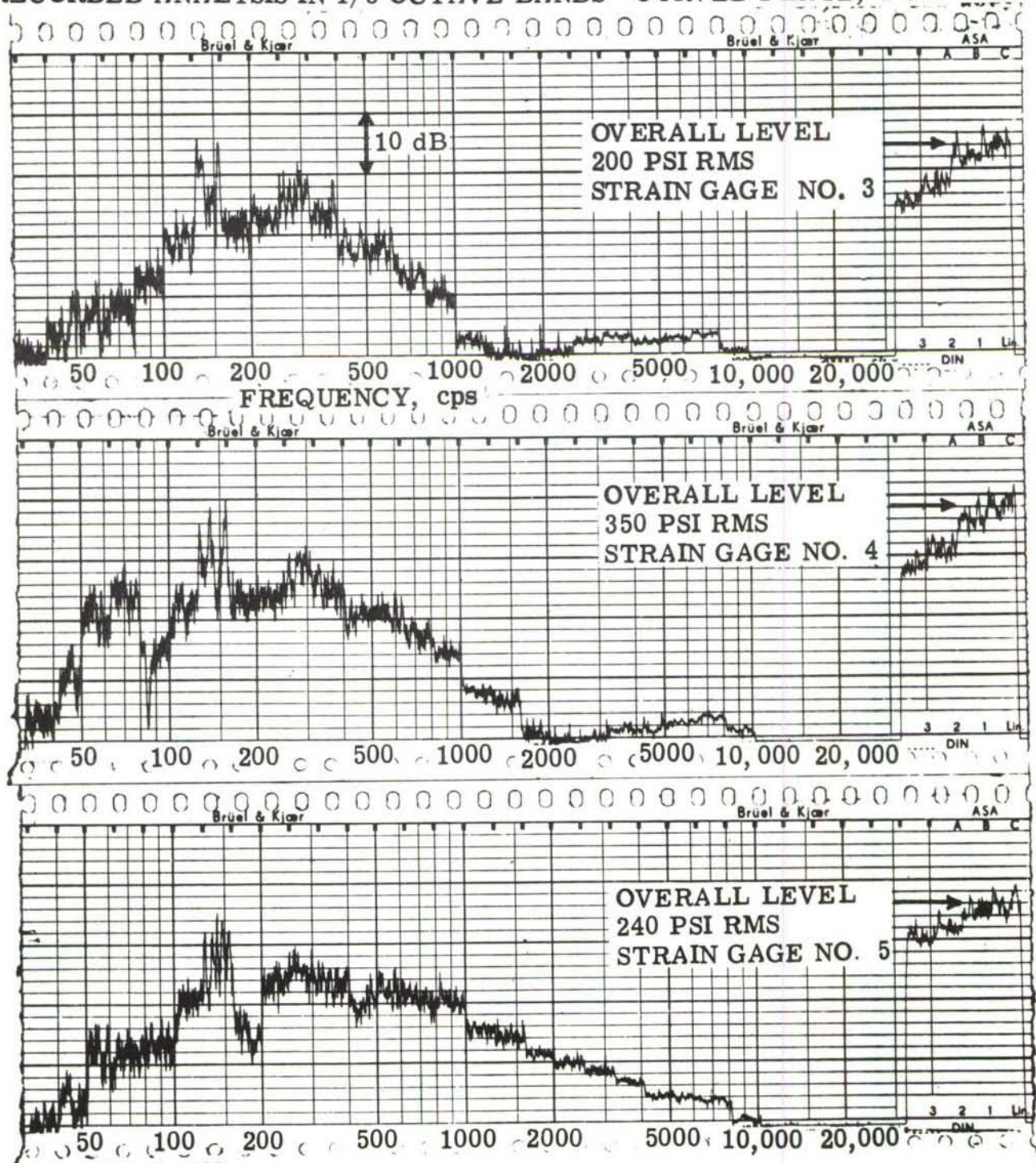
Figure 48b.   Spectrum Analysis of Response

93
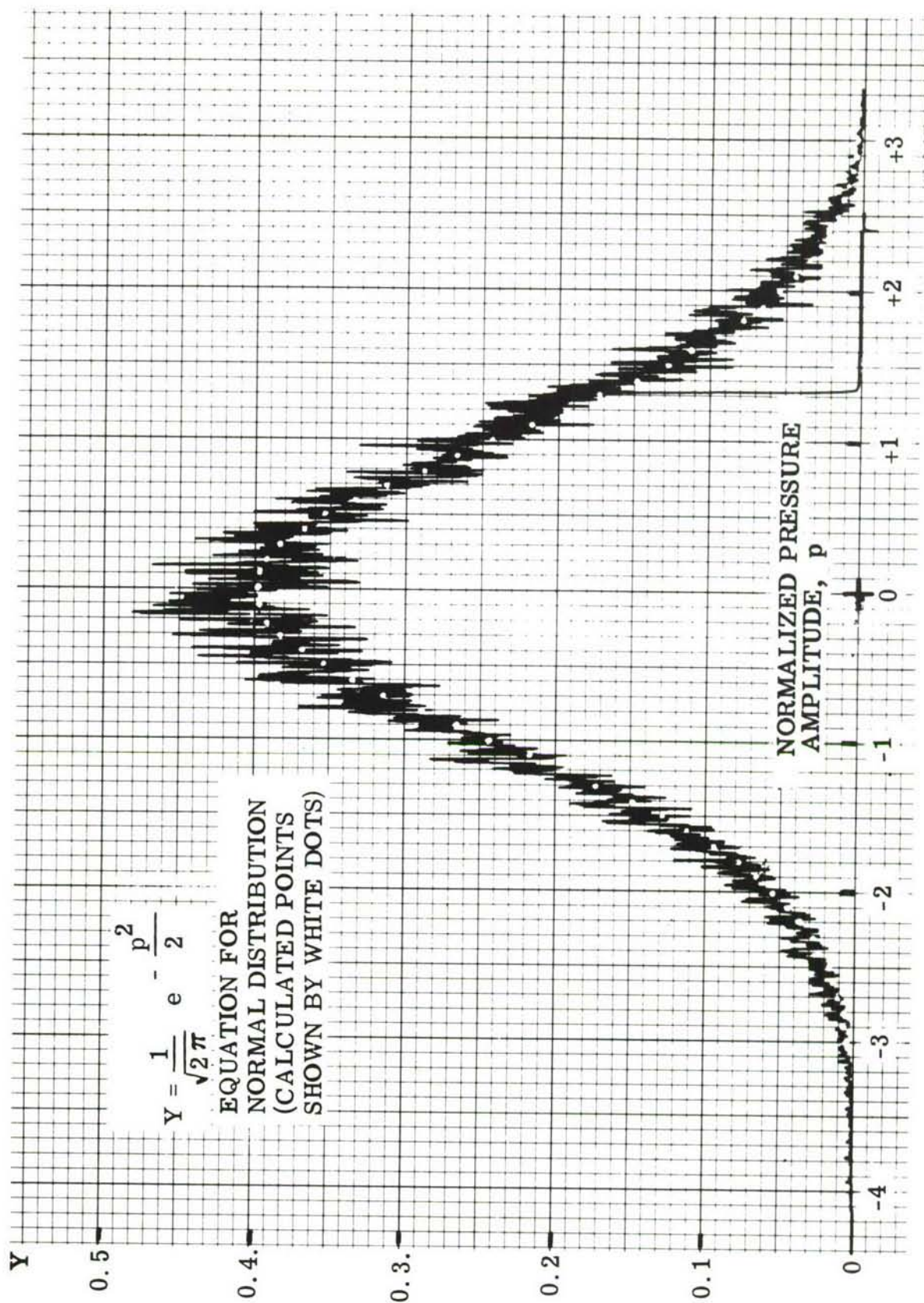
Figure 49. Probability Density of Acoustical Pressure Amplitudes

94

TABLE XII RANDOM - SINUSOIDAL EQUIVALENCE

RANDOM EXCITATION				SINUSOIDAL EXCITATION for SAME rms STRESS RESPONSE			
1/3 Oct. BAND cps	BAND LEVEL dB	SPEC-TRUM LEVEL dB	STRESS READ-ING ± psi	SOUND PRESSURE LEVEL dB	EXCESS over RANDOM SPECTRUM, ΔdB_1		MODE FREQUENCY cps
					Obs.	Cal.	
140/180	141	125	780	129	4	5	154
224/280	139	120	440	121	1	2	260

The agreement in ΔdB, obtained here, is within 1dB. However, larger variations are not intolerable. The calculation of spectrum levels in random analysis in the first place incurs uniform averaging in the bandwidth concerned and is not generally a precise indication. Secondly, a permissible variation in the damping coefficient ratio can easily absorb this difference. At higher modes, the second factor alone becomes increasingly large numerically.

Insofar as random fatigue is concerned, it has already been indicated (Section 2.4 and Fig. 4) that the sinusoidal equivalent stress level, or sound pressure level must be in excess of an equivalent level for equal stress by ΔdB_2 ($= 10 \log \alpha/e$) if failure time is to be reproduced. ΔdB_2 can be added to ΔdB_1 for fatigue considerations.

Another significance cannot be allowed to pass unnoticed. In Figures 48a and 48b considerable amplitude changes occur in the strain gage indications within the 140/180 cps band. The implication is that the fundamental mode at 154 cps in this case has a tendency to disappear or not be excited. This is advanced as an explanation of why this particular mode was overlooked in one out of three specimens tested. In any event the stress analyses here readily establish that the expected stress in a fundamental mode of curved plates may not be produced. At the same time the maximum stress occurring in any one of many higher modes is very much lower than the first mode stress. The frequency and stress magnitude depend on which of the higher modes dominated the response amplitude. Unless the thickness of the modeled plates of this program were further reduced, a fatigue duration test would not be justified.

5. DISCUSSION

5.1 Vibratory Modes and Stress Response Related to Fatigue

While the experimental results presented in Sections 3 and 4 indicated satisfactory correlation in the parameters governing the response of the specimens tested, either as individual elastic units or as modeled components, the attainment of long term fatigue remains dependent on the magnitude of the stress induced by the acoustical forces applied. In this respect, the proven strength obtained in a shorter duration, even though at a mechanically recreated cyclic stress, also correlated with existing data of acoustically induced fatigue for the same plate material in simple geometric configurations. The problem is reduced to defining the vibratory modes prevailing in whatever configuration is being investigated whereby the induced stress can be predicted for known fatigue expectancy. From the test results obtained significant factors in the purely geometrical dimensions have been found which greatly modified the modes obtainable in an acoustical environment and accounted for the stress reductions observed. For this discussion, the basic equations of motion in a linear response may be utilized.

Considering a vibratory particle in any beam configuration restricted to one degree of freedom, in equation A4, Appendix A,

$$\frac{d^4 y}{dx^4} + \frac{\rho A y \omega_r^2}{EI} = 0$$

the implied condition is a simple bending phenomenon. Insofar as the deflection y is linearly related to the forcing intensity p, the frequency solution of ω is independent on the amplitude of y. In most cases, the acoustically applied pressure, p is essentially uniform over the entire configuration whose linear dimensions are significantly less than the wave length of the acoustical forces at mode frequency ω. A convenient constant λ is given in Reference 13 from which ω can be calculated; thus:

$$\lambda_r^4 = \frac{\rho A \, \omega_r^2}{EI}$$

and $\lambda_r \ell$ = a constant for a given configuration and boundary conditions,

where ℓ is a significant length factor. For a uniform plate of rectangular configuration, the frequency f_r in the m,n mode is reduced to $f_r = C h / a^2$ where C is the dimensionalized constant given in Fig. 5, for unity modes m and n. For simply supported square or rectangular plates, C is unchanged whenever m = n. The resulting mode frequencies are shown in Fig. 50 with substantiating data from Reference 28. Some energy loss to the supporting frame due to friction is indicated in the slight reduction in frequency. This frequency reduction becomes progressively negligible in higher modes. In a log-log plot, the idealized relationship for no energy loss follows the calculated line and is unaffected if the mode number m is converted to a normalized length factor A, inverted in the figure for convenience to indicate
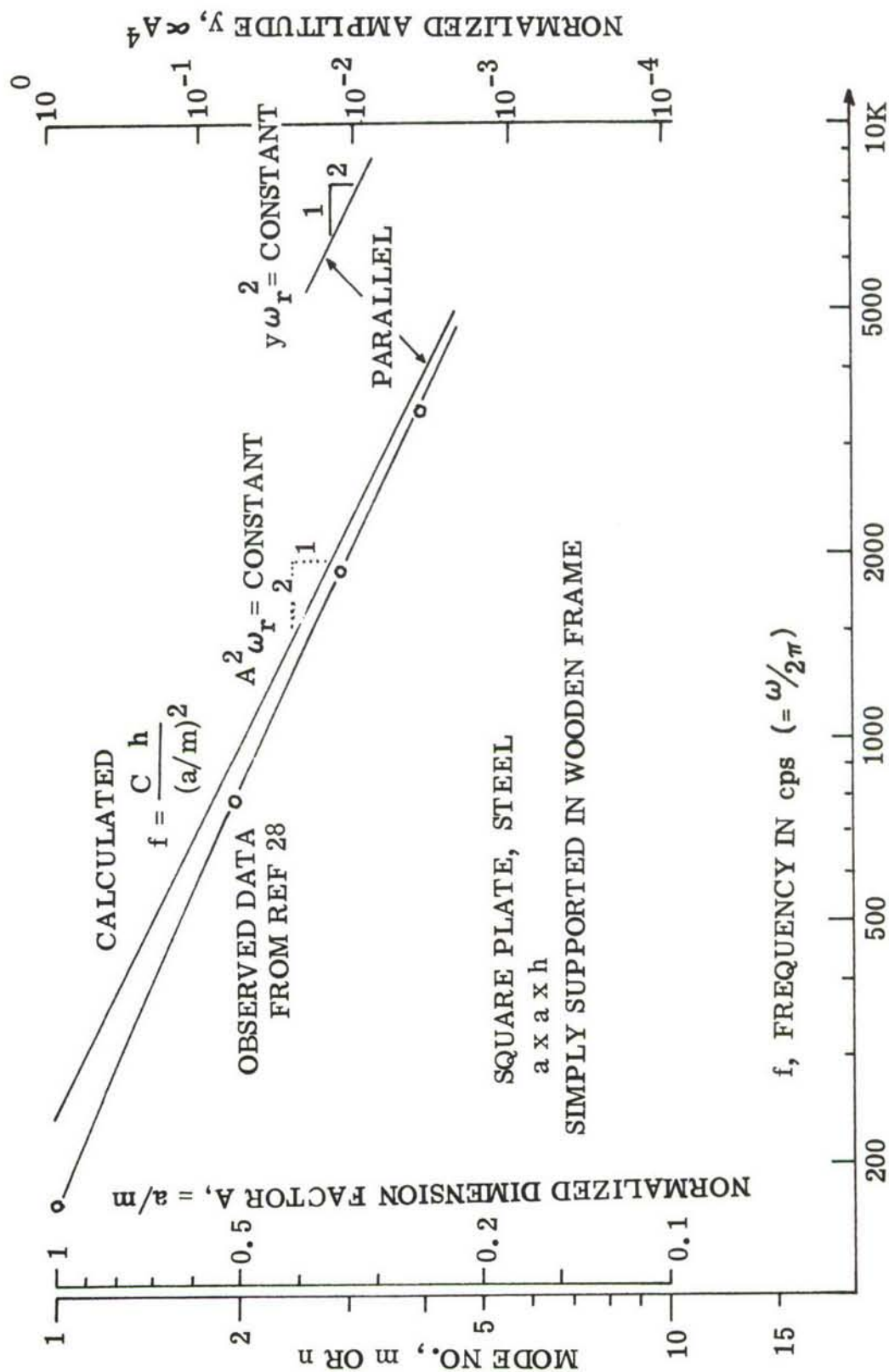
Figure 50. Resonance Frequency of Square Plate

$A = a/m$. The equality is, therefore, transformed to $A^2 \omega_r = $ constant. A second change in the logarithmic scale given at the right-hand side transforms the readings to A^4 and converts the product $A^4 \omega_r^2$ into another constant. The relationship is synonymous to $y \omega_r^2 = $ constant, where y, the dynamic amplitude, is made to be proportional to the fourth power of a length factor. This fact in a linear response at a constant damping coefficient ratio c/c_c (See 3.6.3) demonstrates the amplitude reduction in higher modes, where the length factor being a function of the modal distances decreases for increasing mode orders. For other plate configurations, the initial decrease from a fundamental mode is even more rapid at lower modes but approaches the illustrated conditions as limiting cases, Figs. 23, 28, and 39.

Failure to generate response in the fundamental modes, for whatever causes there may be, invariably results in greatly decreased stress responses. The basis of fatigue similitude at a uniform stress required to correlate scale ratio to duration change becomes quite difficult to realize unless each and all the higher modes can be completely defined. In the honeycomb sandwich panels, the higher modes were so closely related harmonically to the fundamental mode due to the aspect ratio selected that high mode responses became the more dominating. In curved plates, the stiffening effect in the higher modes is much less than the fundamental mode. And at the curvature selected, the generation of a truly fundamental mode is overshadowed by the relative ease in the formation of higher modes. In this regard, the observation is made that a constancy in $y \omega^2$ is equivalent to uniform g^2 units in power spectral densities as well as in total power. The most likely mode combination is predicated upon an equal energy distribution when randomly excited. Thus, from the strain gage responses of Figs. 48a and 48b, a more or less uniform stress in each mode is obtainable when the pressure spectra are equalized at the same level as illustrated at 125 dB in Table XIII.

TABLE XIII   RANDOM RESPONSE AT EQUALIZED FORCING SPECTRA

1/3 Octave Band cps	Equalized Spectrum Level dB	Stress Response		Response per Mode	
		rms psi	Reference	rms psi	Mode Frequency cps
140/180	125	780	Table XII	780	154
224/280		790	By linear extrapo- lation from Table XII	790	260
280/355		1240		870	286
				870	338
355/450		830		830	395
450/560		830		830	540

5.2   Determination of Damping Coefficient and Size Factor

A decay curve for damping coefficient calculation is found to be very
effective and convenient to use. The validity and accuracy of the result
depend only on the linearity between displacement and stress obtainable
at low amplitudes regardless of the manner of excitation. Thus strain gages
may be at any location and all decay signals may be averaged for better
results. Fig. 51 is given here to facilitate calculation. From the correla-
tion of damping coefficients with the span of the beam a size factor can be
determined, indicating a scaling law that the damping coefficient ratio
decreases as the model size is decreased. For flat panels, therefore,
fatigue data on smaller models must be modified by damping characteristics,
known beforehand or determined as part of the test.   For curved plates,
however, if the dominant modes occur in simply supported elements, no appre-
ciable change in damping coefficient needs to be considered.

5.3   Mode Numbers m, n and Parameter Product m·n

From all available information and the data collected in this program,
a lumped argument in the form of the product of mode numbers m and n emerges
as a very useful reference parameter. It appears warranted to continue this
investigation in other cases involving model changes for further substantiation.
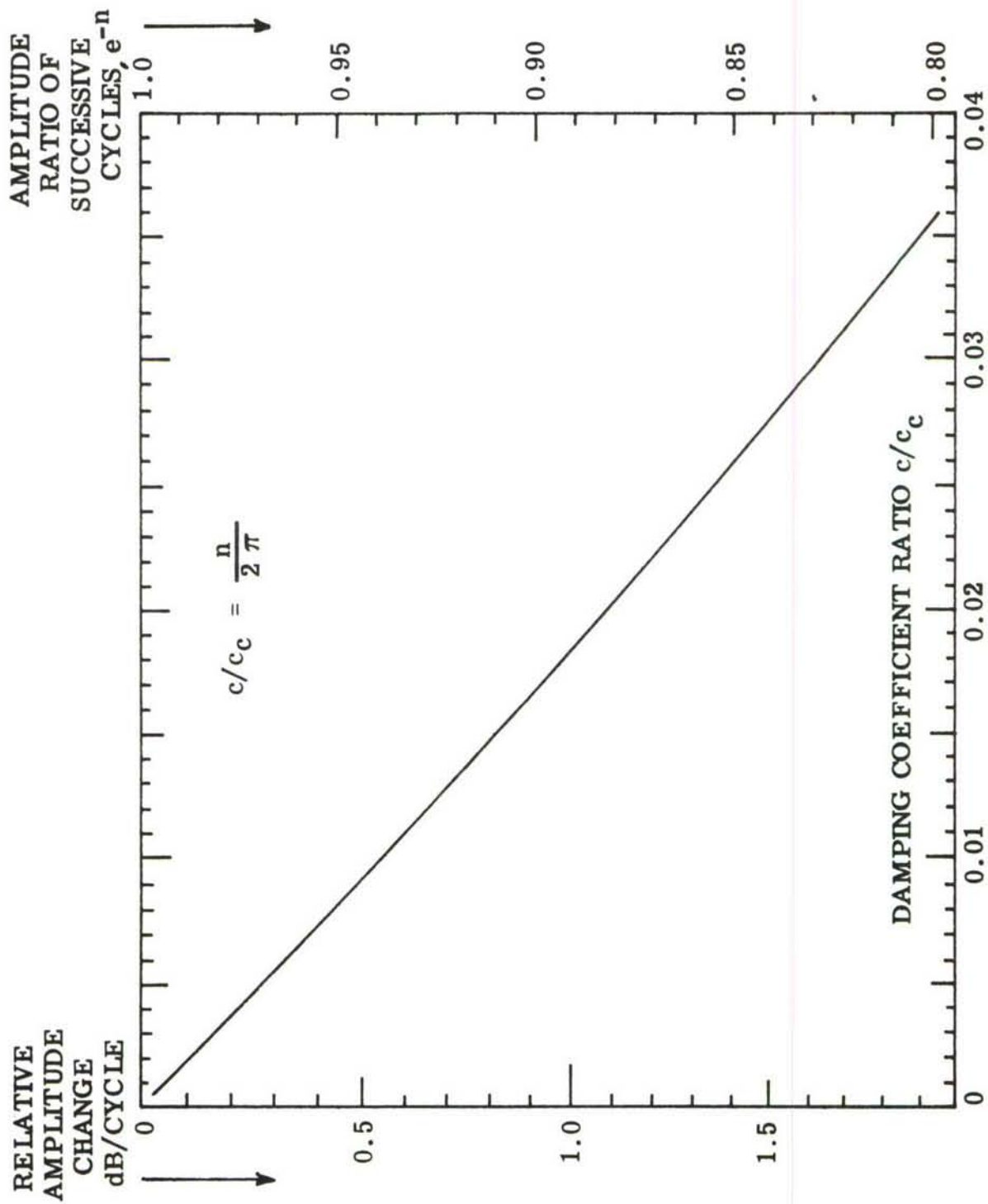
Figure 51. Damping Coefficient Calculation

In the frame supported plate of Fig. 50, the elastic energy can be expressed in terms of a frequency ratio based on the calculated resonance frequency corresponding to a given mode defined by m and n. It will be found that for equal parameter product m n, this ratio remains sensibly constant and approaches unity for no energy loss at higher modes. If knife edge supports are used, such as in Reference 3, the energy loss is reducible to a minimum and is negligible in all modes.

When the conditions at the supporting edges are complicated as in practical structures where deformations in many ways prevail, the response mode is predominated by the components in simply supported constrainment. The results in Tables VI and VII can thus be compared in isolated m,n S modes to reveal a better modeling correlation in parameter products rather than in the complicated compositions pertaining to each mode. For example, the response of the full size specimen at the second harmonic of the excitation frequency (2 x 216 cps) is predominantly a 3,1S mode as indicated in Table VI and Fig. 23. For the modeled specimen, though excitable at the same forcing frequency, the comparable response should occur at a frequency 2.37 times (see p.61) higher, or corresponding to a harmonic order of 4.7 in this case. The closest indication was provided at the 4th and 5th order (of 216 cps) in Table VII as a 1.5,2S and 3,1S modes respectively. The same lumped argument of 3 is obtained. It is therefore, indicated that as the modes become more complicated, there will be many other combinations that can share the same argument, rendering it imperative in modeling studies to analyze each mode completely and to define the elastic response in detail. It must be added that no coupling effect in excessive amplitude change has been observed in this test series.

By extending the use of the mode number product as a parameter defining the stiffening effect in curved plates, the result given in Fig. 38 appears to offer a highly useful guide in the delineation of the potential for altering the response mode by curvature. It would be desirable, however, to secure additional data to substantiate the indicated relationship by varying the parameter dimensions that were held constant in this rather limited test program.

5.4   Application of Beam Test Results to Panels

In view of the fact that the first mode response in all test panels was unobtainable because of the joint influence of the prevailing aspect ratio and edge conditions, a calculated comparison between the beams in honeycomb sections and the anticipated panel strength is presented as follows which can also be applied to curved plates. On the basis that the proven fatigue strength at approximately 10,000 cycles is 30,000 psi in the face sheets, a random spectrum level in the acoustical environment can be readily established to meet a service requirement as defined by a given life duration.

Example: Equivalent fatigue duration = 10^9 cycles with these known parameters:
Panel Size 28" x 41 x 1" Honeycomb; all edges clamped
Radius of gyration = 0.496 in. Area of Face Sheets = 0.024 in^2, d = 0.505 inch
Frequency Correction Factor = $\sqrt{0.183}$ = 0.43 based on Table
Damping Coefficient = 0.01   III
considered here as typical (see Table IV)

Calculations: Let sinusoidal pressure at f_r be **p**

  Max. Bending Moment $= 0.073$ **p** $a^2, \beta/6 = 0.073$ (Reference

  Max. Bending Stress $= \dfrac{0.073 \text{ \textbf{p} } a^2 (d)}{I}$ (A.R.), from p.61

$$= \frac{(0.073)\ (28)^2(0.505)\ (1)\ \text{\textbf{p}}}{(0.024)\ (0.496)^2\ (0.02)}$$

Reduce the fatigue strength of 30,000 psi at 10^4 cycles to 5700 psi at 10^9 cycles by extrapolation of S-N curve shown in Fig. 52 as the bending stress limit and solve for

  p $= 0.0233$ psi peak or 135 dB which is expected to be within the linear response range.

  Calculated mode frequency $= \dfrac{(27.1)\ (4960)\ 12\ (0.43)}{(28)\ (28)} = 250$ cps (Fig. 23)

  $\Delta dB_1 = 2 + 10 \log (0.01)\ (500) = 9$ for equal stress

  $\Delta dB_2 = 4$ (average log log S-N curves) for equal damage

  Random spectrum level $= 135 - (9 + 4) = 122$ dB at 250 cps

The proof required is to secure a maximum stress reading of 5700 psi at 135 dB in this mode. If it is extended nonlinearly to 15,000 psi at 150 dB, it may be used as a test level to secure an accelerated fatigue life at 200,000 cycles. At 250 cps, this takes 13.3 minutes. If the test stress is set at 10,000 psi, the fatigue duration will be 133 minutes. If a higher mode prevails instead, the stress will be greatly reduced. A much extended test is required which is not considered to be within the originally programmed scope for defining applicable modeling techniques.
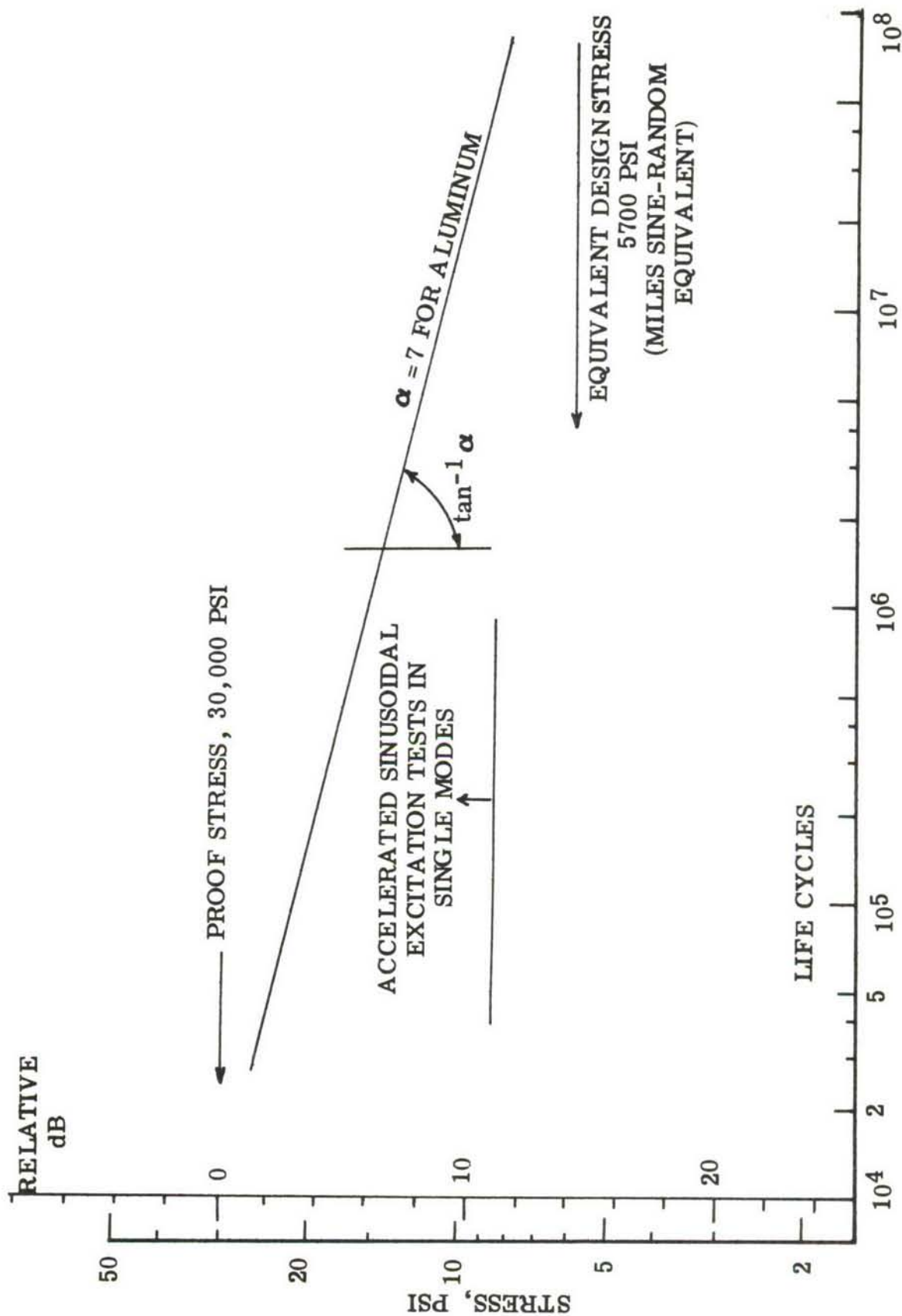
Figure 52. Fatigue Life Cycle Calculations

6. CONCLUSIONS AND RECOMMENDATIONS

Stress correlation is the critical parameter in modeling for acoustic fatigue. True models with exact geometric scaling in all elements are not necessary for achieving the required stress correlation. Adequate models are obtained by maintaining the same aspect ratio and modes for the specimen and models. For curved plates the necessity of maintaining identical modes between specimen and model requires that the radius of curvature must be scaled in the same ratio as the linear dimensions defining the aspect ratio. The frequency and stress of adequate models then vary at predetermined magnitudes with a functional relationship to damping, amplitude, and cross-section (thickness) geometric and material parameters. Nonlinear effects are dependent on excitation levels and may be present in both specimen and model or may appear to be different between the specimen and models. These nonlinearities are amenable to resolution. In general, a prerequisite to sonic fatigue tests is a knowledge of the nonlinearity induced by damping and amplitude for each specimen. Data of this type are obtainable from non-destructive vibration tests. The experimental data confirms the application of basic procedures formulated by Miles, Palmgren, and Miner. The requirement for random excitation in the use of modeling techniques for sonic fatigue prediction is thus minimized.

6.1 Honeycomb Sandwich Construction - Preliminary Tests and Modeling Procedures

6.1.1 Configuration Integrity Test

The structural integrity of all honeycomb sandwich sections should be determined by obtaining specimen failure with mechanical vibratory tests. The use of cantilever beam specimens in a minimum of two span lengths suffices for this requirement. The reasons for the requirement are: (1) To ascertain that failures are confined to tensile (bending) fractures in face sheets, and (2) to compare the maximum available low life-cycle strength in complete stress reversals ($R = -1$) with an applicable S-N curve.

6.1.2 Damping Coefficient Ratios

In testing the configuration integrity, the damping coefficient ratios should be obtained as a function of amplitude prior to the determination of fatigue strength. These ratios, suitably corrected for span changes, are required for panel modeling parameters.

6.1.3 Modeling Procedures

The modeling parameter in frequency is based on the equation

$$f_{m,n} = \frac{C_{m,n} \, k \, \sqrt{X}}{a^2_{m,n}} \quad \text{where}$$

$f_{m,n}$ is the frequency of full-size or model panel at mode numbers m and n in dimensions b and a respectively, cps

$C_{m,n}$ a frequency constant common to all panels at the given mode m,n, in-lb-sec system

k,   the radius of gyration of the section, inch

X,   a weight factor equal to $\dfrac{\text{weight of face sheets}}{\text{total section weight}}$, and

$a_{m,n}$ the short dimension (in b x a) inch

The only restricted constant is $C_{m,n}$ for which the aspect ratio of the specimen and model panels must be kept the same and with the panel edges identically constrained. All other variables may be chosen in suitable proportions.

The modeling parameter of dynamic flexural stress is based on the equation:

$$\sigma_{max} = \frac{\beta \, a_{m,n}^2 (A.R.)}{h^2} = \frac{\beta \, a_{m,n}^2 \, d \, (A.R.)}{6Ak^2} \qquad \text{where}$$

σ_{max} is the maximum reversible bending stress in a fundamental mode defined in length factor $a_{m,n}$;

d, distance of extreme fiber to neutral layer of honeycomb section whose total face sheet area per unit width is A at radius of gyration k,

h, the thickness of an equivalent rectangular section;

(A.R.), an amplification ratio = $\dfrac{1}{2 \, c/c_c}$ at damping coefficient ratio c/c_c; and

β, a maximum bending moment coefficient appropriate to the mode defined by $a_{m,n}$. (Ref. 24 and 25)

By examining these two parametric equations jointly, it can be seen that if all dimensional factors are in proportion to scale ratios in true modeling and the weight correction is neglected, the frequencies would be raised in a scaled (down) model for the same stress if the amplification ratio remained the same. Because the last condition is generally not obtainable, it is unnecessary to use true models. In adequate modeling, by maintaining the same aspect ratio, the frequency and stress in each mode of the specimen and the models are allowed to vary at predetermined magnitudes. These modeling parameters are applicable to isotropic panels by correct interpretation of the terms k, X and A. For a constant gage panel, the sectional width is given a unity value: Thus, $A \propto h$; $k \propto h$; and $Ak^2 \propto h^3$, where h is the panel thickness. X is of course unity.

The modeling parameter between sinusoidal and random environment is based on the Miles' solution and depends on the conditions specified below:

(a) For equal rms stress observation - The equivalent sinusoidal pressure
      level is ΔdB_1 above the spectrum level at mode frequency f_r in
      random excitation. This level change in decibels is given by the
      equation $\Delta dB_1 = 2 + 10 \log \Delta f$ where $\Delta f = 2(c/c_c)f_r$

(b) For equal fatigue or damage stress in mode f_r - The equivalent sinusoidal
      pressure level is ΔdB_1 + ΔdB_2 above the spectrum level at mode
      frequency f_r in random excitation. The level change in ΔdB_2 is
      given by the equation $\Delta dB_2 = 10 \log|\alpha/e|$ where e = 2.72 and
      α is average slope in a conventional S-N curve on log-log scales,
      i.e.

$$ = \frac{\log \text{(Life Cycle Ratio)}}{\log \text{(Stress Ratio)}}, \text{ or} = \frac{\log n_2 - \log n_1}{\log s_1 - \log s_2} \text{ with } s_1 > s_2 \text{ and } n_2 > n_1. $$

If more than one mode is involved, then the damages due to all
relevant modes are cumulated together in accordance with Palmgren-Miner
Rule. However all modes which are not contributory to the stress at a
particular location must be excluded. In this respect, it is evident
that different damages will result due to: (1) variations in the model stress
response and (2) variations in the composition of a random environment.
The model response is best determinable by sinusoidal excitation tests
and can be verified for as many excitation levels as desired. A specific
level is then selected for fatigue test. The lifetime durations between
models can be readily compared with an acceptable S-N curve.

The nonlinearity parameters are dependent on the specific excitation
levels under consideration. In general, a prerequisite knowledge is
required for each specimen or model on the extent of the nonlinearity in-
curred and on the frequency range of respective "jump phenomena" (best
obtainable with sinusoidal excitation forces), before a long range
fatigue relationship can be established. Data of this program indicate that
a well designed honeycomb sandwich structure based on the tensile strength of
the face sheet is predominantly a vibrating body with linear characteristics.
Unless the core is deficient in shear strength or rigidity, nonlinear
response is probably negligible even in random considerations. However,
with undersized cores the failures would be catastrophic in nature; a
contingency that has been ruled out of the current applications.

6.2   Curved Plate Configuration - Modeling Procedures

6.2.1   Definition and Limitation

The curved plate is defined here as a stiffened rectangular flat
plate unit element with linear dimensions a x b and bent to a radius R
in one direction only. Although a lumped argument was introduced involving
the product of mode numbers m and n that appeared to correlate well with
data from this program and one other source, potential independent and/or
interrelated effects of thickness to radius, thickness to length, length
to width, and width to radius ratios have not been specifically considered.
The following procedures are applicable within these limitations.

6.2.2 Aspect Ratio and Radius of Curvature

The modeling requirement is that both the linear dimensions defining the aspect ratio and the radius of curvature are to be scaled in the same ratio, i.e., a, b, and R are the essential modeling dimensions. The subtended central angle for the curvature is the same in all cases.

6.2.3 Frequency Parameter and Stiffening Effect

For each mode the stiffening effect of curvature is the same. The stiffening effect is defined as the ratio of the frequency of the curved configuration to that of an unstiffened flat plate. The variation in the stiffening effect with mode numbers appears to follow the relationship indicated in Figure 38, for which a lumped argument is introduced as the product of mode numbers m and n for the two sides. Frequencies of the referenced flat plate, unstiffened, are calculated for each mode desired on the same basis as illustrated in Section 4. The plate thickness h is, therefore, a parameter dimension and need not be necessarily scaled. Because of the stiffening effect of curvature, it would usually be desirable to scale down the thickness parameter more than by the scaled model reduction in order to maintain important model frequencies within a desirable frequency range for the tests. Observe that in this varied degree of stiffening effect, the fundamental and higher modes are no longer harmonically related as in unstiffened flat plates, even for an aspect ratio of 1.4 as demonstrated in Section 3.

6.2.4 Equivalent Flat Plate and Stress Parameter

An equivalent flat plate designates an imaginary flat plate of the same linear dimensions but with an increased moment of inertia such that its mode frequency is the same as the curved plate. The increase in moment of inertia is, therefore, proportional to the square of the frequency ratio which reflects a corresponding decrease in bending stress in the equivalent flat plate or the curved plate.

6.2.5 Fatigue Consideration Versus Instability

If a comparison is made between the decrease in bending stress in curved plates and acceptable S-N curves, it would be realized that the accrued increase in fatigue life would be more than adequate on a time basis to offset the increase in mode frequency. This is illustrated in Figure 53 for the worst condition in which the slope of the given S-N (log-log) curve is much steeper than most materials within an average fatigue duration range. For a curved plate, moderately stiffened by curvature so that the mode frequency is doubled, the reduced stress would be only 25% of the original value. The fatigue extension in life cycles is 1000 times at the same frequency or 500 times in time-duration based on the calculated strength of the unstiffened flat plate. In other words to maintain the same fatigue strength on a stress basis, it would be permissible to allow a 2/3 decrease in the true section modulus in the curved plate. In reducing the rigidity so drastically it is suggested that this would come very likely under an instability criterion which was not investigated in this program.
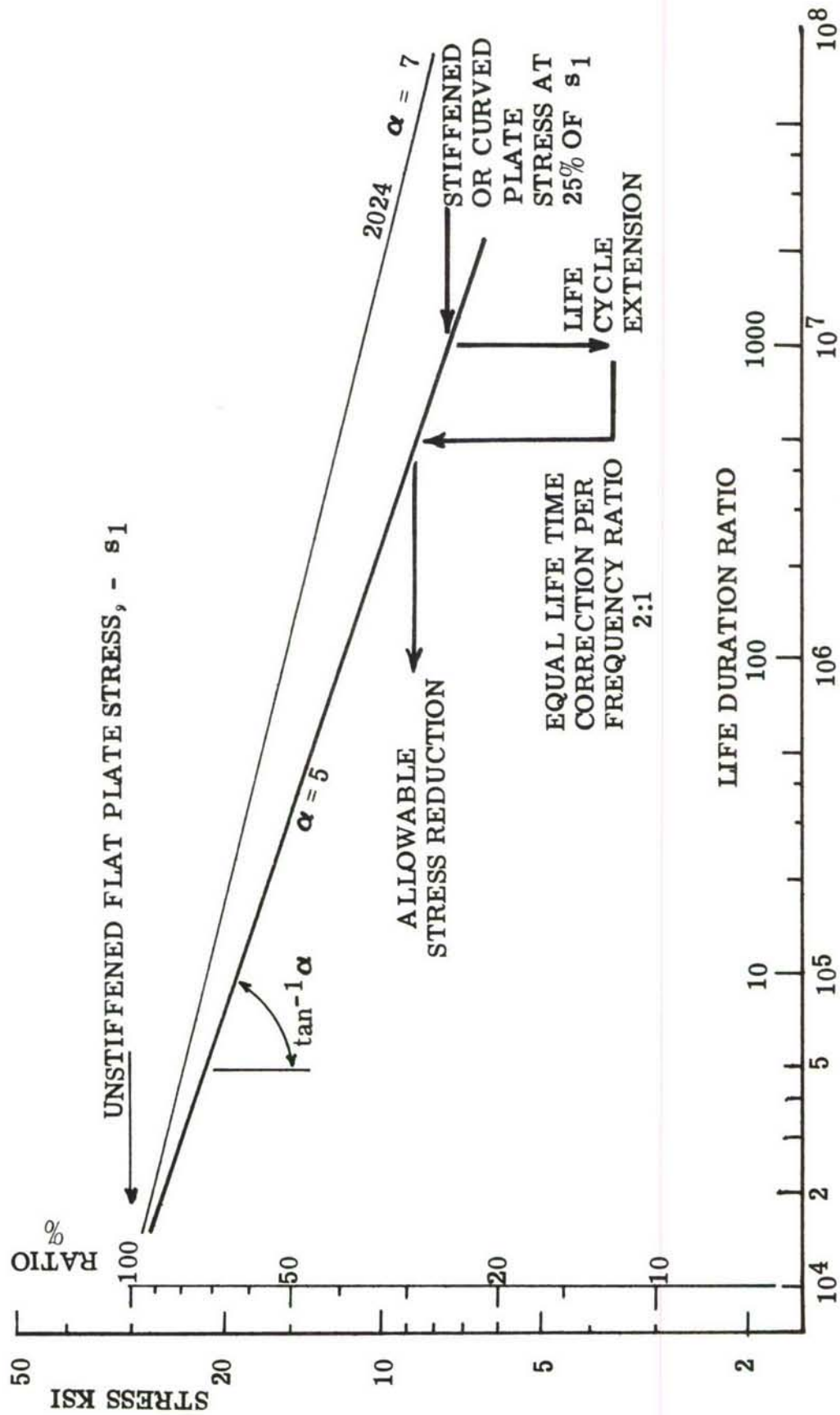
Figure 53. Extension of Fatigue Duration in Curved Plates

6.3   Recommendations for Additional Tests

In fatigue under a random environment, acoustically or otherwise induced, the question appears to be a definition of the environment itself rather than on the mechanics of failure. Data presented in this report are in satisfactory support of the application of Miles, Palmgren-Miner cumulative fatigue hypothesis. In this respect, the use of power spectral densities or spectrum levels in dB per cps is recommended for the definition of acoustical environment in lieu of octave band levels. This definition is also applicable to stress response which is more specific than the overall reading usually taken. Concurrently, it is emphasized that nonlinear response is better revealed with sinusoidal excitation tests than with random signals. A recommendation is also made that the concept of using models for sonic fatigue predictions be extended to establish modeling parameters for anisotropic panels, e.g. corrugation stiffened, or stiffened single faced panels.

6.3.1   Curved Plates

The application of a method using acoustical excitation to resolve the question of increased stiffening in curved plates has been demonstrated. In order to consolidate the findings illustrated in Figure 38, where the stiffness parameter is the subtended angle of curvature, it is recommended that investigations be conducted on at least three more parametric changes to supplement the existing curves. Academically, if the specimens include one plate configuration at a subtended angle of 180°, with axial ends free, the result obtainable by this method should be in agreement with several published treatises on incomplete circular rings where the minimum subtended angle is usually π, e.g., References 29 and 30. In this connection, it must be noted that the subtended angle, held constant in this program, might be a complex function in itself of other characteristic ratios such as thickness to radius, thickness to length, or thickness to width. The latter two ratios may be compounded in turn by the aspect ratio.

6.3.2   Flat Plates

In order to resolve the question of the influence of aspect ratio on plate modes, particularly in the reduced stress at 1.4 aspect ratio, it is recommended that further verification be obtained by extending the investigation to cover a wider range in aspect ratios. A suggested range for aspect ratio would be from 1.1 to 2.5. Better control of edge restraint and uniformity of specimens and models could be obtained by using flat plates (aluminum 2024) on supported edges. It is anticipated that higher modes could then be generated separately for a better evaluation of damping characteristics.

APPENDIX A

BASIC BEAM THEORIES APPLIED IN ANALYZING HONEYCOMB SANDWICH CONFIGURATIONS

1. Bending Rigidity and Stress

The extreme cases in which a honeycomb sandwich construction deflects in resistance to transverse loads only are sketched in Figures 54a and 54b. Sections of width dx along the longitudinal length are shown as isolated elastic units in exaggerated proportions under the action of external shear forces V, the bending moments being deleted for clarity. In Fig. 54a, the two face sheets deflect individually but essentially in the same flexural mode. Both compressive and tensile stresses in bending are induced in each face sheet for a total bending moment resistance of $2EI_f \frac{dy^2}{dx^2}$. In Fig. 54b, the face sheets bend as a unit with plane sections remaining plane at all times. It is, therefore, clear that in the latter case, a simple bending phenomenon in face sheets is depicted for a resistive moment $M_o = EI_{1-1} \, d^2y/d^2x$ where 1-1 represents the neutral axis of the entire section. For a honeycomb sandwich section as dimensioned in Fig. 54c the moment of inertia I_{1-1} of the face sheets is given in the equation

$$I_{1-1} = 2\left[\frac{b\,t^3}{12} + b\,t\left\{\frac{c}{2} + \frac{t}{2}\right\}^2\right]$$

$$= 2\left(I_f + b\,t\,\{c/2 + t/2\}^2\right) \tag{A1}$$

The first term in the bracket, being much smaller than the 2nd term is usually neglected. In other words, the bending rigidity in a honeycomb section rests predominantly in EI_{1-1} and is a maximum when adequate strength is built into the core enabling an element such as 1234 to maintain the coplanar requirement of the face sheet sections. When this condition is fulfilled, the static bending stress σ_o is given by the following equation and distributed in the manner shown in Fig. 54d.

$$\sigma_o = \frac{M_o\, d}{I_{1-1}} \tag{A2}$$

In the above equation, the static bending moment M_o is frequently expressed in the form $M_o = \beta' p\, a^2$ where p is a uniformly distributed pressure, a is the shorter span of a rectangular plate a x b; and β' is the moment coefficient as given in References 22 and 24. A condensed listing is shown below for clarity because of the notational variations involved. The coefficients employed elsewhere in this report are accented.

(a) FACESHEETS IN EQUAL FLEXURES

(c) SECTIONAL VIEW

(b) SANDWICHED SECTION IN BENDING AS A UNIT

(d) BENDING STRESS DIAGRAM
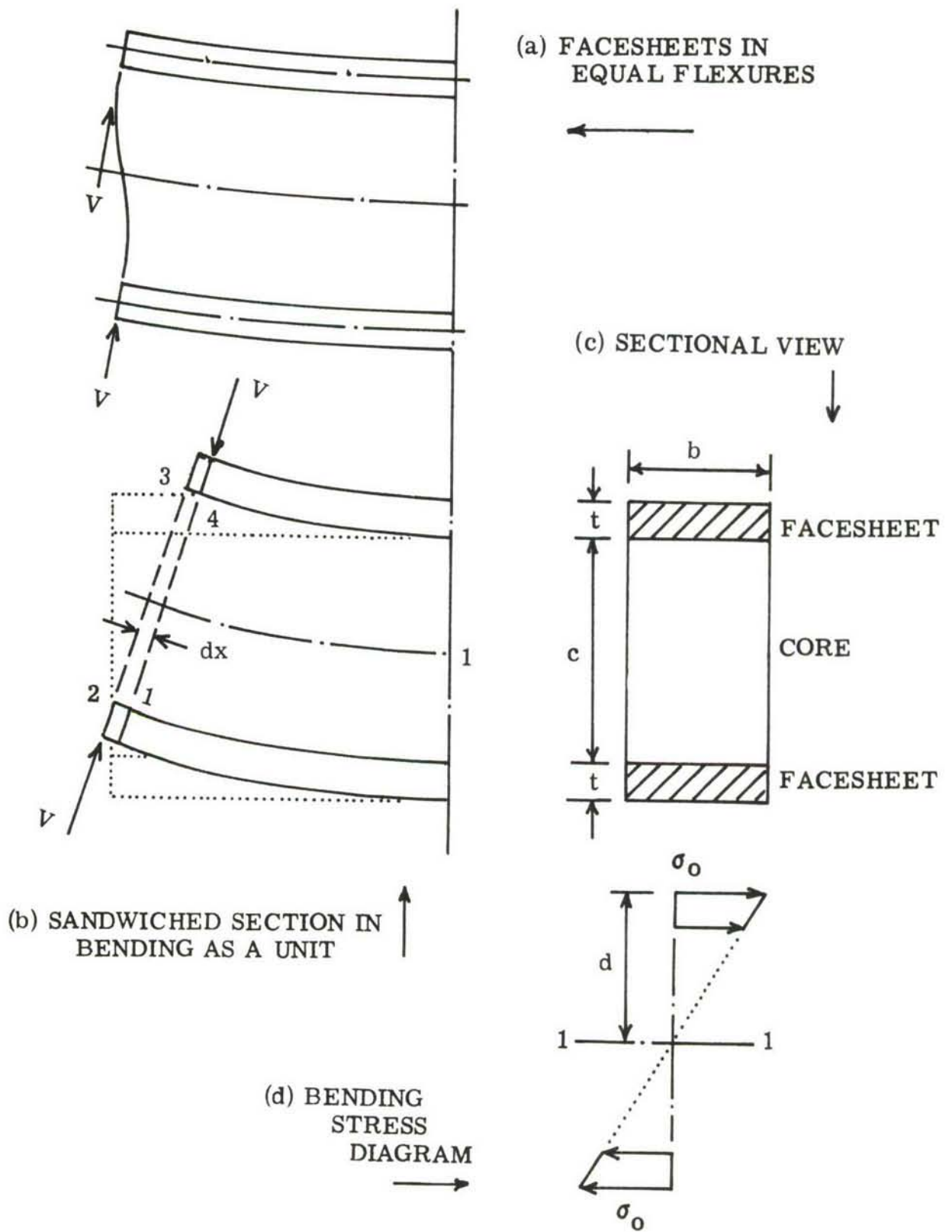
Figure 54. Simple Bending Configurations

b/a	Simply Supported Edges (From Ref. 22)		All Edges Clamped (From Ref. 24)			
	M_X Max.	M_y Max.	M_X Max center of edge b −	center of plate +	M_y Max. center of edge a −	center of plate +
1.0	0.0479	0.0479	0.0513			
1.2	0.0616	0.0501	0.0639	0.0299	0.0554	0.0228
1.4	0.0753	**0.0506**	**0.0726**	**0.0349**	0.0568	0.0212
1.6	0.0862	0.0493	0.0780	0.0381	0.0571	0.0193
1.8	0.0948	0.0479	0.0812	0.0401	0.0571	0.0174
2.0	0.1017	0.0464	0.0829			
∞	0.1250	0.0375				

From the substitution of $\beta' p \, a^2$ for M_0 in equation (A2), it is observed that the bending stress σ_0 is linearly proportional to the pressure intensity p. In dynamic loading the spectral pressure intensity q varies sinusoidally as in the expression $q = p \cos \omega t$ at a maximum value equal to p. The maximum dynamic bending stress is readily obtainable from this equation by considering the maximum amplitudes as derived from a lumped mass system,

$$\sigma = \frac{\sigma_0}{2 \, c/c_c}, \quad \text{or} \quad \sigma = \sigma_0 \, (A.R.) \tag{A3}$$

where c/c_c represents a damping coefficient ratio and (A.R.) stands for the amplification ratio ($= 1/2 \, c/c_c$).

The maximum dynamic flexural stress is simply the amplified maximum static bending stress σ_0. A direct expression of the latter in the form $\sigma_0 = \beta \, p \, a^2/h^2$ is frequently used for a uniform plate of thickness h, β now becoming a stress coefficient having a value of $6\beta'$. The values of stress coefficient β also depend on the aspect ratios and end constraints. In Reference 25 many curves can be found delineating its values in specific cases. A condensed listing is given below with accented values indicating those that were used in this report.

b/a	Max. Bending Stress Coefficient β		Remarks
	Simply Supported, All Edges	Clamped on One Edge Simply Supported on 3 Edges	
1	0.29	0.50	Readings off curves from Ref. 25.
1.4	0.47*	0.67*	*Average **0.57** used in test example, p. 87
2	0.61	0.72	
3	0.71	0.73	
6	**0.73**		Extrapolated reading.

Careful distinction has to be exercised in employing the coefficients of bending moment β' from References 22 and 24 and of bending stress β from Reference 25.

An additional variation is found useful in the substitution of $A\,k^2$ for the moment of inertia term I_{1-1} where A is the sectional area whose radius of gyration is k. The general expression of the maximum dynamic flexural stress is therefore

$$\sigma = \frac{\beta\ p\ a^2 d(A.R.)}{6\ A\ k^2} \tag{A3a}$$

for a bending fiber at distance d to the neutral axis.

2.   Shear Rigidity and Resonance Frequencies

In the application of equations A1 and A2, the prerequisite condition is emphasized that there must be adequate core strength in shear to sustain the bending rigidity in the sandwich structure as being bounded by undistorted plane sections. In order to verify the extent to which this condition is fulfilled, the resonance frequency solution to the general equation governing elastic vibrations is utilized. If the observed resonance frequency agrees with a calculated theoretical value, then adequate shear rigidity prevails.

The general equation (Refs 13, 15, 18)

$$EI\frac{d^4 y}{dx^4} + \frac{wA}{g} y \omega_r^2 = 0 \tag{A4}$$

indicates that the second term represents a vector due to the inertial force at the beam section dx which must, therefore, include the weight of the core carried. In other words, the effective density w is no longer the density of the face sheets only. To the solution

$$\omega_r^2 = \frac{\{\lambda_r \ell\}^4}{w\,A\,\ell^4} EI\ g \tag{A5}$$

derived in Reference 13, a correction term must be added as follows:

$$\omega_r = \left\{ \frac{(\lambda_r \ell)^4\ EI\ g}{w\,A\ \ell^4} \right\}^{\frac{1}{2}} \left\{ \frac{(\text{face sheet weight})}{(\text{total weight})} \right\}^{\frac{1}{2}} \tag{A6}$$

where $(\lambda_r \ell)$ is a known constant for the given configuration.

APPENDIX B

A RE-APPRAISAL OF HONEYCOMB CONSTRUCTION AND ITS

STRENGTH CONTRIBUTION IN SANDWICH CONFIGURATIONS

INTRODUCTION

In this report, the hypothesis has been used that in sandwiched honeycomb structures, core failures would be considered catastrophic for the reason that structural integrity is considerably impaired whereas face sheet failures may be detectable, arrested, or otherwise repaired without the loss of a structural component. The design of the sandwich is, therefore, based on the conception that ultimate failures are confined to face sheets. To insure that adequate strength is built into the core which is usually hidden from view and practically bars normal inspection, this analysis is presented as an aid to core selections. For illustrative purposes, aluminum cores will be used and are composed of hexagonal cells with the width across flats in the direction WW defined as the cell size, corner directions designated TT. The depth of the core is along the direction of the flute, L. Valuable test data from References 31 and 32 are used in this analysis.

1.   Compressive Strength along Axis L and Total Shear Force of Bending

Typical test data from Reference 31 are shown in Fig. 55 with an inset indicating core geometry as defined in the introduction. The cell size was given as 3/8", wall thickness 0.003". The maximum load on a compressive block of 2.01 x 1.98 was given at 1410 lbs. This load will be compared in the following calculation with Euler's column load, considering the effective walls per cell as two columns at right angles.

Cell Area = $\dfrac{1.5}{1.7321}$ $(0.375)^2$ = 0.122 in.^{2}

No. of effective cells 3.98/0.122 = 32.6

Maximum load per cell = 1410/32.6 = 43.3 lbs. (observed data)

Euler's load per cell P_e = n π^2 EI/ℓ^2 where ℓ = core depth = 5.62"

$$n = 1$$
$$E = (10)(10)^6 \text{ lbs/in.}^2$$
$$I = (0.003)(0.375)^3/12 \text{ in}^4$$

The calculated P_e is 41.5 lbs. on the basis that the structural integrity of the stronger column for which the moment of inertia I is used, provides the limiting strength. The agreement is good but is by no means coincidental. Reduced to normal core depths (for example d = ℓ = 1"), the

115
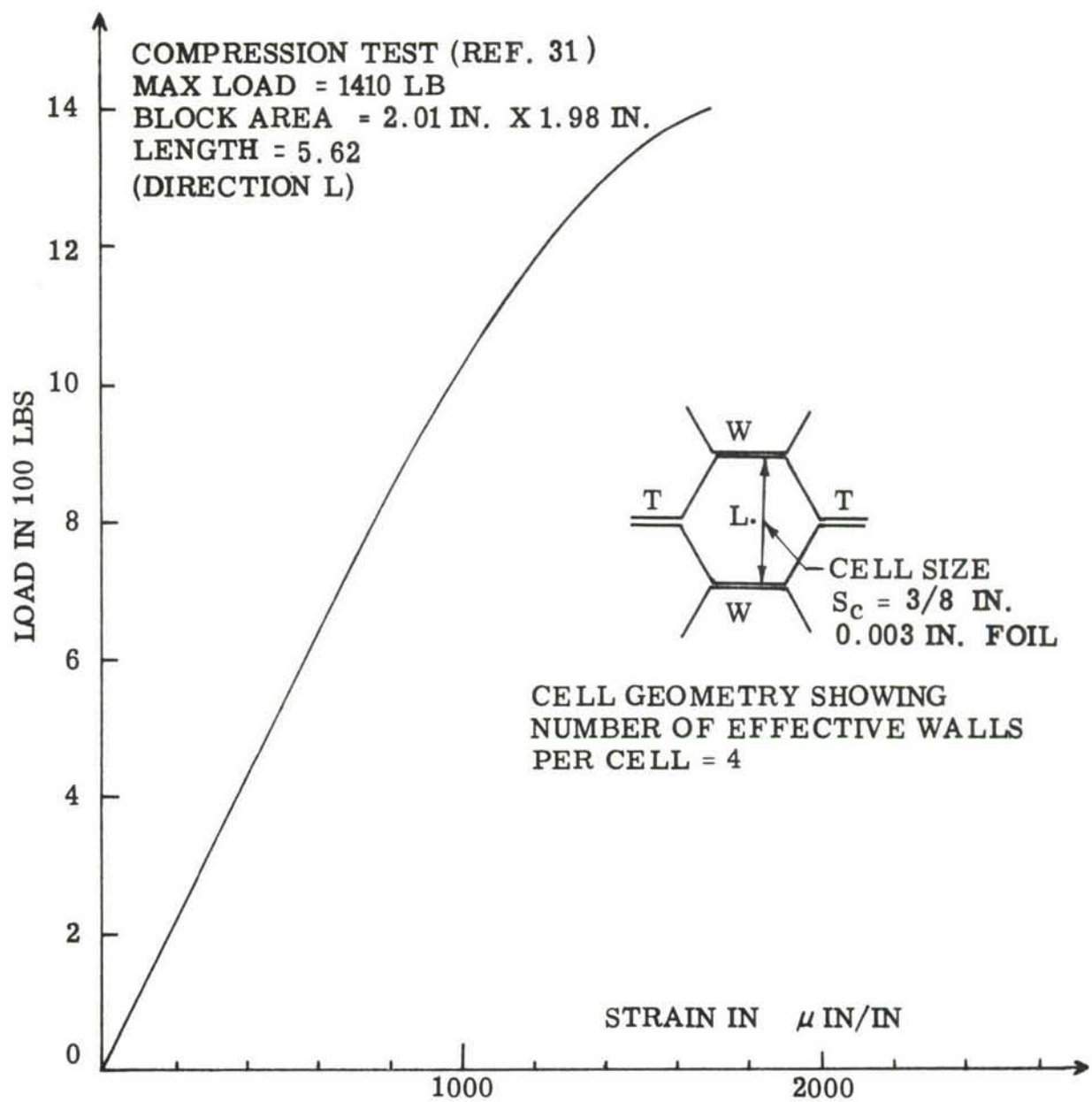
Figure 55. Honeycomb Core Compression Test

permissible compressive load or strength will be greatly increased and
generally exceeds the applied load. The total shear force V (Fig. 12) in
the bending of a beam or plate is a local compressive force on the cells.
Because of this high strength, it ceases to be a design criterion.

2.   Shear Strength in the Ribbon Direction and Shear Stress in Bending

        Some of the test results obtained in a direct application of shearing
forces onto core specimens from Reference 32 are plotted in Fig. 56 with the
test arrangement indicated in the inset. These data delineate a shear
strength that is (i) directly proportional to the foil thickness, and (ii)
inversely proportional to the cell size. At the same time, it may be
identified with the core density scale at the right. A significant but
not much heralded fact is indicated in the strength of the bond between
the core and face sheets' which proves to be stronger than the core at all
times.

        If an entire core is considered, the action of the applied forces P
(See Fig. 56) is of course a shear, but the shear is exerted on the two
bonding surfaces between the core as a unit and the face plates. Insofar
as the core element or a cell section is concerned, forces P may be considered
also as compressive load in planes TW transmitted through the cell walls.
For each cell, therefore, there is a Euler's load limit determined by the
stronger wall column beyond which initial failure will be exhibited in the
weaker column. It is, therefore, not a shearing stress in its true sense
but is conventionally so expressed due to the direction only. The dependency
of this strength upon the sizes is illustrated in the following application
of the Euler's equation.

$$P_e = \frac{n \ \pi^2 \ EI}{\ell^2} \quad \text{or} \quad P_i \propto \frac{I_1}{\ell_1^2}$$

where I_i is the moment of inertia
of either equivalent element TT
or WW and ℓ_i is its length,
subscript i is 1 or 2 for either
TT or WW.

For the same cell size, ℓ_i (or S_c) is constant.

Since $I_i = \dfrac{t \ S_c^3}{12}$, or $\dfrac{S_c \ t^3}{12}$ and $S_c \gg t$, t being the foil thickness;

    P_1 increases linearly as t and is larger than P_2;

    P_2 increases as t^3; - yielding

    P_2/P_1 at a relative rate of change proportional to t^2.

The true strength P_e, therefore, varies also as t^2.
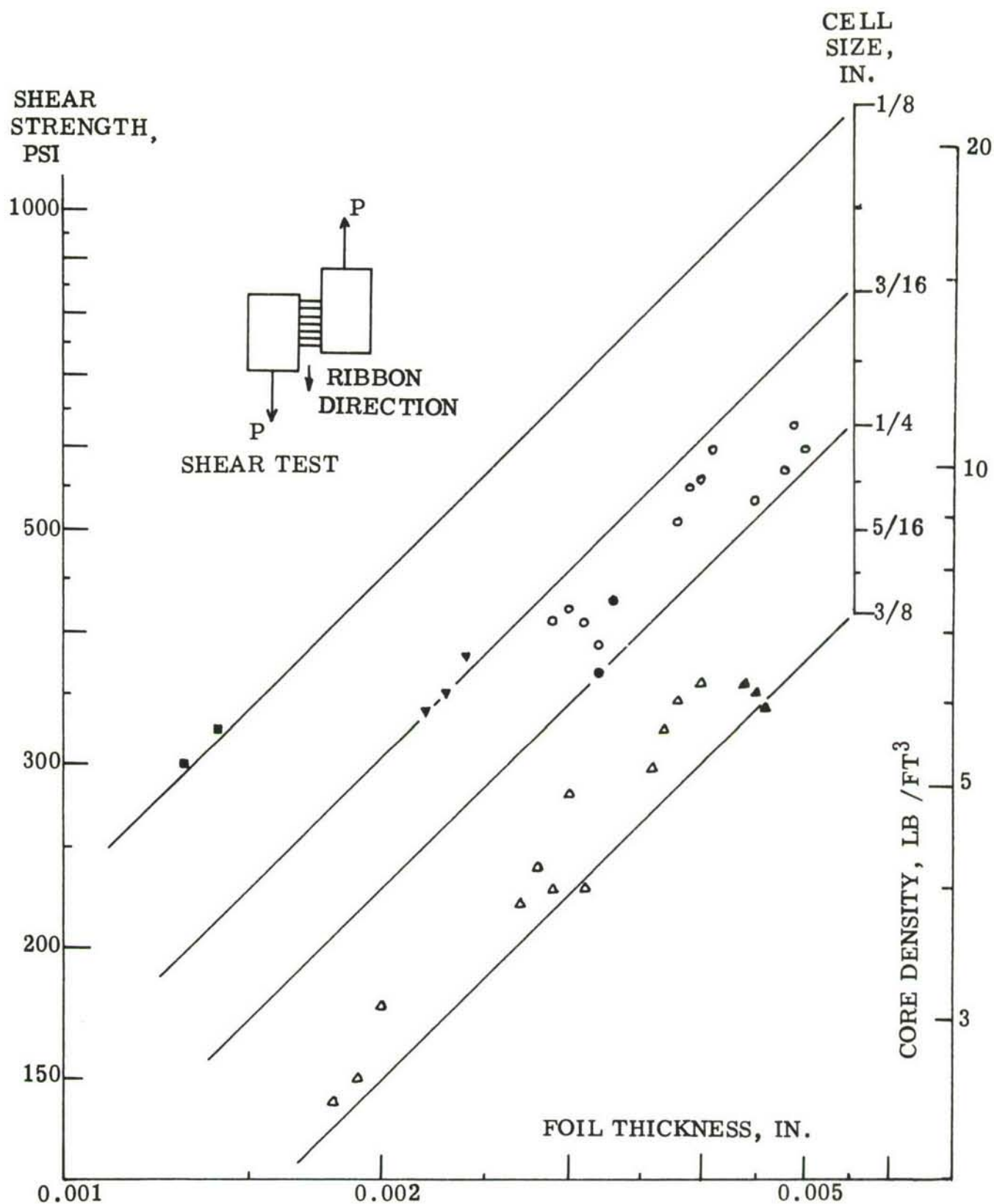
Figure 56. Honeycomb Core Shear Strength and Geometry

The apparent unit strength $(=P_e/A = t^2/t)$ accordingly increases linearly as t in agreement with data indication (i) above. If the thickness is kept constant, P_1 increases linearly as S_c but P_2 is inversely proportional to S_c. The apparent strength in this case is the joint product divided by the area change $(\propto S_c)$ which results in a strength change proportional to S_c^{-1} as per indication (ii) observed.

In these established strength characteristics, a basis is provided in selecting appropriate cores that can be made stronger than the bending strength of the face sheets. For a given design criteria where the maximum shear stress is also known, a core can be selected to meet any degree of overstrength desired. On the basis of available test results, it appears that these strengths as given in Fig. 56 for static shear may also be considered as safe dynamic shear limits.

SIGNIFICANCE OF PANEL ASPECT RATIO IN THE GENERATION OF MODE RESPONSE

The bending frequency of uniform rectangular flat plate, simply supported at the sides, is given by

$$\omega_{m,n} = \pi^2 \sqrt{\frac{D}{\rho}} \left[\frac{m^2}{b^2} + \frac{n^2}{a^2} \right], \quad \text{where}$$

$\omega_{m,n}$ is the frequency of the m,n mode
D   is the plate flexural rigidity
ρ is the plate mass per unit area
a,b   are plate dimensions - aspect ratio $A\!R = b/a, \ b \geqslant a$
m,n   are integers denoting mode number or the number of half-waves, in b,a directions respectively.

The ratio of mode frequency $\omega_{m,n}$ to the fundamental mode frequency $\omega_{1,1}$ is

$$\omega_{m,n}/\omega_{1,1} = \left[\frac{m^2}{b^2} + \frac{n^2}{a^2} \right] \left[\frac{1}{a^2} + \frac{1}{b^2} \right]^{-1}$$

Substituting $b = a\,A\!R$

$$\omega_{m,n}/\omega_{1,1} = \left[A\!R^2 n^2 + m^2 \right] \left[A\!R^2 + 1 \right]^{-1}$$

For a panel aspect ratio of $\sqrt{2}$, $\dfrac{\omega_{m,n}}{\omega_{1,1}} = \dfrac{2n^2 + m^2}{3}$

For another ratio, e.g. $A\!R = 2$, $\dfrac{\omega_{m,n}}{\omega_{1,1}} = \dfrac{4n^2 + m^2}{5}$; the comparison is tabulated as follows:

Mode Number		Node Pattern	$\omega_{m,n}/\omega_{1,1}$		Aspect Ratio between Node Lines	
n	m		$A\!R = \sqrt{2}$	$A\!R = 2$	$A\!R = \sqrt{2}$	$A\!R = 2$
1	2		2	8/5	$\sqrt{2}$	1
2	1		3	17/5	$2\sqrt{2}$	4
2	2		4	4	$\sqrt{2}$	2
1	3		11/3	13/5	$3/\sqrt{2}$	3/2
1	4		6	4	$2\sqrt{2}$	2
2	3		17/3	5	$3/2\sqrt{2}$	4/3
2	4		8	32/5	$\sqrt{2}$	1
3	3		9	9	$\sqrt{2}$	2

For all simply supported plates, mode frequencies for m = n are integer multiples of the fundamental with 4 being the lowest multiple (from m=n=2). However, in aspect ratio $\sqrt{2}$ plates, there are lower modes with frequencies at integer multiples of 2 and 3, which facilitate the formation of modes in the two harmonic series of 1-2-4-8 and 1-3-6-9 etc. in sharp contrast to the reduced number of modes in the harmonic series of 1-4-5-9 with $\mathcal{R}$ = 2.

The presence of four modes at frequencies 1,2,3, and 4 times the fundamental led to the ready excitation of all modes in the tests reported with discrete frequency excitation or with an applied "haystack" shaped spectrum peaking near the excited mode (e.g. spectrum shape of -6dB per octave below peak and -6 dB per octave above peak). With the applied energy being absorbed by a large number of modes rather than concentrated in the fundamental mode, it was found that the stress levels were dominated by the higher complexity modes and were so low as to preclude obtaining fatigue failures in a reasonable time with the maximum sound pressure level available (168 dB overall).

Although the mode analysis is based on a simply supported plate, the same reasoning applies to the actual system for two reasons. At an aspect ratio of $\sqrt{2}$ the first mode (1,1C) in fully clamped boundaries has practically the same frequency as the simply supported 2,2 mode (2,2S). Secondly, in any physical condition, some degree of edgewise rotation approaching pinned or simply supported restraint does exist. All modes were accordingly identified as clamped (m,nC) or simply supported (m,nS) in the results presented.

REFERENCES

1. Gray, C. L.   Study in the Use of Structural Models for Sonic Fatigue
    ASD TR 61-547, 1962
    Wright-Patterson Air Force Base, Ohio

2. Murphy, G.   Similitude in Engineering
    Ronald Press Co., New York, 1950

3. Dyer, I.
    Smith, Jr., P. W.
    Malme, C. I.
    Gogos, C. M.   Sonic Fatigue Resistance of Structural Designs
    ASD TR 61-262, 1961
    Wright-Patterson Air Force Base, Ohio

4. Wang, P.   A Linear Approach in Sonic Fatigue Analysis and Calculations
    SAE Paper No. 671B April 1963

5. Koval, L. R.
    Cranch, E. T.   On the Free Vibrations of Thin Cylindrical Shells Subjected to an Initial Static Torque
    Space Technology Report No. EM 11-20
    July 1961

6. Miles, J. W.   "On Structural Fatigue Under Random Loading"
    Journal Aero Sc. p 753, November 1954

7. Hess, R. W.
    Fralich, R. W.
    Hubbard, H. H.   Studies of Structural Failure Due to Acoustical Loading
    NACA TN 4050, 1957

8. Miner, M. A.   "Cumulative Damage in Fatigue"
    Journal Appl. Mech., Vol. 12, pA159, September 1945

9. MacDuff, J. N.
    Felgar, R. P.   "Vibration Frequency Charts"
    Methods of Space Vehicle Noise Prediction
    WADC TR 58-343 Appendix, 1958
    Wright-Patterson Air Force Base, Ohio

10. Warburton, G. B.   "The Vibration of Rectangular Plates"
    Proc. Inst. of Mech.Eng. Vol. 168, p 371, 1954

11. Young, D.   "Vibration of Rectangular Plates by the Ritz Method"
    Journal Appl. Mech. ASME Vol. 17, p 448, 1950

12. Hearmon, R.F.S.   "The Frequency of Flexural Vibration of
                              Rectangular Orthotropic Plates with
                              Clamped or Supported Edges"
                              Journal Appl. Mech. Vol. 81, p.537, 1959

13. Bishop, R.E.D.   The Mechanics of Vibration
     Johnson, D.C.   Cambridge University Press, New York, 1960

14. Kerr, L.   Damping and Fatigue Properties of Sandwich
     Lazan, B. J.   Configurations in Flexure
                             ASD TR 61-646, 1961
                             Wright-Patterson Air Force Base, Ohio

15. Timoshenko, S.   Vibration Problems in Engineering
                             D.Van Nostrand Co. Inc., New York, 1955
                             3rd Edition

16. Stoker, J. J.   Nonlinear Vibrations in Mechanical and
                             Electrical Systems
                             Interscience Publishers, New York, 1950

17. Ku, Y. H.   Analysis and Control of Nonlinear Systems
                             Ronald Press Company, New York, 1958

18. Den Hartog, J.P.   Mechanical Vibrations
                             McGraw Hill Book Co., New York, 1956
                             4th Edition

19. Wang, P.   "Application of Linear Response Techniques
                             to Stress and Fatigue Analyses in Acoustical
                             Loading Problems"
                             Journal Acoustic Soc.of Am. Vol. 34
                             No. 9, p. 1161, September 1962

20. Smith, Jr. P.W.   "Nonlinear Response of Simply
     Malme, C.I.   Clamped Panel"
     Gogos, C.M.   Journal Acoustic Soc.of Am. Vol.33, No.11
                             p.1476, November 1961

21. Lyon, R. H.   Observation on the Role of Nonlinearity
                             in Random Vibration of Structures
                             NASA TND-1872, 1963

22. Timoshenko, S.   Strength of Materials, Part II
                             D. Van Nostrand Co. Inc., New York, 1956
                             3rd Edition

23. Chu, H. N.   "Influence of Large Amplitudes on Free
     Herrmann, G.   Flexural Vibrations of Rectangular Elastic
                             Plates"
                             Journal of Appl. Mech., Vol. 23, p.532
                             December 1956

24. Evans, T. H.
   "Table of Moments"
   ASME Trans. (Jour.of Appl. Mech.)
   Vol. 61, p.A-7, 1939

25. Wojtaszak, I.A.
   "Design Data"
   ASME Trans. (Journal of Appl. Mech.)
   Vol. 58, p.A-71, 1936

26. Mead, D. J.
   "The Practical Problems of Assessing
   Damping Treatments"
   Journal Sound Vib. Vol. 3, p.270, 1964

27. Hess, R. W.
   Herr, R. W.
   Mayes, W. H.
   A Study of The Acoustic Fatigue
   Characteristics of Some Flat and Curved
   Al. Panel Exposed to Random and
   Discrete Noise
   NASA TN D-1, 1959

28. Robbins, M. S.
   "Demonstration of Model Patterns in
   Vibrating Plates"
   Sound, Vol. 2, No. 4, p.8, 1963

29. Ojalvo, I. U.
   Newman,M.
   "Natural Frequencies of Clamped Ring
   Segments"
   Design and Development, p.219
   May 21, 1964

30. Archer, R. R.
   "Small Vibrations of Thin Incomplete
   Circular Rings"
   Int. J. Mech. Science, Vol. 1, p.45, 1960
   (Pergamon Press, Ltd., Poland)

31. Dept. of Defense
   Document
   ANC-23 "Sandwich Construction for
   Aircraft, Part II"
   Second Edition, 1955

32. Kuenzi, E. W.
   Mechanical Properties of Aluminum
   Honeycomb Cores
   Forest Product Lab. Report No. 1849
   September 1955

33. North American
   Aviation,Inc.
   Los Angeles Div.
   Establishment of The Approach To, and
   Development of, Interim Design Criteria
   for Sonic Fatigue
   ASD-TDR-62-26 1962
   Wright-Patterson Air Force Base, Ohio

DOCUMENT CONTROL DATA - R&D

(Security classification of title, body of abstract and indexing annotation must be entered when the overall report is classified)

1. ORIGINATING ACTIVITY (Corporate author)	2a. REPORT SECURITY CLASSIFICATION
North American Aviation, Inc.	Unclassified
International Airport, Los Angeles, Calif.	2b. GROUP N/A

3. REPORT TITLE

Modeling Techniques and Sonic Fatigue Prediction

4. DESCRIPTIVE NOTES *(Type of report and inclusive dates)*

Final Report - May 1964 to October 1965

5. AUTHOR(S) *(Last name, first name, initial)*

Wang, Paul

6. REPORT DATE	7a. TOTAL NO. OF PAGES	7b. NO. OF REFS
June 1966	140	33

8a. CONTRACT OR GRANT NO.	9a. ORIGINATOR'S REPORT NUMBER(S)
AF33(615)-1743	
b. PROJECT NO.	AFFDL-TR-65-171
1471	
c.	9b. OTHER REPORT NO(S) (Any other numbers that may be assigned this report)
d. Task Nr. 147101	NAA TFD-64-490-13

10. AVAILABILITY/LIMITATION NOTICES

Qualified requesters may obtain copies of this report from DDC. This report will be furnished to CFSTI for sale to the public.

11. SUPPLEMENTARY NOTES	12. SPONSORING MILITARY ACTIVITY
	Air Force Flight Dynamics Laboratory
	Wright-Patterson AFB, Ohio 45433

13. ABSTRACT

    The principles of static and dynamic similitude were applied to typical complex structural components for the purpose of examining the application of modeling techniques to sonic fatigue predictions. Modeled specimens of curved panels, honeycomb sandwich flat panels, and honeycomb sandwich cantilever beams have been tested. The tests were conducted on full scale, 5/8, and 3/8 size models. The tests and analyses demonstrated that scale reductions of linear panel dimensions, and other size factors necessary in the fabrication of models, may be separately considered in maintaining the established similitude relationships. Both random spectra and discrete frequency acoustic excitation are considered.

    Correlation of available data from other sources has established a frequency parameter defining the effects of radius of curvature along one side of a curved panel. This frequency parameter converts to a stress reduction factor that has been verified experimentally in many modes. Although the section modulus for honeycomb sandwich panels need not be controlled by the scaling factors, the generation of response modes is significantly related to the aspect ratios of surface dimensions. This panel aspect ratio effect can yield a dominant excitation of higher complexity modes at low stresses and impose difficulties in fatigue duration tests. Experimental data are used to identify these complexities and differences between modes without introducing consideration of coupling effects.

(continued on next page)

DD FORM 1 JAN 64 **1473**

DOCUMENT CONTROL DATA - R&D

(Security classification of title, body of abstract and indexing annotation must be entered when the overall report is classified)

1. ORIGINATING ACTIVITY (Corporate author)	2a. REPORT SECURITY CLASSIFICATION
	2b. GROUP

3. REPORT TITLE

4. DESCRIPTIVE NOTES *(Type of report and inclusive dates)*

5. AUTHOR(S) *(Last name, first name, initial)*

6. REPORT DATE	7a. TOTAL NO. OF PAGES	7b. NO. OF REFS

8a. CONTRACT OR GRANT NO.	9a. ORIGINATOR'S REPORT NUMBER(S)
b. PROJECT NO.	
c.	9b. OTHER REPORT NO(S) (Any other numbers that may be assigned this report)
d.	

10. AVAILABILITY/LIMITATION NOTICES

11. SUPPLEMENTARY NOTES	12. SPONSORING MILITARY ACTIVITY

13. ABSTRACT

Stress correlation is the critical parameter in modeling for acoustic fatigue. True models with exact geometric scaling in all elements are not necessary. Adequate modeling is obtained by maintaining the same aspect ratio and modes for the specimen and model. The frequency and stress then vary at predetermined magnitudes with a functional relationship to damping, amplitude, and cross-section (thickness) geometric parameters. Non-linear effects are dependent on excitation levels. In general, a prerequisite to sonic fatigue tests is a knowledge of the non-linearity induced by damping and amplitude for each specimen. The experimental data confirms the application of basic procedures formulated by Miles, Palmgren, and Miner which minimize the requirement for random excitation in the use of modeling techniques for sonic fatigue predictions.

DD $_{1\ JAN\ 64}^{FORM}$ 1473

14. KEY WORDS	LINK A		LINK B		LINK C	
	ROLE	WT	ROLE	WT	ROLE	WT
Modeling Techniques						

INSTRUCTIONS

1. ORIGINATING ACTIVITY: Enter the name and address of the contractor, subcontractor, grantee, Department of Defense activity or other organization (*corporate author*) issuing the report.

2a. REPORT SECURITY CLASSIFICATION: Enter the overall security classification of the report. Indicate whether "Restricted Data" is included. Marking is to be in accordance with appropriate security regulations.

2b. GROUP: Automatic downgrading is specified in DoD Directive 5200.10 and Armed Forces Industrial Manual. Enter the group number. Also, when applicable, show that optional markings have been used for Group 3 and Group 4 as authorized.

3. REPORT TITLE: Enter the complete report title in all capital letters. Titles in all cases should be unclassified. If a meaningful title cannot be selected without classification, show title classification in all capitals in parenthesis immediately following the title.

4. DESCRIPTIVE NOTES: If appropriate, enter the type of report, e.g., interim, progress, summary, annual, or final. Give the inclusive dates when a specific reporting period is covered.

5. AUTHOR(S): Enter the name(s) of author(s) as shown on or in the report. Enter last name, first name, middle initial. If military, show rank and branch of service. The name of the principal author is an absolute minimum requirement.

6. REPORT DATE: Enter the date of the report as day, month, year; or month, year. If more than one date appears on the report, use date of publication.

7a. TOTAL NUMBER OF PAGES: The total page count should follow normal pagination procedures, i.e., enter the number of pages containing information.

7b. NUMBER OF REFERENCES: Enter the total number of references cited in the report.

8a. CONTRACT OR GRANT NUMBER: If appropriate, enter the applicable number of the contract or grant under which the report was written.

8b, 8c, & 8d. PROJECT NUMBER: Enter the appropriate military department identification, such as project number, subproject number, system numbers, task number, etc.

9a. ORIGINATOR'S REPORT NUMBER(S): Enter the official report number by which the document will be identified and controlled by the originating activity. This number must be unique to this report.

9b. OTHER REPORT NUMBER(S): If the report has been assigned any other report numbers (*either by the originator or by the sponsor*), also enter this number(s).

10. AVAILABILITY/LIMITATION NOTICES: Enter any limitations on further dissemination of the report, other than those imposed by security classification, using standard statements such as:

(1) "Qualified requesters may obtain copies of this report from DDC."

(2) "Foreign announcement and dissemination of this report by DDC is not authorized."

(3) "U. S. Government agencies may obtain copies of this report directly from DDC. Other qualified DDC users shall request through

_____."

(4) "U. S. military agencies may obtain copies of this report directly from DDC. Other qualified users shall request through

_____."

(5) "All distribution of this report is controlled. Qualified DDC users shall request through

_____."

If the report has been furnished to the Office of Technical Services, Department of Commerce, for sale to the public, indicate this fact and enter the price, if known.

11. SUPPLEMENTARY NOTES: Use for additional explanatory notes.

12. SPONSORING MILITARY ACTIVITY: Enter the name of the departmental project office or laboratory sponsoring (*paying for*) the research and development. Include address.

13. ABSTRACT: Enter an abstract giving a brief and factual summary of the document indicative of the report, even though it may also appear elsewhere in the body of the technical report. If additional space is required, a continuation sheet shall be attached.

It is highly desirable that the abstract of classified reports be unclassified. Each paragraph of the abstract shall end with an indication of the military security classification of the information in the paragraph, represented as (TS), (S), (C), or (U).

There is no limitation on the length of the abstract. However, the suggested length is from 150 to 225 words.

14. KEY WORDS: Key words are technically meaningful terms or short phrases that characterize a report and may be used as index entries for cataloging the report. Key words must be selected so that no security classification is required. Identifiers, such as equipment model designation, trade name, military project code name, geographic location, may be used as key words but will be followed by an indication of technical context. The assignment of links, rules, and weights is optional.

PO 886-551